ELECTROSTATIC FORCES FOR SATELLITE SWARM NAVIGATION AND RECONFIGURATION

Final Report

Authors: Chakravarthini M. Saaj[1], Vaios Lappas[1], Dave Richie[1]
Mason Peck[2] , Brett Streetman[2], Hanspeter Schaub[3]

Affiliation: [1]Surrey Space Centre, University of Surrey, UK
[2]Mechanical & Aerospace Engineering, Cornell University, US
[3]Aerospace and Ocean Engineering Department, Virginia Tech, US

ESA Research Fellow/Technical Officer: Dario Izzo

Contacts:

Vaios Lappas
Tel: +44(0)1483 683412
Fax: +44(0)148389503
e-mail: V.Lappas@surrey.ac.uk

Dario Izzo
Tel: +31(0)71 565 3511
Fax: +31(0)715658018
e-mail: act@esa.int

Available on the ACT website
http://www.esa.int/act

Ariadna ID: AO4919 05/4107
Study Duration: 4 months
Contract Number: 19697/06/NL/HE

ACRONYMS & ABBREVIATIONS

ACT	Advanced Concepts Team
AIAA	American Institute of Aeronautics and Astronautics
APF	Artificial Potential Field
CSF	Coulomb Spacecraft Formation
ESA	European Space Agency
ESTEC	European Space Research & Technology Centre
EP	Electric Propulsion
GEO	Geostationary Earth Orbit
LEO	Low Earth Orbit
LAO	Lorentz Augmented Orbit
PD	Proportional Derivative
PID	Proportional Integral and Derivative
SMC	Sliding Mode Control
SM	Sliding Mode
WPs	Work Packages

CONTENTS

LIST OF FIGURES

LIST OF TABLES

ABSTRACT

Natural charging due to ambient plasma and the photoelectric effect can produce Coulomb forces of 10-1000 μN, which could disturb the configuration of swarms of spacecraft in formations close enough that Debye shielding is negligible. Even in the presence of Debye shielding, charged spacecraft interact with the planetary magnetosphere and generate Lorentz forces, which can also disturb precision formations. The magnitude of these disruptive inter-satellite Coulomb forces is comparable to typical ion thrusters proposed for spacecraft formation flying. Rather than fighting them, it would be wise to make use of these effects. In this work, we developed an efficient hybrid propulsion system combining Coulomb forces and standard electric thrusters for formation flying of the order of tens of meters in Geostationary or other high earth orbits. We also investigated extensions of this concept to lower-earth orbits, where the Lorentz effect dominates. Following its initial investigation of Coulomb and Lorentz force interactions with electric propulsion, we designed a candidate hybrid propulsion system for satellite-swarm formation flying. This novel approach is fuel-efficient and also minimizes potentially damaging exhaust plumes, reduce mass, and eliminate an important class of disturbances. The path-planning algorithm used in this study for autonomous spacecraft navigation is based on artificial potential-field method. This method is rapidly gaining popularity, as it is computationally less expensive than global approaches and provides a simple but effective path planner for real-time obstacle avoidance. The results in the report would serve as a “proof of concept” for propellant-less propulsion using electrostatic forces and Lorenze force. However, much work is needed to fully exploit electrostatic forces to make the concept of propellant-less propulsion true for a real satellitron mission.

Key words: Satellitrons, Coulomb force, Lorentz force, Formation flying, Artificial potential field.

1. STUDY OBJECTIVES

Phase 1 (14 March 2006-14 May 2006)

The study objectives are:

- To study the dynamical interaction among inter-satellite Coulomb forces, Lorentz Forces, and conventional electric thrusters and to develop an efficient hybrid propulsion system for satellite swarm formation flying in high Earth orbits.

Phase 2 (14 May 2006-15 August 2006)

The study objectives are:

- To develop a fully autonomous path planning and collision avoidance algorithm for satellite swarm using an artificial potential-field method.
- To evaluate the viability of a candidate formation-flying controls architecture based on this hybrid propulsion concept, with a view toward establishing systems-engineering principles for the design of such systems.

1.1 WORK SCHEDULE

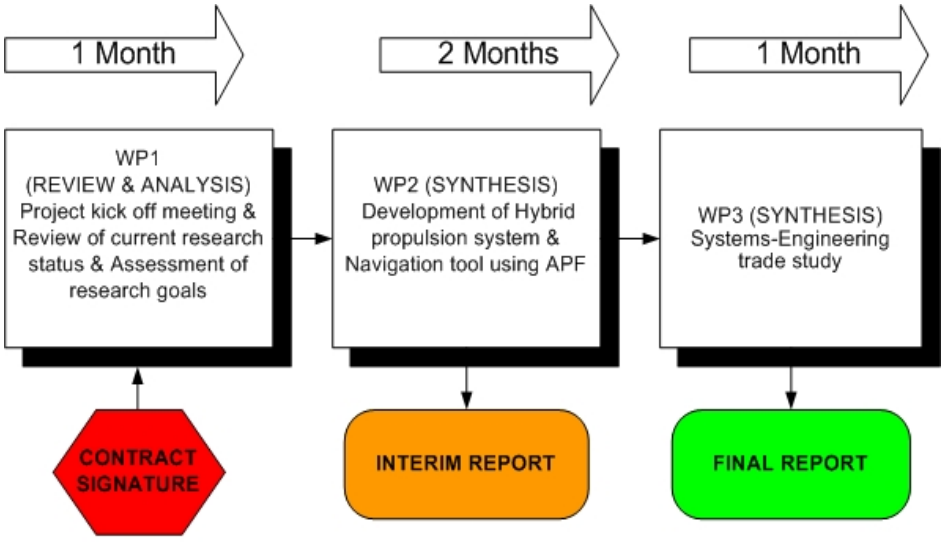

We used a three-phase consecutive work breakdown structure as shown in Figure 8. The work package WP1 (REVIEW & ANALYSIS) comprised of a project kick-off meeting, research survey on inter-satellite Coulomb force, Lorentz-augemented orbits for various space applications and artificial potential-field methods for spacecraft swarm path planning. This phase also assessed the various research goals proposed in the work. This phase was conducted over one month. Work package WP2 (SYNTHESIS) comprises two major goals. The first task consisted of analyzing the interaction between Coulomb forces, Lorentz forces and the standard thrusters used for satellite formation flying. Based on this a new hybrid propulsion system is developed which will be a nearly propellant-less propulsion system. The second task is to develop the collision avoidance algorithm by combining the artificial potential field method with this hybrid propulsion system for autonomous navigation of satellite swarms in high earth orbits. This phase comprises the core of the project and was conducted over two months. The end of this WP is a milestone defined by the mid-term review. Work package WP3 (SYNTHESIS) proposes to identify and evaluate systems-engineering trade studies whose outcome will be a robustly optimized design for future swarm spacecraft that use the proposed hybrid propulsion and AFP approaches. At the end of this one-month period, the final work report will be delivered and this would mark the final milestone and the successful completion of this project.

2. LITERATURE REVIEW

2.1 PLASMA ENVIRONMENT AND SPACECRAFT CHARGING

The growing sophistication of spacecraft has lead to increasing concern over spacecraft environment interactions associated with plasmas. Spacecraft surface charging due to plasma interaction continue to be a major source of spacecraft anomalies and pose a continuing problem for the spacecraft builders. Surface charging refers to charging effects and electrostatic discharge effects on the visible surface of the spacecraft. The literature on spacecraft charging is extensive (Garett 1980, James et al. 1994, Hasting and Garret 1996, Garrett and Whittlesey, 2000, Tribble 2003). Garett (1980) reviewed the field of spacecraft surface charging in 1980. A detailed discussion of the space plasma environment can be found in the textbook by Hasting and Garret (1996). Coulomb spacecraft charging and plasma interactions have been of great concern to spacecraft designers and operators even twenty-five years after the highly successful geostationary SCATHA spacecraft program (Mullen et al., 1986). Differential spacecraft charging occurs when portions of the satellite assume different potentials. The exposed vehicle surfaces will interact with the ambient plasma differently depending on the material composition of the surface, whether the surface is in sunlight or shadow, and the flux of plasma particles to this surface. These potentials can result in arcing from one component to another or sputtering of surfaces and are to be avoided, whether by the choice of materials, charge management (by grounding to the surrounding plasma), or by careful placement of components and incorporation of Faraday cages (James et al., 1994; Garrewtt and Whittlesey, 2000). Catastrophic electrostatic discharges can occur from potential differences of only a few hundred volts between sensitive components. Thus, great design effort needs to be placed in the elimination of spacecraft differential charging. Besides potentially causing electrostatic discharge, differential spacecraft charging can also affect the motion of the spacecraft. The natural distributed charge that would occur during worst case plasma conditions at GEO could result in torques as large as 0.1 μNm at 10 meter separation distance. A more recent review on this issue has been done by Garett and Whittlesey (2000). In recent years spacecraft designers are concerned about internal charging that would adversely affect the electronics in addition to differential charging. This issue has been addressed in the NASA handbook, “Avoiding Problems Caused by Spacecraft On-orbit Internal Charging Effects” (1998). Spacecrafts orbiting in low altitudes are also subject to charging (Stone, 1981). Low altitude plasma interactions and charging effects are slowly yielding to detailed computer analysis and experiment. However, “critical ionization velocity” phenomenon proposed by Alfven (1954) remains an intriguing issue (Lai and Murad, 1989). Moreover, the effect of “dusty plasma” on spacecraft operation needs further investigation (Chutijian, 2000).

2.2 GEO COULOMB SPACECRAFT FORMATION FLYING

The formation concept, first explored in the 1980's to allow multiple geostationary satellites to share a common orbital slot (Walker, 1982), has recently entered the era of application with many successful real missions (a few examples are: EO-1 in formation with LandSat-7, TechSat21). The main advantage of spacecraft formation flying is that by successfully controlling a formation, one may have them cooperate in a way that enables missions that would have required an enormous single spacecraft. Swarms of micro-satellites are currently envisioned as an attractive alternative to traditional large spacecraft. The ability to distribute the functionality of one large spacecraft among several much smaller may reduce the total weight and in turn the launch costs. However, an important concern with spacecraft formation flying is how to control the relative motion using a fuel and power efficient solution. Formation flying involves position maintenance of multiple spacecraft relative to measured separation. This requires identifying stable formation configuration, maintain the configuration (station keeping) for a finite period of time and depending on the mission requirements reconfigure the formation autonomously. Dispersing the functions of a single spacecraft over a formation of spacecraft produces a more robust and fault-tolerant system architecture. The failure of a single spacecraft in a formation does not necessarily lead to system failure as it would in a single larger spacecraft. Upgrades or repairs could be performed by simply replacing any obsolete or disabled spacecraft (Das et al. 1998). The cost of repairs and upgrades to the system is reduced because of the natural modularity of a spacecraft formation. Spacecraft formations offer higher performance and more efficient system architectures. A free flying (no booms or tethers) formation facilitates greater resolution through the use of spatially distributed simultaneous measurements (Leitner et al. 2002). Long baseline optical interferometry is an example of a high performance system that requires distributed measurements (DeCou, 1991). Another benefit of free-flying spacecraft formations is their ability to change the relative positions and attitudes of the spacecraft to achieve optimal configurations for different missions throughout the lifetime of the system. Thereby adding greater functionality to the system than a single spacecraft could provide (Das et al. 1998). Constellation of micro-satellites will require propulsion system with micro-to milli-Newton thrust levels for deployment, orbit maintenance, disposal and attitude control (Janson et al, 1999). Formation-keeping thrusters must be capable of producing finely controlled, highly repeatable impulse bits. Although no suitable thruster has yet been proven in flight, recent research suggests that the best current technologies are micro-Pulsed-Plasma Thrusters (micro PPT), Field Emission Electric Propulsion (FEEP) thrusters and colloid thrusters (Hoskins et al., 1999, Tajmar et al., 1999, Martinez-Sanchez and Pollard, 1998). However, it has been identified that in close proximity, the propellant emitted by these

conventional thrusters will impinge upon neighboring vehicles and damage payloads. Moreover, the orbital mechanics for many clusters of interest mandate continuous thruster firings pointed directly towards other spacecrafts in the formation. This contamination problem will be amplified as the formation spacing is reduced.

In recent years there has been increasing interest in close-proximity (10-100m) spacecraft formation flying. Unfortunately, close-proximity missions are not feasible with the current electric propulsion technology available today. Formation flying of the order of tens of meters is very difficult using conventional electric or ion propulsion methods, because the exhaust plumes can interfere with on-board sensors and payload elements (such as optical instruments). King et al. (2002a, 2002b, 2003) and Schaub et al. (2003) proposed a novel spacecraft formation flying concept by exploiting the inter-spacecraft electrostatic force. By expelling either positively or negatively charged particles, the charge of a spacecraft can be controlled. Currently, the CLUSTERS mission demonstrates this technology by emitting charged particles so that the spacecraft maintain electrostatic neutrality relative to the charged plasma environment (Torkar et al. 2001). By generating different charges on spacecraft in close proximity, each craft exerts a force on all the other spacecraft. This force can potentially be exploited to control the relative motion of the spacecraft and thus the formation shape. There are numerous other research papers on Coulomb Spacecraft Formation (CSF) (Schaub, 2004; Joe et al., 2004; Schaub and Kim, 2004; Parker et al., 2004; Berryman and Schaub, 2005; Natarajan and Schaub, 2005). Using Coulomb forces would allow the relative motion of satellites to be controlled without such contaminations (Schaub et al., 2003). Coulomb thrusting makes use of renewable electric energy and is therefore free from contaminations and hence sounds promising for future close formation flying missions. An isolated spacecraft will assume equilibrium potential (voltage) such that the net environmental current due to plasma and photoelectron emission is zero. It is possible to change this passive equilibrium potential by actively emitting electrical current from the spacecraft. By controlling the net charge of the spacecraft, Coulomb forces can be generated to keep the formation near a desired configuration. Unlike conventional electric thrusters, Coulomb control would be essentially propellant-less. It has been estimated that Coulomb forces of the order of 10-1000 μN can be produced on short timescales with less than 1 Watt of on board power which is comparable with that produced by conventional electric thrusters (Garrett and Whittlesey, 2000). This shows that virtually zero fuel mass would be consumed to generate these forces. This essentially propellantless mode of propulsion comes at the price of a greatly increased level of complexity of the relative motion dynamics. The electrostatic fields directly tie together and couple the motion of all charged satellites. If one charged satellite were to change its position, then the motion of all other charged satellites in the formation will be affected. Moreover, the electric field strength will drop off with the inverse

square of the separation distance, this relative motion control concept is only viable for relatively tight formations with 10-100 meters separation distance. Beyond such distances, electrostatic discharge among spacecrafts components becomes an increasing concern. CSF applications range from wide field of view sparse radar interferometry systems and autonomous robotic scouts flying about a mother craft to swarms of pico-satellites that will provide a distributed sensing platform. This method is based upon the attraction and repulsion of charged bodies. Coulomb controlled formations offers an alternative to other candidate propulsions systems because it weigh less and are more fuel efficient. Programs such as LISA (Vitale et al., 2002) and TPF (Kong et al., 2004) may depend on precise formations and, of course, benefit from fuel-efficient designs. In Geostationary Orbits (GEO), the spacecraft charging is significant (Mullen at al. 1986). The charged plasma environment in space has a large effect on Coulomb force. First, interactions with plasma tend to drive the charge of a spacecraft to a particular value, requiring a constant power input to maintain a desired potential. The second main effect of the plasma environment is Debye shielding. A positively charged particle in a plasma will be surrounded by negatively charged particles. Outside a certain distance, called the Debye length, the system of the positively charged particle and the sheath of negative ions or electrons surrounding it will appear to be a charge neutral system. Thus, for Coulomb effects to be experienced among spacecraft, they must be closer to each other than the Debye length of the surrounding plasma. In GEO, Debye length is large and is of the order of tens of meters. This allows close-proximity CSF in GEO. However, this method of control has certain disadvantages. With Coulomb control, all forces are internal and the linear and rotational momentum cannot be altered by Coulomb forces (Schaub and Parker, 2004; Schaub and Kim, 2004). The dynamics is highly coupled and non-linear. However, if the dynamics can be better understood, then the Coulomb control might one day be a fuel efficient, inexpensive, long lasting and dependable method for controlling close proximity formations. Much work has been done to understand static Coulomb formation (Berryman and Schaub, 2005). However, there is no guarantee that they are stable or controllable. Further research is essential to demonstrate their stability and controllability of both static and dynamic Coulomb formations.

2.3 LORENTZ-AUGMENTED ORBIT AND LEO FORMATION FLYING

A charged particle moving relative to Earth's magnetic field accelerates in a direction perpendicular to its velocity and the magnetic field due to the Lorentz force. The use of the Lorentz force for spacecraft control is a new idea, and relatively unstudied. The phenomenon of Lorentz force distributed orbits has been observed in natural systems (Schaffer and Burns, 1987; Schaffer and Burns 1994). Schaffer and Burns have developed the dynamics of dust particles charged by the plasma environment around Jupiter. They have shown that the motions

of these small charged grains can be greatly affected by Lorentz mechanics. Peck (2005) conducted a study on Lorentz force and has proposed several applications for the Lorentz effects. It turns out that a Lorentz-Augmented Orbit (LAO) may be used to address a number of problems of current relevance, including design of stable formations, orbit raising, inclination control, and drag mitigation. But perhaps more remarkable, advancing the technology represents a way to achieve propellant-less earth or solar-system escape. The Lorentz force is experienced individually by any charged spacecraft, and is not the result of an interaction between two charged vehicles, as is the case for the Coulomb force. The Lorentz force is due to the spacecraft's velocity with respect to the Earth's magnetic field, which rotates with the Earth. Note that the direction and magnitude of the Lorentz force is determined by the satellite's orbital geometry and current position. The direction of the force is also always perpendicular to the craft's velocity in a non-inertial earth-referenced frame. A detailed derivation of the motion of a spacecraft subject to the Lorentz force is available in a soon-to-appear paper (Streetman and Peck, 2006).

Lorentz-force propulsion does not involve the use of electrodynamic tethers, although the physics is related. In the case of a tether, the current flowing through a long conductor induces a magnetic field that interacts with the planet's magnetic field to produce a force on the tether. Electrons travel through the tether at low speed but at as high a current as possible. For an LAO, the spacecraft may be very compact. The charge it carries travels at perhaps thousands of meters per second relative to the magnetic field, and this moving charge represents the current that results in a force similar to what a tether experiences. Furthermore, an LAO does not work though electrostatic levitation. That is, an LAO does not take advantage of Coulomb forces that act on the charged spacecraft. Depending on the orbit geometry of a formation, Debye shielding and the geomagnetic field cause Coulomb and Lorentz effects to vary in importance. In LEO the Debye length is small, and orbital speed are much larger than the speed of the magnetic field; so, Coulomb effects are dominated by Lorentz effects. In fact, the Debye shield improves the performance of a Lorentz-capable spacecraft, because it increases the capacitance of the body, allowing more charge to be stored on a given area. Near GEO, the Debye length is much larger and the spacecraft's velocity relative to the magnetic field approaches zero, so Coulomb effects dominate. Formations of LAO-capable spacecraft are not designed to interact through Coulomb attraction or repulsion. Both Coulomb and Lorentz forces can significantly alter the orbits of charged spacecraft. However no studies of Coulomb formations to date include the effects of the Lorentz force. If the formation is operated significantly away form GEO or in an elliptical orbit, Lorentz effects may cause significant undesirable results in formation keeping, especially if the Coulomb control strategy calls for spacecraft of both positive and negative charges, as these will be driven in opposite directions. For a practical electromagnetic

formation control system to be designed, a model needs to be developed that takes into account both Coulomb and Lorentz effects on charged spacecraft.

Much of the studies on spacecraft charging is concerned with the deleterious effects of differential charge, a problem that arises when dissimilar or discontinuous materials acquire potential as the spacecraft travels through the space plasma (Tribble, 2003). The photoelectric effect, in which photons cause some materials to emit electrons, can also be responsible. These studies are concerned primarily with predicting charge levels and assessing the risks of material damage due to interactions with the natural environment. By contrast, Peck (2005) consider the active application of charge to a spacecraft body; and although the influence of the plasma is very relevant for the design Lorentz-capable spacecraft, the equilibrium potentials achieved passively are not of direct interest here. Hough (1982) studied the impact of the Lorentz force on the comparatively short trajectory of a missile, with no effort at modulating the charge for the sake of control. In contrast, Peck's approach for satellites includes both control and the assumption that these forces may innovativeness require a long time to effect a significant orbit change. So, despite the of Hough's work, this approach look elsewhere for insight. The most in-depth treatment of Lorentz-augmented celestial mechanics is found in the work of Burns and Schaffer on planetary dusty plasmas (Burns and Schaffer, 1989; Schaffer and Burns, 1987). Their work offers explanations for gaps in Jupiter's and Saturn's rings that are based on identifying resonances in the orbit dynamics. The resonances arise thanks to interactions among gravity and small effects such as solar pressure, lunar perturbations, and the Lorentz force. The success of these studies validates models of particle charging and demonstrates that the Lorentz force leads to non-Keplerian orbits, at least for micron-size particles at a few Volts of potential. Dusty plasma researchers have also considered the problem of dust grains in orbit, but with a primary interest in plasma dynamics rather than celestial mechanics (Cui et al., 1994).

Another class of studies on spacecraft charging stems from ballistic missile defense research during the past two decades, much of it for the Strategic Defense Initiative of the Reagan era. This work has involved high-energy ion and electron beam emission from sounding rockets and spacecraft. Some examples of rocket platforms include the Beam Experiment Aboard Rocket (BEAR), Space Power Experiment Aboard Rockets (SPEAR) I through III (Rustan et al., 1993; Mandell et al., 1998; Friedrich and Torkar, 1991), and MAIMIK (Friedrich and Torkar, 1991). Satellite-based experiments include the high-altitude Application Technology Satellite 6 (ATS-6) and Spacecraft Charging at High Altitude (SCATHA) satellites. Theoretical studies have also been undertaken (Lai, 1989; Lai, 2002). The Space Shuttle has also been the subject of charging studies (Bilen et al., 1995), for example during the 1992 flight of the Tethered Satellite System (TSS). The LEOSynch spacecraft architecture represents a way to operate a LEO

spacecraft whose ground track is a pattern fixed on the rotating earth (Peck and Morgowicz, 2006). To do so, they take advantage of the Lorentz force that acts on charged, polar-orbiting satellites as they travel through Earth's magnetic field to cause a nodal-precession rate equal to 360 deg./day. The orbit mechanics of such a spacecraft resemble those of a sun-synchronous satellite, whose orbit precesses around the earth's poles at about 1 deg/day due to the J_2 perturbation. For this reason, the proposed technology can also be used to cancel or augment J_2. The obvious benefit of a geosynchronous LEO satellite to earth observation (whether military or scientific) is that this ground track allows repeated LEO imaging of the same ground target for a large fraction of a satellite's orbit. A constellation of such satellites can offer persistent LEO coverage of such a target. Furthermore, such a spacecraft can be retargeted to cover a new longitude in less than 6 hours. The implementation issues, such as the interaction of this spacecraft with the plasma environment, approaches for maintaining the charge are addressed in this work.

2.4 PATH PLANNING TECHNIQUES

One of the most challenging problems with spacecraft swarming, formation flying and station keeping is that the spacecrafts must be autonomous and able to generate and correct their own relative positions with limited guidance from the ground. The first work in this field, as in the relative position case, stems from the work done on automatic rendezvous and docking control of two spacecraft, as was done on the Apollo missions. Later it was utilized in the Space Shuttle, Skylab and Gemini (Wang et al. 2003). A spacecraft formation can be considered as a distributed system. The position control systems of the individual spacecraft act as the local control agents. The control decisions of the local control agents must be coordinated to ensure the stability and convergence of the global system. Coordinated controllers are generally split into centralized and decentralized types. The distinction is based on where and who makes the control decisions. Centralized control (leader-follower) is a type of coordinated control where a single control agent, called the global control agent, determines the control actions for the distributed system (Wang et al. 1999, Pan and Kapila 2001, Kang and Yeh 2002 and Mesbahi and Hadaegh 2001). Wang et al. (1999) proposes a control technique to rotate the entire formation about a given axis and synchronize the individual spacecraft with the formation. Both position and attitude are controlled, and the error is proven to decay to zero exponentially, though under the assumption of no environmental disturbances and implementation difficulties. In (Pan and Kapila 2001) an adaptive nonlinear controller is proposed, which assumes a unknown mass and inertia, and coupled translational and attitude dynamics. Based on a Lyapunov framework they derive a controller, which leads to globally asymptotic convergence of the follower spacecraft relative position and attitude. Kang and Yeh (2002) proposed a more general way to achieve leader/follower synchronization, through the use of reference projections. The control input to each satellite is a function of its own state and the reference

projection. Where the reference projection defines a desired state for the closed-loop system, as a function of the measured and desired states of the other satellites. Mesbahi and Hadaegh (2001) have developed a leader-follower approach based on linear matrix inequalities and logic based switching. Izzo (2002) developed an extension of the Hill-Clohessey-Wiltshire equation that is used to study a simple 100m leader-follower formation in near polar orbit at 600Km of altitude that takes into account the Earth oblateness and the air drag. Izzo et al. (2003) has proposed an accurate linear model capable of capturing first order dynamics, as in the Hill-Clohessey-Wiltshire equation and the motion due to the presence of the J_2 effect. Izzo and Pettazzi (2005) has developed a novel approach for autonomous path planning of satellite swarm using behaviour based approach. In this method, it is possible to achieve a highly distributed control over the relative geometry of the satellite swarm. Krogstad (2005) developed a nonlinear observer-controller structure for leader-follower satellite formation attitude control by applying methods from synchronization of mechanical systems and nonlinear control theory.

In decentralized control, control decisions are relegated to the local control agents. The local control agents use local observations and any information communicated by the other control agents to determine control actions. The two primary benefits of decentralized control over centralized control are robustness and relatively simple control laws. The failure of a single local control agent in a decentralized controlled system does not lead to the destabilization of the entire system (Davison, 1974). The failure is confined to the region of the failed local control agent resulting in a graceful degradation of system performance. Decentralized control uses relatively simple control laws, because the design of the global controller can be broken up into smaller control agents. The local control agents are designed so that they perform their local control tasks, as well as coordinate with one another to control the global system (Davison, 1974). The coordination is implemented by means of communication between the local control agents. Centralized controllers require greater information and information processing than what is required by the local control agents of a decentralized controller (Aoki and Li, 1973). One of the most popular ideas for decentralized cooperative control are behavioral (or reactive) models (Balch and Arkin, 1998). Behavior-based control is implemented when a control system has multiple, and sometimes competing, objectives or behaviors. The behaviors could include goal attainment, collision avoidance, obstacle avoidance, and formation keeping. The overall control action is determined by a weighted average of the control actions for each of the behaviors. This is a useful tool for the coordinated formation attitude control problem. For the coordinated attitude control problem, behavior-based control is used to arrive at a compromise between the control actions required for the formation-keeping and station-keeping behaviors (Beard et al. 2001). Formation-keeping is the behavior that tries to drive the spacecraft to its absolute desired attitude while station-keeping is the behavior that tries to align the spacecraft with the other

spacecraft in the formation. These are easily implementable (Lawton et al. 2000), (Fredslund and Mataric 2002) but generally fail to yield any formal guarantees of convergence. The “emerging” formation configurations depend primarily on initial conditions. This is also the case in flocking cooperative control schemes (Olfati-Saber and Murray 2004; Tanner et al. 2003; Gazi and Passino 2002) although the asymptotic synchronization of agents velocities is formally proven. In most schemes that use nearest interaction rules (Lin et al. 2004; Klavins 2003; Lin et al. 2003) the resulting relative positions or the final rendezvous point are unpredictable. Other decentralized approaches rely on ideas based on Internet protocols (Sandoval-Rodriguez and Abdallah 2003). Voronoi diagram-based, decentralized non-smooth cooperative control techniques (Cortes and Bullo 2004) have shown to globally optimize certain objective functions, yet still, the final arrangement of agents cannot be foretold. A decentralized cooperative control methodology that does guarantee the convergence of agents in particular relative positions while navigating amongst sphere like obstacles is (Dimarogonas et al. 2003). However, the approach to decentralization is similar to that of (Ren and Beard 2004): each agent essentially carries a copy of some centralized coordination scheme, thus still requiring full knowledge of the system and environment state. A drawback of decentralized controllers is that it is difficult to prove convergence analytically. Matthew (2004) has developed a decentralized attitude controller utilizing behavior-based control is developed for controlling the attitude of a formation of free-flying spacecraft. Tanner and Kumar (2005) has developed decentralized cooperative controllers, which are based on local navigation functions and yield global asymptotic stability of a group of mobile agents to a desired formation and simultaneous collision avoidance. A comprehensive survey of spacecraft formation flying guidance for both deep space and planetary orbital environments can be found in (Scharf et al. 2003). Recently, Izzo and Pettazzi (2005) presented a new technique for satellite path planning that exploits a behaviour-based approach to achieve an autonomous and distributed control of identical spacecrafts over the relative geometry making use of limited sensorial information. Ayre et al. (2005) developed a novel control scheme termed ‘Equilibrium shaping’ based on behaviour-based control suitable for self-assembly and formation flying applications.

Another approach to coordinated control is based on virtual structure. A great deal of work has been done in this area using mobile robots (Lewis and Tan 1997), and has recently been applied to spacecraft formations (Ren and Beard 2004; Beard 1998; Beard and Hadaegh 1998; and Beard et al. 2001). In this approach, the spacecraft formation is viewed as a virtual rigid body. The desired states of a single spacecraft may be specified by the place holders in the virtual structure such that the formation moves as a single structure. One advantage of the virtual structure approach is that it is easy to prescribe the coordinated behaviour for the group. Another advantage is that the virtual structure can maintain the formation very well during the

manoeuvres in the sense that the virtual structure can evolve as a whole in a given direction with some given orientation and maintain a rigid geometric relationship among multiple vehicles. The disadvantage is that requiring the formation to act as a virtual structure limits the class of potential applications of this approach. For example, when the formation shape is time-varying or needs to be reconfigured frequently, the virtual structure approach may not be the best option. The idea of formation feedback is addressed by Ogren et al. (2002), Beard et al. (2001), Young et al. (2001) and Ren and Beard (2002). In (Beard et al. 2001), the authors introduce a coordination architecture for spacecraft formation control which subsumes leader-following, behavioural, and virtual structure approaches to the multi-agent coordination problem. In (Young et al. 2001), formation feedback is used for the coordinated control problem for multiple robots. In the case of spacecraft control, system dynamics are more complicated than the double integrator dynamics applied in (Young et al. 2001). Ren and Beard (2004) has proposed a different approach of formation feedback from (Ogren et al. 2002) and has applied this idea to the more complicated spacecraft interferometry problem so that formation keeping is guaranteed throughout the manoeuvre and the total system robustness is improved. Optimal control has proven relevant in the absence of the second zonal harmonic (J_2) of the non-spherical Earth. Kumar and Seywald (1995) used optimal control to solve for the relative motion of two satellites in very low Earth orbits. Inalhan et al. (2000) considered the micro-satellite reconfiguration as a distributed and hierarchical control problem. Milam et al. (2001) developed a general optimization based control methodology to solve constrained trajectory generation problems for station keeping and reconfiguration of fully actuated low thrust micro-satellites. Campbell (2003) designed an off-board computed procedure using the theory of optimal control for the design of formation reconfiguration. Ren et al. (2004) introduced the virtual-structure method in order to design a decentralized formation scheme for spacecraft formation flying. Campbell (2003) applied some results from optimal control theory in order to design an off-board computed procedure for the design of a formation-reconfiguration method. In addition to controller design, many researchers are focussing on the necessary architecture required to maintain the precise flight of several spacecrafts at the same time and the communications equipment necessary for this (Smith and Hadaegh, 2002). Although these results are encouraging, much work is needed before this technology is feasible for actual space applications.

A well-known approach to collision-free path planning of terrestrial robots is using Artificial Potential Field (APF) developed by Khatib (1986). Since then it has been widely explored and discussed (Khosla and Volpe, 1988; Rimon and Koditschek, 1992). APF is rapidly gaining popularity in many practical applications, as it is computationally less expensive than the global approach and provides a simple and effective path planner for obstacle avoidance for real-time

implementation. In this approach the robots steering direction is determined by assuming that the obstacles (and forbidden regions) assert repulsive forces on the robot and the goal asserts attractive forces. Consequently, the robot experiences a generalized force equal to the negative of the total potential gradient that drives the robot towards the goal. Koren and Borenstein (1991) presented a systematic and a critical discussion on the inherent problems of PFMs which includes trap situations due to local minima (cyclic behaviour), no passage between closely space obstacles, oscillations in the presence of obstacles, oscillations in narrow passages. The robot is said to be in a structural local minimum only when there exists at least one possible trajectory and the robot is in static equilibrium with repulsive forces from obstacles and attractive force from the goal sink. The first problem, the local minima, is not the problem of potential field approach but the problem of purely reactive systems. Such a problem can be resolved integrating the deliberative approach (plan based). The remaining three problems are due to the information loss between the behaviours and blending module. Kim and Khosla (1991) proposed a trial and error method that involves incorporating an artificial obstacle, which could remove one possible trajectory that causes structural local minimum. Khosla and Volpe (1988) proposed the super quadratic potential function to model obstacles with arbitrary shapes. By this approach local minima can be removed with limited success in configuration space but at the cost of increased computational complexity. Kim and Khosla (1992) proposed a harmonic potential function for real-time obstacle avoidance that completely eliminates local minima even for cluttered environment. The panel method was used to represent arbitrarily shaped obstacles and to derive the potential over the whole space. However, this method is suitable only for point mobile robots and does not eliminate local minima for mobile robot or a manipulator, which cannot be approximated as a point. Rimon and Koditschek (1992) developed a new methodology for constructing navigation function from a geometric description of the free configuration space. However, this method guarantees to bring a bounded-torque actuated robot to a desired configuration with out hitting obstacles only in a perfectly known and stationary environment. Akishita *et al.* (1993) proposed a velocity potential approach to path planning and avoiding moving obstacles for an autonomous mobile robot by use of the Laplace potential. This navigation function comes from the introduction of fluid flow dynamics into path planning. However, this navigation algorithm is feasible only in bounded space. Khatib and Chatila (1995) introduced a potential field approach for sensor-based motion control for mobile robots. An attractive potential function having a quadratic behaviour at the goal neighbourhood and an asymptotic linear behaviour away from it was proposed. Chengqing et al. (2000) proposed a potential field based navigation algorithm in conjunction with virtual obstacle concept for overcoming the local minima. The algorithm was implemented for maneuver of a fast moving cylindrical mobile robot in unstructured environments. Koren and Borenstein (1991) presented a systematic and a critical discussion on the inherent problems of APF for mobile

robots, which includes trap situations due to local minima (cyclic behaviour), no passage between closely spaced obstacles, oscillations in the presence of obstacles, and oscillations in narrow passages. Kirkpatrick et al. (1983) first proposed simulated annealing, as a method for solving combinatorial optimization problems. Park et al. (2001) presented an artificial potential-field approach based on simulated annealing for local and global path planning of mobile robots.

The APF method has a wide range of space applications, like path-constrained proximity manoeuvres, large-angle attitude slew manoeuvres, autonomous rendezvous and docking, self assembly and on-orbit servicing, and spacecraft formation and station keeping. The application of APF for autonomous navigation of single spacecraft and reconfiguration of a swarm of spacecraft has not received wide attention. An artificial potential field based approach for autonomous satellite navigation was proposed by McInnes (1995) and self-assembly in space was proposed by McQuade (1997). Kong (2002) considered the operation of multi-spacecraft systems in three different potential fields such that spacecraft formation can be held with as little effort as possible. The first potential field considered is the Earth's gravitational field. The second potential field considered is based on the operation of a multi-spacecraft interferometer operating in a gravity-free environment. The third potential field exploited in his work is the self-induced electromagnetic field within which the terrestrial planet finder interferometer operates. This approach has proved less computationally burdensome for real-time implementation. Moreover, due to the ease with which state-space path constraints are included, complex manoeuvres can be undertaken with simple control laws. However, the major inherent drawback is the existence of local minima that differ from the desired configuration. Park et al. (2001) has proposed a method to avoid local minima using simulated annealing for local and global path planning of mobile robots. For space-related applications, the swarm of satellites will fail to attain the final target configuration if it is trapped in an undesirable local minimum.

2.5 CONTINUOUS-TIME SLIDING MODE CONTROL

Variable structure control with a sliding mode was first described by Soviet authors including Emel'yanov *et al*. (1964), Utkin (1971) and Itkis (1976). A survey paper by Utkin (1977) references many of the early contributions available in translation. Since then significant interest on variable structure systems and sliding mode control has been generated in the control community worldwide. Numerous theoretical advances and practical applications have been reported in literature (Heck and Ferri, 1989; Hung et al., 1993; Young et al., 1999; Chakravarthini et al., 2002) to list a few. In the early stage of its development, the plant considered was a linear second order system modelled in the phase variable form [2]. Since then, the initial expectations of such systems have been re-evaluated, their real potential has been revealed, new research directions have originated due to the appearance of a new class

of control problems, new mathematical methods, recent advances in switching circuitry, and new control principles. Today SMC is used as a general design method and is being examined for a wide spectrum of systems including nonlinear systems, multi-input/multi-output systems, discrete-time models, large scale and infinite-dimensional systems and stochastic systems. One of the most interesting aspects of sliding mode is the discontinuous nature of control action. The primary function of each of the non-linear feedback channels is to switch between two distinctively different system structures so that a new type of motion called *Sliding Mode* exists in a manifold (Young et al., 1999). A SMC system may be regarded as a combination of subsystems, each with fixed structure and each operating in a specified region of the state space. The sliding mode control design problem is to select the parameters of each of the structures and to define the switching logic [1]. Utkin suggested partitioning of the state-space of an *m*-input system into 2^m regions and associating each with a linear control having a particular state feedback gain. The control law is then piecewise linear state feedback, with gains that switch at the *m* hypersurfaces, partitioning the state space. While it is possible for each hypersurface to be a sliding surface, their intersection is the sliding surface of predominant interest. Thus the SMC problem is to choose the 2^m state feedback gains and the *m* linear switching surfaces such that a stable sliding mode is obtained on this intersection [73]. It can be shown that a system having *m* inputs can have *m* switching functions and up to 2^m -1 sliding surfaces. Though this introduces additional complexity, it is possible to combine the useful properties of each of the structures. Also a SMC would then possess new properties not present in any of the subsystems used. For e.g., an asymptotically stable system may consist of two structures neither of which is asymptotically stable (Utkin 1977). SMC results in superb system performance which is robust against parameter variations and complete rejection of disturbance which affects the system behavior adversely. The motion of a SMC system includes two phases; the reaching phase and the sliding phase. During the reaching phase, the system state is pushed toward the switching surfaces. During this period, however, the tracking error cannot be controlled directly and the system response is sensitive to parameter uncertainties and noise. Thus, one would ideally like to shorten the duration or even eliminate the reaching phase. One easy way to minimize the reaching phase and hence the reaching time is to employ a larger control input. This, however, may cause extreme system sensitivity to unmodelled dynamics, actuator saturation and undesirably higher chattering as well. The robustness can be improved by shortening the reaching phase or may be guaranteed during whole intervals of control action by eliminating the reaching phase (Choi et al., 1993; Chang and Hurmuzlu, 1993). These approaches reformulate the sliding domain equation so that the initial state of the system resides on the modified sliding domain. When this is achieved, and since the system state never leaves the sliding domain, the reaching phase is eliminated from the motion of the resulting system. Variable structure control systems are high speed switching feedback control systems

which are known to be insensitive to matched uncertainties (Drazenovic, 1969). However, unmatched uncertainties in physical systems may be present and may destroy the stability of the sliding mode. In other words, if the invariance condition (matching condition) is not satisfied, unmatched uncertainties will enter into the dynamics of the system in the sliding mode. Thus the system behaviour in the sliding mode is not invariant to unmatched uncertainties. In VSS design, several important issues should be discussed. The important tasks are reduced-order property, invariance property and to reduce the very high frequency of switching points. Thus the only obstacle for sliding mode to become one of the most significant discoveries in modern control theory is the high frequency switching which results in chattering phenomenon. One of the causes for the chattering phenomenon is the presence of finite time delays for control computation. In the absence of switching delays, the switching device switches ideally at an infinite frequency. The second cause is the limitations of physical actuators and sensors, which are often neglected. These parasitic dynamics in series with the plant causes a small amplitude high-frequency non-decaying oscillations to appear in the neighborhood of the sliding manifold (Hung et al., 1993). These oscillations are referred to as chattering. They also serve to excite the unmodelled high frequency dynamics of the system. These oscillations are not preferable from practical point of view because it results in low control accuracy, high heat losses in electrical power circuits and high wear of moving mechanical parts. Thus the controller with a high switching frequency will cause fatigue of plant and reduce the service life of a machine. One approach to reduce chattering is to replace the relay control by a saturating continuous approximation or hyperbolic tangent (Young et al., 1999).

3. FUNDAMENTALS

3.1 PLASMA INTERACTION AND COULOMB SPACECRAFT CHARGING

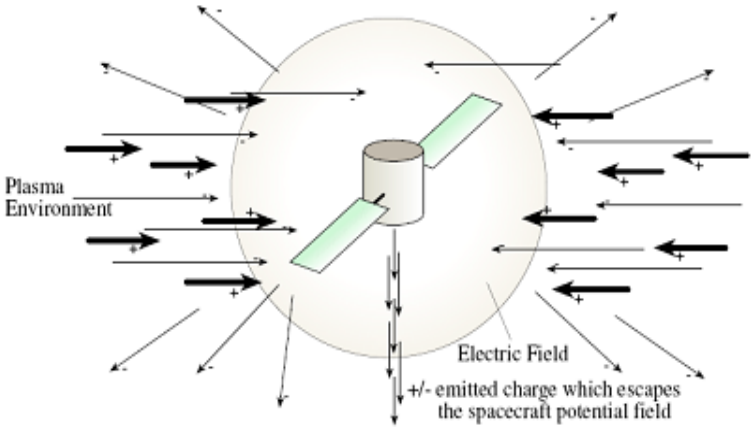

Figure 1 Simple Illustration of the spacecraft charging in a plasma environment

An isolated spacecraft will assume equilibrium potential (voltage) such that the net environmental current due to plasma and photoelectron emission is zero. It is possible to change this passive equilibrium potential by actively emitting electrical current from the spacecraft as illustrated in Figure 1 (reprinted from Ref. Schaub et al, 2003). By controlling the net charge of the spacecraft, Coulomb forces can be generated to keep the formation near a desired configuration. It has been estimated that Coulomb forces of the order of 10-1000 μN can be produced on short timescales with less than 1 Watt of on board power which is comparable with that produced by conventional electric thrusters (Garrett and Whittlesey, 2000). The natural distributed charge that would occur during worst case plasma conditions at GEO could result in torques as large as 0.1 μNm at 10 meter separation distance. Analogous torques occur due to the Lorentz force, which arises from the charged body's velocity relative to an external magnetic field (such as the earth's magnetosphere). The plasma environment around Earth has a large effect on Coulomb force. First, interactions with plasma tend to drive the charge of a spacecraft to a particular value, requiring a constant power input to maintain a desired potential. The second main effect of the plasma environment is Debye shielding. A positively charged particle in a plasma will be surrounded by negatively charged particles. Outside a certain distance, called the Debye length, the system of the positively charged particle and the sheath of negative ions or electrons surrounding it will appear to be a charge neutral system. Thus, for Coulomb effects to be experienced among spacecraft, they must be closer to each other than the Debye length of the surrounding plasma. Formation flying on the order of tens of meters is very difficult using conventional ion propulsion methods, because the exhaust plumes can interfere with on-board sensors and payload elements (such as optical instruments). Using Coulomb forces would allow the relative motion of satellites to be controlled without such contaminations (Schaub et al., 2003). Let the Coulomb formation consist of N satellites of different mass m_i. A vector r_i will denote a satellite position vector relative to the inertial center of Earth point. The Coulomb force magnitude between two satellites (assumed spheres) with charges q_i and q_j in such a plasma field is given by

$$F_{ij} = k_c \frac{q_i q_j}{r_{ji}^2} \; e^{\frac{-r_{ji}}{\lambda_d}} \tag{1}$$

where, r_{ji} is the satellite separation, λ_d is the Debye length and $k_c = (4\pi\varepsilon_0)^{-1} = 8.99 \times 10^9$ Nm^2/C^2 is a constant of proportionality that depends on the permittivity of free space, ε_0. Consider a close formation with N satellites. Then the electric field E_i experienced by the i^{th} satellite having charge q_i is given by (Schaub et al. 2003)

$$E_i = k_c \sum_{j=1}^{N} q_j \frac{r_{ji}}{|r_{ji}|^3} e^{-\frac{|r_{ji}|}{\lambda_d}} \tag{2}$$

where, $i \neq j$ and $r_{ji} = r_i - r_j$ is the relative position vector. The Coulomb force experienced by i^{th} satellite is $F_i = q_i E_i$. Assuming a standard inverse square gravitational attraction and infinite λ_d, the full nonlinear inertial equations of motion of the i^{th} spacecraft is

$$\ddot{r}_i + \frac{\mu}{r_i^3} r_i = \frac{1}{m_i} \sum_{j=1}^{N} f_{ij}, i \neq j \tag{3}$$

Figure 2 shows a conceptual plasma sheath and a numerical example computed by NASA's Charging Analyzer Program (NASCAP). NASCAP computes an eccentric sheath, which is caused by the spacecraft travelling at orbital velocity, compressing the sheath forward of the spacecraft and elongating it aft. The plasma environment contributes to CSF dynamics in subtle ways. First, as has been observed in earlier CSF work, a conductive plasma sheath forms around a charged spacecraft. The sheath's polarity is opposite that of the spacecraft. In fact, the total charge in the sheath is roughly equal to the total charge on the spacecraft but is of opposite sign. The shape of the sheath is such that it follows the surface of the spacecraft at short distances from the spacecraft. In the far field, the shape approaches a sphere.

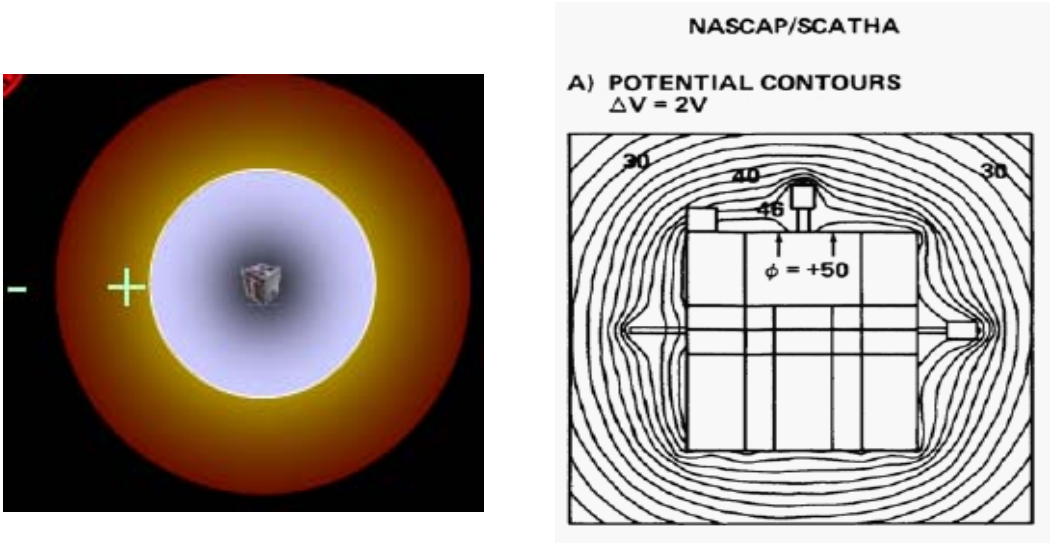

Figure 2 Conceptual Plasma Sheath (left) and NASCAP analysis of potential in SCATHA plasma sheath

This sheath's thickness is on the scale of the Debye length, the scale of Coulomb interactions in a plasma. More precisely, a test charge at some distance *r* from the center of a spherical charged body of radius s_1 feels a force $\boldsymbol{F}_{test}$ that resembles the familiar Coulomb effect but with a

more precipitous drop-off due to the sheath's exponential attenuation of the spacecraft's electrical field beyond simply the $1/r^2$ dependency:

$$\boldsymbol{F}_{test} = k\frac{q_1 q_{test}}{r^2} e^{-\frac{r-s_1}{\lambda_1}} \hat{\boldsymbol{r}}, \tag{4}$$

where $k=(4\pi\varepsilon_0)^{-1}$ is a constant of proportionality that depends on the permittivity of free space, ε_0; q_1 is the charge on the spacecraft, q_{test} is the test charge, λ_1 is the length scale of Coulomb interactions (possibly the Debye length) in this sheath, and $\hat{\boldsymbol{r}}$ is a unit vector extending from the test charge to the nearest point on the surface. A few such lengths away from the charged surface, the electric field has been almost entirely canceled by the oppositely charged sheath.

This model is not quite appropriate for two charged spacecraft, i.e. bodies of finite physical extent, because it neglects the important shielding from the second body's sheath. We account for this effect by incorporating the second spacecraft's sheath in the force acting on this second spacecraft as follows:

$$\boldsymbol{F}_{1-2} = k\frac{q_1 q_2}{r^2} e^{-\frac{r-s_1}{\lambda_1}} e^{-\frac{r-s_2}{\lambda_2}} \hat{\boldsymbol{r}},$$

or

$$\boldsymbol{F}_{1-2} = k\frac{q_1 q_2}{r^2} e^{-\left(\frac{r-s_1}{\lambda_1}+\frac{r-s_2}{\lambda_2}\right)} \hat{\boldsymbol{r}} \tag{5}$$

where, q_2 is the charge on the second spacecraft, λ_2 is the length scale the second sheath, and s_2 is the second spacecraft's radius. Naturally, this result assumes that one spacecraft is never inside the other. Figure 3 is a diagram of two such spacecraft. Refer (Friedman and Kennedy, 2004) for definitions of the fundamentals. Experts have different views about the suitability of Equation (5) when compared to Equation (1). Discussions with the plasma experts such as L. Brad King at Michigan Tech., Mason Peck at Cornell and H. Schaub reveal that this is a still open issue in the space community (personal communication, September 6, 2006). This analysis is included in this report to draw the reader's attention to both of these concepts. However, we use the conventional definition of Coulomb force in Equation (1) for our analysis throughout this report.

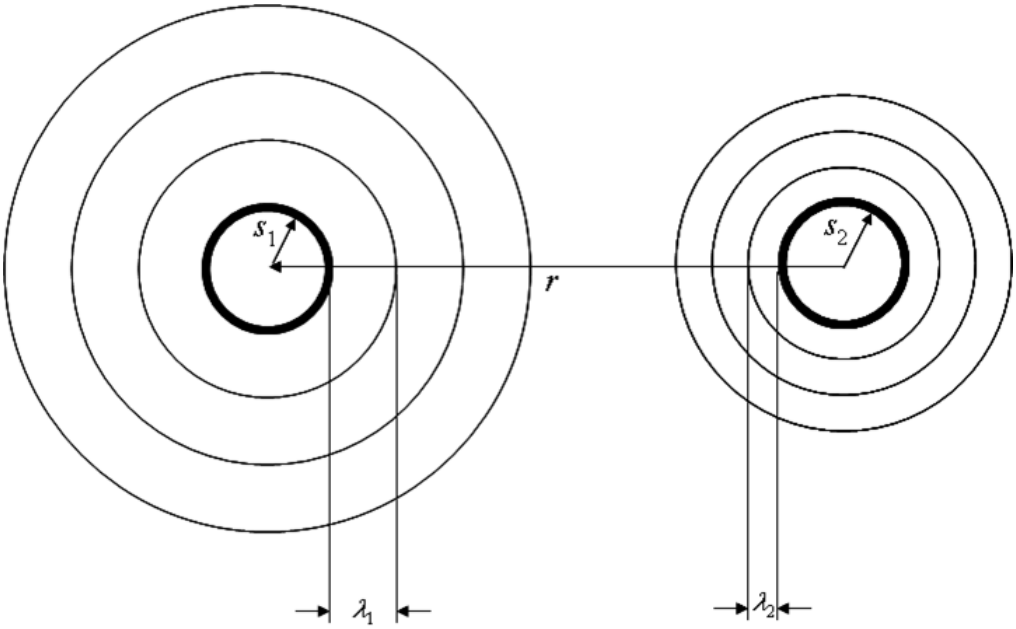

Figure 3 Math model for two charged spacecraft

Even this representation has its flaws. One is that as the spacecraft approach one another, the sheaths merge and cannot be represented as simple spheres. That level of precision deserves attention, but doing so requires a degree of subtlety that is beyond the scope of this description. One often encounters the Debye length as a parameter that characterizes Coulomb interactions in a plasma. It is given by

$$\lambda_{De} = \sqrt{\frac{\varepsilon_0}{n_{e0} e^2 \left(1/T_e + 1/T_i\right)}} \tag{6}$$

where e e is the electron charge 1.602×10^{-19} C, n_{e0} is the quasi-neutral plasma concentration for electrons and ions as explained in Fridman and Kennedy, and we assume a Boltzmann distribution for electrons (temperature T_e) and ions (temperature T_i). This result derives from a linearization that assumes the potential at the spacecraft surface (in Volts) is less than the electron temperature (in eV). In LEO the electron temperature is about 0.1 eV, implying that even a few Volts of potential violates these assumption for LEO spacecraft. If the situation is otherwise, which is quite likely in the case of CSF or Lorentz-force control, this simple result cannot be used. Instead, numerical integration of the Poisson equations describing the charge distribution is necessary. The effect of higher potential is to thicken the sheath (i.e. increase λ). So, referring to λ as the Debye length, which is defined via that linearization, can be misleading. A thicker sheath can benefit a CSF because thicker sheaths attenuate the electric field more slowly with distance, allowing larger-scale formations to be realized. The thickening with voltage also complicates the control, since the force is an implicit function of the potentials V_1 and V_2 on the two spacecraft of interest:

$$\boldsymbol{F}_{12} = k\frac{q_1 q_2}{r^2} e^{-\left(\frac{r-s_1}{\lambda_1(V_1)}+\frac{r-s_2}{\lambda_2(V_2)}\right)}\hat{\boldsymbol{r}},$$

Another subtlety is the fact that the spacecraft's velocity relative to the plasma, ***v***, deforms what would have been a spherical sheath in the case of a stationary body. The sheath on the windward side is compressed, and the sheath on the leeward side is stretched out, similar to the shape of the earth's magnetosphere as it encounters the solar wind. Figure 4 shows a numerical solution for the sheath on such a spacecraft. In GEO, this phenomenon vanishes because the spacecraft travels with the plasma. A final issue to be considered in any CSF implementation is the power required to maintain this charge. Without the plasma, the matter would be trivial: the charge on the spacecraft would be limited only by the work function of the surface material. When the Coulomb repulsion of a particle from the surface exceeds the limit imposed by the material, no more charge can be held. This limit might be about 1 MV for typical materials. However, plasma particles are highly mobile and have no trouble falling toward the spacecraft surface, tending to drive the surface to the plasma floating potential (a few Volts, depending on the environment). To estimate the power required for maintaining a charge, one has only to consider the cross-sectional area of the spacecraft-and-sheath system as it travels through the plasma. Particles that encounter this area likely impact the surface of the spacecraft by way of the plasma sheath. So, the sheath size, and indirectly the spacecraft potential, determine the rate of change in the charge (i.e. the current) to the spacecraft.

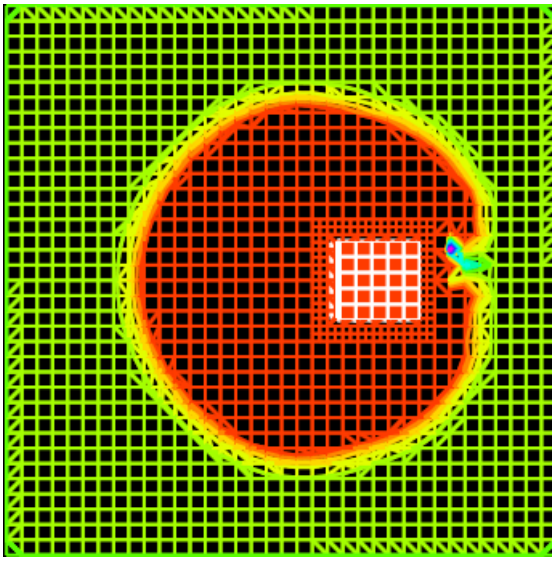

Figure 4 NASCAP solution for the sheath around a 1 kV, cube-shaped spacecraft (2.5 m on a side) in LEO

This cross-sectional area in the direction of the spacecraft velocity (A_v) determines the plasma current to the spacecraft *I* by the following approximation:

$$I(V) = A_v(V)\left(i_e + i_i\right),$$

where i_e is the electron current, and i_i is the ion current (likely atomic oxygen in LEO). In LEO, i_e is about -6×10^{-4} A/m^2, and i_i is about 3.5×10^{-6} A/m^2. Again, the area's dependence on the voltage is not a simple function, but rather one that has to be computed numerically and probably implemented in a sort of curve fit or look-up table for real-time control. If the spacecraft is to maintain its potential by emitting ions or electrons via a high-energy beam, it must do so at this level of current but with a beam energy equal to the potential of interest. This principle, that the spacecraft charges to the beam energy, has been demonstrated in numerous spacecraft-charging experiments. For example, a beam consisting of 5 MeV electrons ought to be able to charge a spacecraft to 5 MV as long as the beam current is at least equal to the plasma current. Estimating the power used is further complicated by the fact that the capacitance of a body, modeled as a sphere, increases in the presence of the plasma sheath. Specifically, the capacitance *C* for the spacecraft is given by the solution for two concentric, oppositely charged spheres, one of which represents the spacecraft surface and the other of which represents the surrounding plasma sheath:

$$C = 4\pi\varepsilon_0 \frac{s\left(s + 3\lambda\right)}{3\lambda},$$

where 3λ is taken to approximate the sheath thickness for purposes of computing the capacitance. However, as we have argued, the sheath thickness depends on the potential. So,

$$C\left(V\right) = 4\pi\varepsilon_0 \frac{s\left(s + 3\lambda\left(V\right)\right)}{3\lambda\left(V\right)}.$$

Therefore, the charge on the spacecraft is

$$q = VC\left(V\right),$$

and the power is

$$P = I\left(V\right)V.$$

Solving this system of equations involves numerical evaluation of the electrodynamics, coupled with a model of the plant and compensation dynamics, in an iterative manner. Other issues, such as the order-of-magnitude variability in the plasma environment due to solar activity may suggest that adaptive control is the only feasible approach for a real-time implementation.

3.2 LORENTZ FORCE AND LAO CONCEPT

A charged particle moving relative to Earth's magnetic field accelerates in a direction perpendicular to its velocity and the magnetic field due to the Lorentz force. The Lorentz force $\boldsymbol{F}_{\mathrm{L}}$ experienced by a particle that carries an electrical charge q with a velocity v relative to a magnetic field $\boldsymbol{B}$ is given by $\boldsymbol{F}_{\mathrm{L}} = \mathrm{q}v \times \boldsymbol{B}$. Figure 5 shows a particular implementation of this concept. In this scenario, a spherical self-capacitor holds electrical charge at some potential relative to the surrounding plasma. As the spacecraft travels at some velocity relative to the magnetic field, the Lorentz force it feels accelerates it, ultimately toward earth escape. The details are subtle and include important effects due to the rotating earth and interactions with the plasma environment. The Lorentz force is experienced individually by any charged spacecraft, and is not the result of an interaction between two charged vehicles, as is the case for the Coulomb force. The Lorentz force is due to the spacecraft's velocity with respect to the Earth's magnetic field, which rotates with the Earth. Note that the direction and magnitude of the Lorentz force is determined by the satellite's orbital geometry and current position. The direction of the force is also always perpendicular to the craft's velocity in a non-inertial earth-referenced frame. Depending on the orbit geometry of a formation, Debye shielding and the geomagnetic field cause Coulomb and Lorentz effects to vary in importance. Table 1 provides a summary.

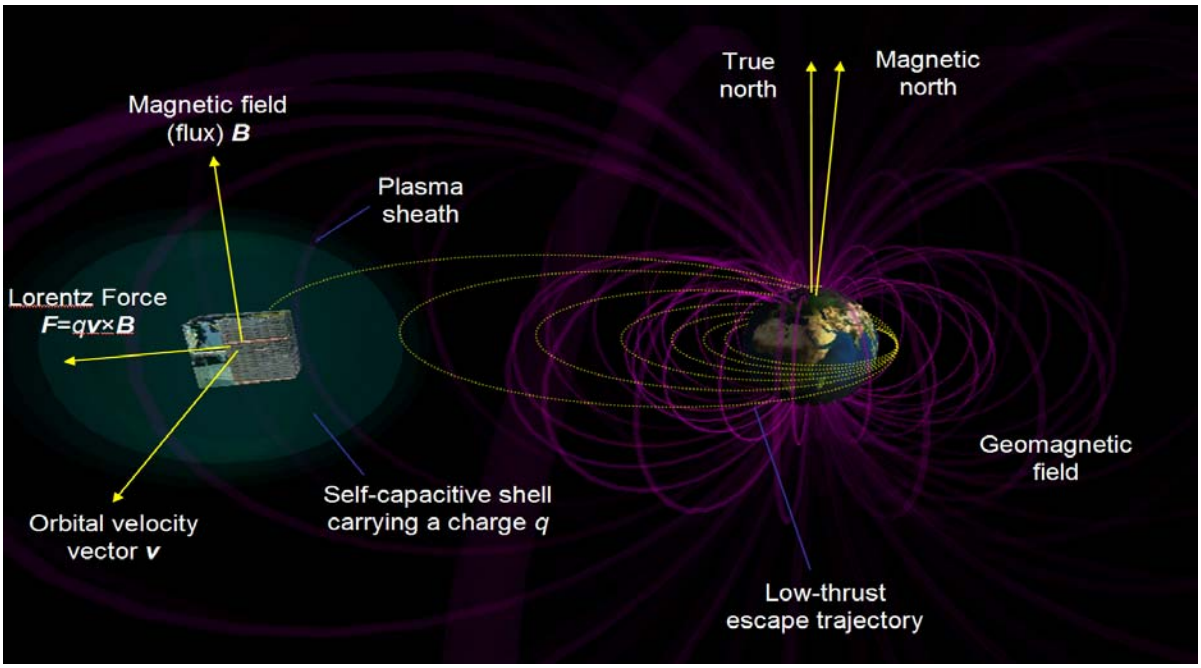

Figure 5 LAO concept realized as a spacecraft with a capacitive Faraday-cage shell providing Lorentz force for Earth escape.

In LEO the Debye length is small, and orbital speed are much larger than the speed of the magnetic field; so, Coulomb effects are dominated by Lorentz effects. In fact, the Debye shield improves the performance of a Lorentz-capable spacecraft, because it increases the capacitance of the body, allowing more charge to be stored on a given area. Near GEO, the Debye length is much larger and the spacecraft's velocity relative to the magnetic field approaches zero, so Coulomb effects dominate. Figure 6 (reprinted from Ref. Peck, 2005) depicts the LAO spacecraft concept. In this architecture, a conductive sphere (serving as a Faraday cage) surrounds most of the spacecraft and maintains a high electric charge. Lorentz-force propulsion does not involve the use of electrodynamic tethers, although the physics is related. In the case of a tether, the current flowing through a long conductor induces a magnetic field that interacts with the planet's magnetic field to produce a force on the tether. Electrons travel through the tether at low speed but at as high a current as possible. For an LAO, the spacecraft may be very compact. The charge it carries travels at perhaps thousands of meters per second relative to the magnetic field, and this moving charge represents the current that results in a force similar to what a tether experiences. Furthermore, an LAO does not work though electrostatic levitation. That is, an LAO does not take advantage of Coulomb forces that act on the charged spacecraft. Formations of LAO-capable spacecraft are not designed to interact through Coulomb attraction or repulsion.

	LEO	**GEO**
Debye Length	O(1cm)	O(10m)
Ratio of circular speed to speed of magnetic field	High	Near 1
Coulomb Force	Near zero	High
Lorentz Force	High	Near zero

Table 1. Effect of orbit height on relative importance of Lorentz and Coulomb effects.

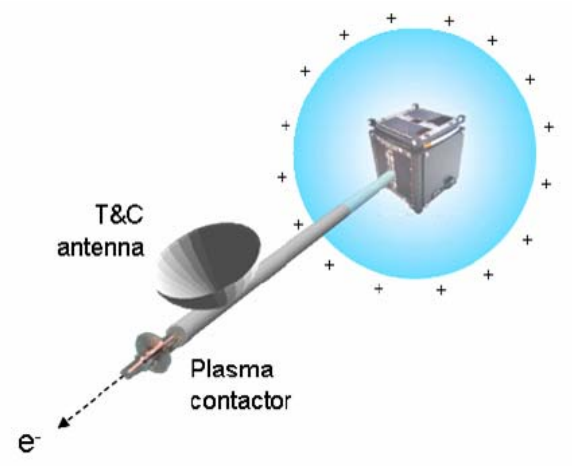

Figure 6 LAO Spacecraft Concept: Spherical Faraday Cage and Electron Beam

Both Coulomb and Lorentz forces can significantly alter the orbits of charged spacecraft. However no studies of Coulomb formations to date include the effects of the Lorentz force. If the formation is operated significantly away form GEO or in an elliptical orbit, Lorentz effects may cause significant undesirable results in formation keeping, especially if the Coulomb control strategy calls for spacecraft of both positive and negative charges, as these will be driven in opposite directions. Augmented with the Lorentz Force, Newton's law of gravitation for a particle of mass *m* moving in the r^{-2} gravitational field of a fixed point mass *M* becomes

$$m\frac{{}^{N}d^{2}}{dt^{2}}\boldsymbol{r} = -m\frac{\mu}{r^{2}}\hat{\boldsymbol{r}} + q\left(\frac{{}^{N}d}{dt}\boldsymbol{r} - \boldsymbol{\omega}_{e}\times\boldsymbol{r}\right)\times\boldsymbol{B}, \tag{7}$$

where the superscript N indicates a derivative taken with respect to a Newtonian, or inertial, frame, $\boldsymbol{r}$ is the vector position (magnitude *r* and direction $\hat{\boldsymbol{r}}$) of the particle relative to the system barycenter, $\mu = MG$ where *G* is the universal gravitational constant, *q* is the electric charge on the particle, $\boldsymbol{\omega}_{e}$ is the earth's angular velocity vector (hereafter taken to be constant in *N*), and *B* is the magnetic field vector. This expression acknowledges that it is the particle's velocity relative to the magnetic field $\boldsymbol{v} = \frac{{}^{N}d}{dt}\boldsymbol{r} - \boldsymbol{\omega}_{e}\times\boldsymbol{r}$ that determines the Lorentz force. In the simplest model, the earth's magnetic field rotates with the earth. By relativity, this time-varying magnetic field represents an electric field, which is the means by which work can be done on the Lorentz-augmented orbit.

In a frame E that rotates with the earth, the equation of motion in terms of the relative velocity $\boldsymbol{v} = \frac{{}^{E}d}{dt}\boldsymbol{r}$ and a gravitational potential Φ_{gr} is

$$\frac{{}^{E}d}{dt}\boldsymbol{v} = -\nabla\Phi_{gr} + \frac{q}{m}\boldsymbol{v}\times\boldsymbol{B} - 2\boldsymbol{\omega}_{e}\times\boldsymbol{v} - 2\boldsymbol{\omega}_{e}\times\left(\boldsymbol{\omega}_{e}\times\boldsymbol{r}\right), \tag{8}$$

where dividing through by *m* introduces the commonly used charge per mass $\frac{q}{m}$ as a parameter that determines the scale of the Lorentz force. Following Schaffer and Burns (1994), we project this equation onto $\boldsymbol{v}$

$$\frac{{}^{E}d}{dt}\boldsymbol{v}\cdot\boldsymbol{v} = \frac{1}{2}\frac{d}{dt}v^{2} = -\nabla\Phi_{gr}\cdot\frac{{}^{E}d}{dt}\boldsymbol{r} + \frac{d}{dt}\left(\frac{1}{2}r^{2}\omega_{e}^{2}\sin^{2}\theta\right), \tag{9}$$

where θ is a coordinate of a spherical coordinate system (r,θ,Φ) with origin at the planet's center and associated with an E-fixed basis. Integrating between arbitrary t_1 and t_2 shows that the total mechanical energy in the rotating frame *H* is constant:

$$H(t_2) - H(t_1) = 0\,, \tag{10}$$

Schaffer and Burns point out that this function is the appropriate Hamiltonian in the noncanonical variables ($\boldsymbol{r}$, $\boldsymbol{p} = m\dot{\boldsymbol{r}}$) as demonstrated by Littlejohn (1982; 1979), who used these coordinates in a perturbation theory for highly charged particles in slowly varying electromagnetic fields. The fact that this constant Hamiltonian exists in a rotating frame suggests that only the rotation of the magnetic field, which causes the co-rotational electrical field, can do work in the inertial frame. A propellant-based system for orbit control can deliver only finite ∇V. By contrast, devices like electrodynamic tethers, solar sails, and LAO capable spacecraft offer the prospect of indefinite thrust, all at some cost (such as technical risk, operational schedule, and development budget). The radial force applied to a satellite in a circular Lorentz-augmented orbit alters the spacecraft's potential energy—not by much, but enough to establish a formation of spacecraft with different altitudes and identical orbit angular rate ω. Using the earlier inverse-cube model for $\boldsymbol{B}$ we find that circular orbits of a given period can be achieved at radii

$$r = \sqrt[3]{\frac{1}{\omega^2}\left(\mu - \frac{q}{m}(\omega - \omega_e)B_0 r_0^3\right)}\,. \tag{11}$$

Figure 7 shows the radial distance between two satellites in equatorial circular orbits, one with 0.001 C/kg charge, and one with no electrical potential. The curve goes through 0 at geostationary altitude because, as explained above, at that height the spacecraft exhibits no velocity relative to the rotating magnetic field (and therefore experiences no Lorentz force). Absent perturbations, this formation is in equilibrium and requires no propellant for stationkeeping.

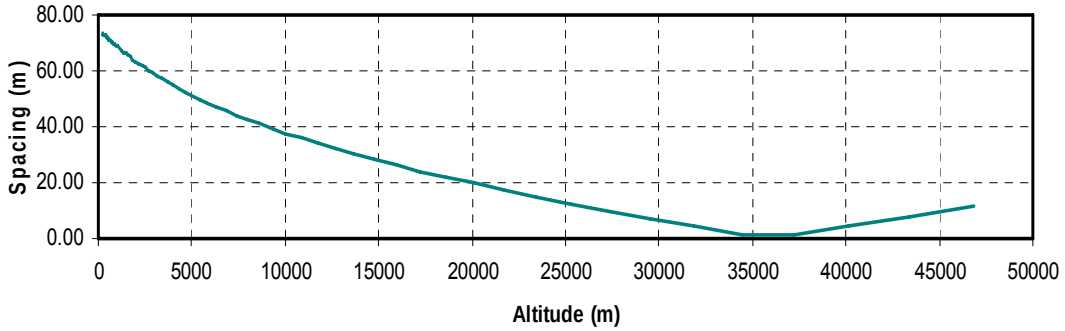

Figure 7 Vertical Spacing for Circular Prograde Orbits: q/m=0.001

Numerous formations can be achieved with such a capability: for example, a string-of-pearls style constellation in which the satellites form a straight line across the circular orbit. Rotating formations (based on modified Clohessy-Wiltshire equations) may be able to form a paraboloid

arrangement of spacecraft for sparse optical observation of terrestrial or astronomical targets. Augmenting the Lorentz effect with Coulomb forces is probably unqorkable at low altitudes where, again, the Debye sheath interferes with the propagation of the electric field. However, at intermediate or higher altitudes, the pairing of these effects can offer significant advantages by saving propellant in satellite swarms. For a practical electromagnetic formation control system to be designed a model needs to be developed that takes into account both Coulomb and Lorentz effects on charged spacecraft. We propose to study the best way to devise a novel formation-control strategy that takes advantage of both Coulomb forces and Lorentz forces. We propose to evaluate applications of Coulomb forces and Lorentz forces that will illustrate its value as a low-thrust propulsion concept for satellite swarms. The LAO concept offers propellant-less orbital maneuvers in a variety of applications. The mass savings alone represent a watershed opportunity in the design of space-system architectures. Some applications are summarized in Figure 8. They are categorized roughly by the technology readiness of the technologies that enable them. Because the Lorentz force is proportional to the charge, maximizing *q/m* is a natural goal. However, the rate at which this charge is lost to the environment determines the power required to keep the spacecraft charged, and the susceptibility of a design to discharge is therefore also of interest. It is important to distinguish between the concept of a body with potential *V* relative to the plasma and the concept of charge as applied to a capacitor. The capacitance *C* of an LAO spacecraft is clearly of relevance: the charge *q* it carries goes with *q*=*CV*. However, the capacitance one commonly encounters in electrical engineering is the result of energy storage via two oppositely-charged surfaces. A capacitor of this type, one which contains both positive and negative charge, does not experience a net Lorentz force (although individual components of it may). Very high-capacitance, low-mass devices like Maxwell Technologies' Boostcap Ultracapacitors offer over 2000 C at 2.5V for 0.5 kg (Maxwell.com, 2005), but these devices offer no net electrical field because the charges inside them cancel. Instead, the charge on an LAO spacecraft is likely best achieved on the surface of a conducting sphere. The sphere's shape precludes charge concentrations, which would otherwise encourage arcing and discharge into the plasma. Perhaps most important, surrounding the spacecraft with a conducting sphere establishes a Faraday cage that completely protects components in the interior from electrical discharge (because there can be no electrical field inside a conducting surface (Jackson, 1999)). This sphere has the added benefit that it may be deployed by inflation, as have other metallized space inflatables (Space.com, 2000), for a lightweight solution that is compact for launch. Practical considerations (such as communications) will require a hole in this shield, but small-enough holes do not affect the Faraday cage's ability to shield electric fields. The time constant τ for spacecraft charging is surprisingly low. In less than a second a spacecraft may reach a "floating" potential, which is maintained by interactions with the environment. This equivalent

RC circuit turns out to be the most important sizing parameter for LAO capable spacecraft. Data from the SPEAR 1 experiment helps establish the charge-decay time constant at low altitudes (200-350 km), (Rustan, 1988). Approximated as a linear decay, and with I_{beam}=0, spear data suggests τ =1.35s^{-1} for a spacecraft with V=42 kV. Maintaining this high voltage requires only 0.06 A, or 2520 W, if one assumes that the power is associated with a beam of this energy (42 keV). Thus, fast modulation of charge is not difficult and opens up the possibility of agile orbit manoeuvring. Establishing the charge on the surface of the sphere may be achieved in several ways, including ion beams and electron beams. These approaches and others will be considered in the proposed study. For a general architecture, we propose storing the charge on the surface of a sphere, from which a partly insulated plasma contactor extends. The sphere is envisioned as an inflatable structure, made of Kapton (for example), to which is bonded a transparent conductive film. Transparency allows some sunlight to enter the sphere, offering the possibility of operating a solar array within the Faraday cage. The charge built up in this fashion may be deposited on the surface of the sphere directly, through simple harness, or through a belt mechanism like that of a Van De Graaff generator (Van de Graaff, 1933). Small electrostatic generators of this familiar variety store megavolts of charge on the surface of a sphere in air for very low current. Rather than depending on a heavy AC motor, the LAO spacecraft would likely use a plasma contactor with a high-voltage electrode.

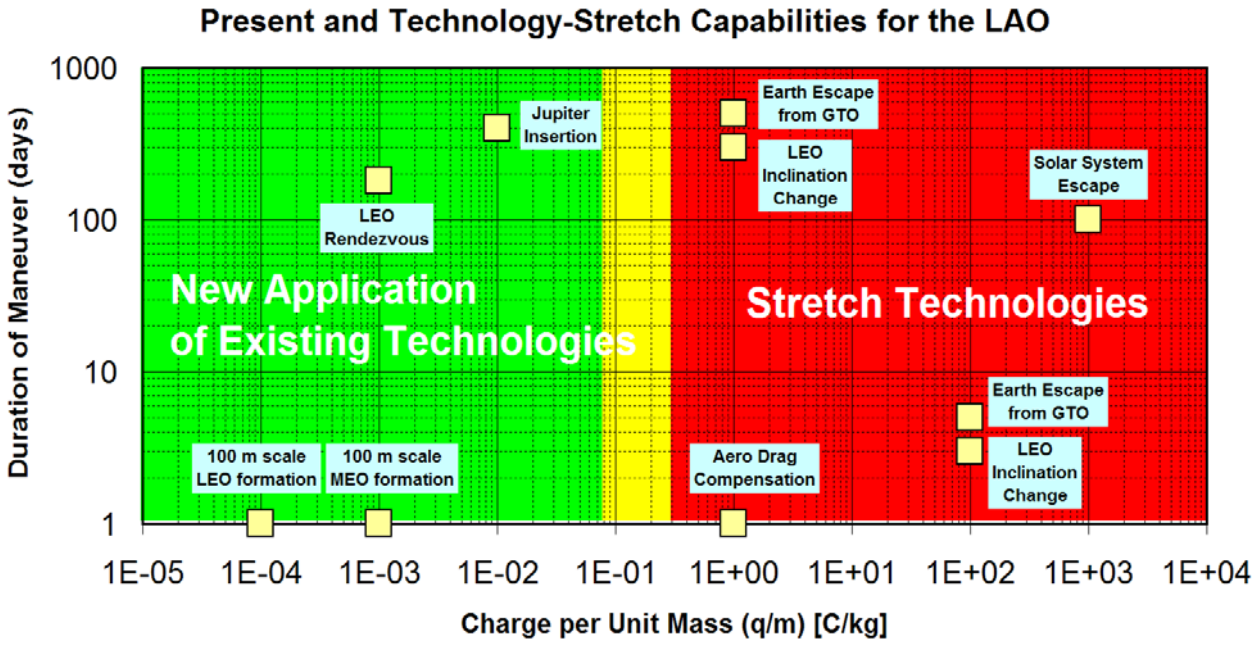

Figure 8 Capability Summary: Present Technology and Stretch Goals

3.3 PATH PLANNING USING ARTIFICIAL POTENTIAL FIELD

In artificial potential field method, the dynamic environment in which the spacecraft exists is represented by a scalar potential function, which has a minimum potential (sink) at the desired terminal state of the vehicle dynamics and has maximum potential (source) at path constraints (near-by satellites or obstacles). The source and sink fields are illustrated in Figure 9. The potential of the spacecraft swarm will be constructed by identifying each satellite in the swarm as a region of high potential. The obstacles (near-by spacecrafts) are represented by repulsive artificial and the goal position is represented by an attractive potential. A repulsive force between them, which is simply the negative gradient of the potential field, avoids collisions between the neighbouring spacecrafts. Since the rate of descent of the potential function is rendered negative definite, the potential-field approach guarantees that the spacecraft will converge to the desired terminal state without violating the defined path constraints. The convergence time depends on dissipative terms (damping) in the control law. The final formation will be achieved only if every member of the swarm is in a sink corresponding to the target configuration. An excellent description of using artificial potential field and sliding mode control for swarm aggregation and formation can be found in (Gazi 2005; Gazi and Passino 2004, 2003). Izzo and Pettazzi (2005) has also proved that sliding mode control for satellite formation control is an effective way of implementing distributed architecture based on swarm methods. Some of the results in (Gazi 2005; Gazi and Passino 2004) are repeated in the following section for convenience as we use this autonomous path planning methodology with the proposed hybrid actuation for spacecraft swarm aggregation and formation control using artificial potential field and sliding mode control.

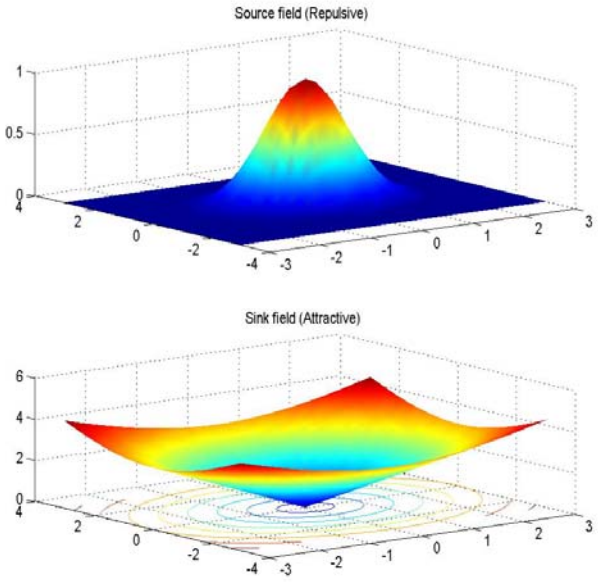

Figure 9 Example of APF source and sink field

3.3.1 THE CLASS OF ATTRACTION/REPULSION FUNCTIONS FOR SWARM MODEL

Let the swarm consists of N individual members or agents in the n dimensional Euclidean space. The position of i^{th} agent is described by $x^i \in R^n$. It is assumed that synchronous motion exists and there is no time delay, i.e. all the individuals move simultaneously and know the exact relative position of all the other individuals. In this model agents are considered as points and their dimensions are ignored. The distance moved and direction of motion of each individual depends on the net attraction and repulsion exerted by all other member in the swarm. The motion of each agent in the swarm is governed by the equation (Gazi and Passino, 2003, 2004)

$$\dot{x^i} = \sum_{j=1, j\neq i}^{N} g(x^i - x^j), i = 1, \ldots, N \tag{12}$$

where, $g(.) \in \Psi$ is an odd function which represents the sum of the function of attraction and repulsion between the agents i.e., $g(.) = g_a(.) + g_r(.)$ and Ψ is the set of all attraction/repulsion functions. The function $g_a : R^+ \to R^+$ represents (the magnitude of) the attraction term, where as $g_r : R^+ \to R^+$ represents (the magnitude of) the repulsion term. Again $g(.)$ can be represented by

$$g(y) = -y\left[g_a(\|y\|) - g_r(\|y\|)\right]$$

where $y \in R^n$ is arbitrary and $\|y\| = \sqrt{y^T y}$ is the Euclidean norm. It is assumed that on large distances attraction dominates, that on short distances repulsion dominates. Equation (12) can be represented by

$$\dot{x^i} = -\nabla_{x^i} J(x), i = 1, \ldots, N \tag{13}$$

where, $J : R^{nN} \to R$ is a potential function that represent the inter-individual interactions. Note that here the potential function $J(x)$ is not static. It depends on the relative positions of the individuals in the swarm. Therefore, uncertainties and disturbances including those acting on the system dynamics can affect the time derivative of $J(x)$. Consider potential function of the form

$$J(x) = \sum_{i=1}^{N-1} \sum_{j=i+1}^{N} J_{ij}\left(\|x^i - x^j\|\right)$$

where, $J_{ij}\left(\left\|x^i - x^j\right\|\right)$ is the potential between i and j and can be different for different pairs. Moreover, it is assumed that $J_{ij}\left(\left\|x^i - x^j\right\|\right)$ satisfies the following conditions:

A1) The potentials $J_{ij}\left(\left\|x^i - x^j\right\|\right)$ are symmetric and satisfy

$$\nabla_{x^i} J_{ij}\left(\left\|x^i - x^j\right\|\right) = -\nabla_{j^i} J_{ij}\left(\left\|x^i - x^j\right\|\right) \tag{14}$$

A2) There exist corresponding functions $J_a : R^+ \to R^+$ and $J_r : R^+ \to R^+$ such that

$$\nabla_y J_a\left(\|y\|\right) = y g_a\left(\|y\|\right) \text{ and } \nabla_y \boldsymbol{J}_r\left(\|\boldsymbol{y}\|\right) = \boldsymbol{y}\boldsymbol{g}_r\left(\|\boldsymbol{y}\|\right)$$

where, $\boldsymbol{J}_a\left(\|\boldsymbol{y}\|\right)$ the attractive potential function dominates on long distances and $\boldsymbol{J}_r\left(\|\boldsymbol{y}\|\right)$ the repulsive potential function that dominates on short distance. In other words $g_a\left(\|y\|\right)$ and $g_r\left(\|y\|\right)$ are chosen such that these conditions are satisfied. For $g_{ar}^{ij} : R^+ \to R^+$ we have $g_{ar}^{ij}\left(\|y\|\right) = g_a^{ij}\left(\|y\|\right) + g_r^{ij}\left(\|y\|\right)$. Then, the above assumption restricts the motion of the individuals toward each other along the gradient of these potentials (i.e. along the combined gradient field of these potentials).

A3) There exists unique distance δ_{ij}, at which we have $g_{ar}^{ij}\left(\left\|\delta_{ij}\right\|\right) = 0$ and $g_{ar}^{ij}\left(\|y\|\right) > 0$ for $\|y\| > \delta_{ij}$ and $g_{ar}^{ij}\left(\|y\|\right) < 0$ for $\|y\| < \delta_{ij}$. Here δ_{ij} is the unique distance at which the attraction and the repulsion balance i.e., $g_a^{ij}\left(\delta_{ij}\right) = g_r^{ij}\left(\delta_{ij}\right)$. Functions satisfying the above conditions A1-A3 result in aggregating swarm behaviour. Assuming that the motion of the individuals is given by (1) it can be shown that the following hold.

R1) The center $\bar{x} = \left(1/N\right)\sum_{i=1}^{N} x^i$ of the swarm is stationary for all time.

R2) If $J(x)$ is bounded from below. i.e., $J(x) > a$ for some finite $a \in R$, then, for any initial condition $x(0) \in R^{nN}$, as $t \to \infty$ we have $x(t) \to \Omega_e$ where $\Omega_e = \left\{x : \dot{x} = 0\right\}$.

R3) The swarm size will be bounded, and the position x^i of all the agents will converge asymptotically to a small region around its center $\bar{x}$, which is a hyperball of size ε, $B_\varepsilon\left(\bar{x}\right) = \left\{x : \left\|x - \bar{x}\right\| \le \varepsilon\right\}$. Moreover, the convergence to B_ε will occur in a finite time.

The result in (**R1**) implies that the relative motions of the individuals will balance each other and will result in a stationary center. This is expected due to the reciprocity in (3). The center of the swarm moves along the average of the gradient of the profile evaluated at the current positions of the individuals. However, this does not necessarily mean that it will converge to a minimum. Moreover, this does not imply anything about the motions of the individuals. The convergence

properties of the swarm to minimum points of the profile depends on the properties of the profile. The result in (**R2**) states that as time tends to infinity all the individuals will stop motion and the swarm will converge to a constant configuration. The size ε of the region in which the agents converge and the speed of convergence stated in (**R3**) depend on the attraction and repulsion parameters of the potential function $J(x)$. The result in (**R3**) does not say anything about where these positions will be. It is inferred that given the initial positions of the individuals $x^i(0), i = 1,\ldots,N$, the final configuration to which the individuals will converge is unique. However, it is difficult to find a direct relation between $x(0)$ and the final position $x(\infty)$. This is a shortcoming of this approach. An example of a potential function that satisfies the above assumptions is the function with linear attraction and exponential repulsion

$$\boldsymbol{g}(\boldsymbol{y}) = -\boldsymbol{y}\left(\boldsymbol{a} - \boldsymbol{b}\exp\left(-\frac{\|\boldsymbol{y}\|^2}{\boldsymbol{c}}\right)\right) \tag{15}$$

where $\boldsymbol{a}, \boldsymbol{b}$ and $\boldsymbol{c}$ are positive constants such that $\boldsymbol{b} > \boldsymbol{a}$. The constant a is in a sense the magnitude of the attraction and b is in a sense the magnitude of the repulsion and the constant $\boldsymbol{c}$ is its spread or repulsion range but the actual repulsion is some combination from effects of both. It can be observed that in Equation (15) increasing parameter a decreases the size of the bound ε where as increasing parameter or parameter c increases. By equating $y\left(a - b\exp\left(-\frac{\|y\|^2}{c}\right)\right) = 0,$ it can be seen that $g(y)$ switches sign at the set of points defined by $\Psi = \left\{ y = 0 \text{ or } \|y\| = \delta = \sqrt{\frac{c}{\ln\left(\frac{b}{a}\right)}} \right\}$. For case with $\boldsymbol{a} = 1, \boldsymbol{b} = 20$ and $\boldsymbol{c} = 0.2$ this function is shown in Figure 10 and δ =0.774 and $\varepsilon = 3.8$. The convergence to B_ε will occur in a finite time bounded by $\bar{t} = \max_{i=1,\ldots,N}\left\{-\frac{1}{2a}\ln\left(\frac{\varepsilon^2}{\left\|x^i(0) - \bar{x}(0)\right\|^2}\right)\right\}$.

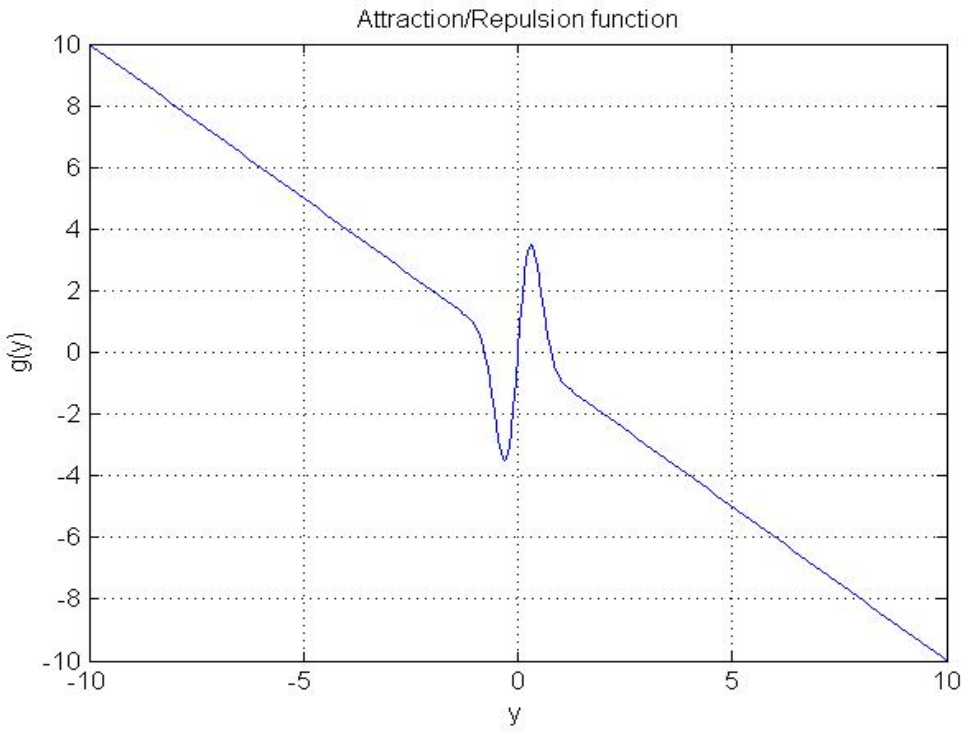

Figure 10 Plot of linear attraction and exponential repulsion type potential function

For individuals with finite body size (i.e, with mass and some private or safety area), Gazi and Passino (2004) has proposed a the 'hard-limiting' type repulsion function. The individuals are assumed to be hyperspheres in R^n. Let η be the radius of the hypersphere and x^i be the center of the hypersphere for individual i. If the individuals in the swarm are initially far apart from each other i.e., $\left\|x^i(0) - x^j(0) > 2\eta\right\|$ for all $(i, j),\ j \neq 1$, then in order for two individuals i and j not to collide we need $\left\|x^i(t) - x^j(t)\right\| > 2\eta$ for all $(i, j),\ j \neq 1$. The "hard-limiting" type repulsion function can incorporate for the body size or to create a safety area for the individuals in the swarm. It can be represented by

$$g_r\left(\left\|x^i - x^j\right\|\right) = \frac{b}{\left(\left\|x^i - x^j\right\| - 2\eta\right)^2}$$

and it satisfies the condition $\lim_{\left\|x^i - x^j\right\| \to 2\eta} g_r\left(\left\|x^i - x^j\right\|\right)\left\|x^i - x^j\right\| = \infty$. The hard-limiting repulsion will guarantee that the swarm size will scale with the number of individuals N, and therefore will result in a swarm density which is, in a sense, more uniform. In R^n, finally the individuals will be enclosed in a sphere of radius r, around the swarm center $\bar{x}$ such that $4\pi r^2 \geq N\pi\eta^2$. From

this we obtain the lower bound on the radius of the smallest sphere which can enclose all the individuals is $r_{\min} = \eta\sqrt[n]{N}$.

3.3.2 FORMATION CONTROL

The swarm model in discussed earlier can be extended for formation control problem. Consider the case in which the attraction/repulsion functions $g(.)$ are pair dependent i.e.,

$$\dot{x}_i = \sum_{j=1,\, j\neq i}^{N} g_{ij}\left(x_i - x_j\right), i = 1,\ldots,N$$

where $g_{ij}(.) \in \Psi$ for all pairs (i, j) and $g_{ij}(x_i - x_j) = g_{ji}(x_j - x_i)$. For formation control the attraction and repulsion functions and therefore the equilibrium distance δ_{ij} for different pairs of individuals can be different. The desired formation can be uniquely specified with respect to rotation and translation by the formation constraints $\left\|x_i - x_j\right\| = d_{ij}$ for all $(i, j), j \neq i$. The idea is to chose each of the attraction/repulsion functions $g_{ij}(.)$ such that $\delta_{ij} = d_{ij}$ for every pair of individuals (i, j). The generalized Lyapunov function

$$J(x) = \sum_{i=1}^{N-1} \sum_{j=i+1}^{N} \left[J_a\left(\left\|x_i - x_j\right\|\right) - J_r\left(\left\|x_i - x_j\right\|\right)\right]$$

then have its minimum at the desired formation and once the formation is achieved $\dot{x}_i = 0$ for all i.

If $J(x)$ is chosen as a formation function, which has a unique minimum at the desired formation (Egerstedt and Hu 2001), then the desired formation will be asymptotically achieved. If $J(x)$ is composed of inter-individual potentials, which hold only on certain range (Leonard and Fiorelli 2001; Olfati and Murray 2002), then (**R2**) still holds but only locally. The size ε of the region in which the agents converge and the speed of convergence stated in (R3) depend on the attraction and repulsion parameters of the potential $J(x)$.

3.3.3 SLIDING MODE CONTROL DESIGN

Sliding mode control is a powerful robust nonlinear control technique that enables separation of the overall system motion into independent partial components of lower dimensions, and as a result reducing the complexity of the control design. The aim is to design each of the control inputs such that a cohesive swarming is achieved thereby preserving the results in the previous section. To ensure this, we need to enforce satisfaction of Equation (a). In short, the control

inputs are designed such that the velocity of the agents are enforced along the negative gradient of the potential function $J(x)$. The controller design is based on the procedure developed in (Utkin et al. 1991; Guldner and Utkin 1995). Consider the swarm model (Gazi and Passino, 2005)

$$M_i(x^i)\ddot{x}^i + f_i(x^i, \dot{x}^i) = u^i, 1 \le i \le N \tag{16}$$

where $x^i \in R^n$ is the position vector of agent i, $M_i \in R^{n \times n}$ is the mass or inertia matrix, N is the number of agents in the swarm , $f_i(x^i, \dot{x}^i) \in R^n$ is the centripetal, Corriolos, gravitational effects and additive disturbances, and $\boldsymbol{u}^i \in \boldsymbol{R}^n$ represents the control inputs. It is assumed that M_i is non-singular and $\underline{M}_i \le M_i \le \overline{M}_i$ where $\underline{M}_i > 0$ and $\overline{M}_i$ are the known lower bound and upper bounds of the inertia matrix respectively. For all i the matrix $M_i(x^i)$ satisfies

$\underline{M}_i \|y\|^2 \le y^T M_i(x^i) y \le \overline{M}_i \|y\|^2$

Let

$$f_i(x^i, \dot{x}^i) = f_i^k(x^i, \dot{x}^i) + f_i^u(x^i, \dot{x}^i), 1 \le i \le N$$

where $f_i^k(.,.)$ represents the known part and $f_i^u(.,.)$ represents the unknown part and $\bar{f}_i$ are known constants for all i such that $\left\| f_i^u\left(x^i, \dot{x}^i \right) \right\| \le \bar{f}_i, 1 \le i \le N.$

In classical sliding mode control problems, the surface $s = 0$ is chosen such that on it, the tracking error asymptotically decays to zero. The design of the sliding mode surface considered by Gazi and Passino (2005) is a little different from conventional approach. In their approach, the surfaces $s^i = 0$ are chosen so that the system motion obeys certain dynamics. The major difference is that the sliding surfaces s^i's are not constant surfaces and they can move as the agents move even though $\dot{x}^i$ can be viewed as the output of the system and s^i as the output error and at $s^i = 0$ the output errors becomes zero.

The n-dimensional sliding manifold for agent i is

$$s^i = \dot{x}^i + \nabla_{x^i} J(x) = 0, i = 1, \ldots, N \tag{17}$$

Once all the agents reach their sliding manifolds $s^i = 0$ Equation (17) reduces to $\dot{x}^i = -\nabla_{x^i} J(x)$ which is same as the motion equation (a) of the agents in the swarm. A sufficient condition for sliding mode to occur is given by (Utkin 1977)

$$s^{iT}\,\dot{s}^i < 0, \forall i = 1, \ldots N \tag{18}$$

This guarantees that starting from any initial point in the state space the sliding manifold is reached asymptotically and sliding mode occur in finite time. Differentiating the sliding manifold equation (17) we obtain

$$\dot{s}^i = \ddot{x}^i + \frac{\partial}{\partial t}\left[\nabla_{x^i} J(x)\right] \tag{19}$$

From Equation (16) we get

$$\ddot{x}^i = M_i^{-1}(x^i)\left[u^i - f_i(x^i, \dot{x}^i)\right] \tag{20}$$

Substituting Equation (20) in Equation (19) and then in (18) we get the necessary conditions for occurrence of sliding mode as

$$s^{iT}\left[M_i^{-1}(x^i)u^i - M_i^{-1}(x^i)\,f_i(x^i, \dot{x}^i) + \frac{\partial}{\partial t}\left[\nabla_{x^i} J(x)\right]\right] < 0\,.$$

If the potential function $J(x)$ chosen such that $\nabla_y J(x)$ is bounded i.e., $\left\|\frac{\partial}{\partial t}\nabla_y J(x)\right\| \le \bar{J}$ for some known bound $\bar{J}$ and for all $y \in R^n$, then the control input u^i will enforce the sliding mode condition (18). The sliding mode controller enforce the occurrence of sliding mode takes the form

$$u^i = -u_o^i(x)\,sign(s^i) + f_i^k(x^i, \dot{x}^i) \tag{21}$$

where, $sign(s^i) = \left[sign(s_1^i) \quad \ldots \quad sign(s_N^i)\right]^T$. The gain of control input is chosen as

$$u_o^i > \frac{1}{\underline{M_i}}\left(\overline{M_i}\,\bar{f}_i + \bar{J} + \varepsilon^i\right),$$

for some $\varepsilon^i > 0$, it is guaranteed that $s^{iT}\,\dot{s}^i < -\varepsilon^i \left\|s^i\right\|$. In the above controller only the known part $f_i^k(x^i, \dot{x}^i)$ of the vehicle dynamics is utilized. If there are no known parts, then the controller would reduce to $u^i = -u_o^i(x)\,sign(s^i)$. Also note that the controller design does not

need the exact mass/inertia matrix $M_i(x^i)$ of the robot. It only needs the upper and lower bounds on them as is the case also with disturbances. Consider the Lyapunov function of the form

$$V_i = \frac{1}{2} s^{iT} s^i, \quad \text{(4a)}$$

Differentiating (4a) with respect to time gives $\dot{V}_i \le -\varepsilon^i \sqrt{V_i}$ and this guarantees that the sliding surface is reached in a finite time bounded by $t^i_{\max} = \frac{2V_i(0)}{\varepsilon^i}$ and sliding mode occurs on all the surfaces $s^i = 0$ in a finite time bounded by $\bar{t}_{sm} = \max_{i=1,..,N} \left\{ \frac{2V_i(0)}{\varepsilon^i} \right\}$. In order to reduce the chattering phenomenon, the $\boldsymbol{sign}(\boldsymbol{s}^i)$ term in the controller can by replaced by $\tanh(\beta \boldsymbol{s}^i)$ or the saturation function $\boldsymbol{sat}\left(\frac{\boldsymbol{s}^i}{\phi}\right)$ using the boundary layer approach. The saturation function is defined as

$$\boldsymbol{sat}\left(\frac{\boldsymbol{s}^i}{\phi}\right) = +1 \text{ if } \boldsymbol{s}^i > \phi,$$

$$= \frac{\boldsymbol{s}^i}{\phi} \text{ if } \left|\boldsymbol{s}^i\right| \le \phi,$$

$$= -1 \text{ if } \boldsymbol{s}^i < -\phi$$

A comparison shows that '$\tanh(\beta \boldsymbol{s}^i)$' and '$\boldsymbol{sat}\left(\frac{\boldsymbol{s}^i}{\phi}\right)$' can produce similar responses. A guage for the performance of the above controllers can be their rate of convergence near $\boldsymbol{s}^i = 0$. In case of $\boldsymbol{sign}(\boldsymbol{s}^i)$, this rate is infinity. Hence, the convergence occurs in finite time. In case of '$\tanh(\beta \boldsymbol{s}^i)$' and '$\boldsymbol{sat}\left(\frac{\boldsymbol{s}^i}{\phi}\right)$' the rate is finite and so they converge asymptotically. So, to get an idea of the rate we have to know which has a higher derivative near $\boldsymbol{s}^i = 0$ i.e, among $\frac{\boldsymbol{d}}{\boldsymbol{dt}}\left(\boldsymbol{sat}\left(\frac{\boldsymbol{s}^i}{\phi}\right)\right) = \frac{1}{\phi}$ at $\boldsymbol{s}^i = 0$ and $\frac{\boldsymbol{d}}{\boldsymbol{dt}}\left(\tanh\left(\beta \boldsymbol{s}^i\right)\right) = \left(1 - \tanh\left(\beta \boldsymbol{s}^i\right) \wedge 2\right)\beta$ at $\boldsymbol{s}^i = 0$. So, for different combinations of phi and gamma we get one or the other to look good. '$\tanh(\beta \boldsymbol{s}^i)$' can

be preferred to '$sat\left(\frac{s^i}{\phi}\right)$' in cases where responses are much similar. The reason is that '$\tanh(\beta s^i)$' induces a smoother control as compared to '$sat\left(\frac{s^i}{\phi}\right)$' which produces only continuous control but not continuously differentiable control. In situations where similar responses are obtained, $\tanh$ is preferred over sat. In spite of using chattering reductions in practical implementations, it may not be able to possible to ideally recover all the stability results in previous section. For example the statement (**R1)** that the center of the swarm is stationary for all time may not necessarily hold and there might be small deviations of the center. Nevertheless, it is expected that most of the results (such as swarm cohesiveness and finite time convergence) can be obtained will only small perturbations.

4. HYBRID PROPULSION USING COULOMB FORCE AND ELECTRIC PROPULSION

The objective of designing a Coulomb-actuated spacecraft is to provide maximum acceleration for limited electrical power. The goal of this section is to develop a suite of spacecraft architecture concepts that take advantage of the proposed hybrid actuation scheme, artificial potential field and sliding mode control of swarm steering. Some of the critical questions to be answered involve power, charge management, sensing, and actuation strategies. The outcome of this phase is a detailed set of trade studies that identify technological solutions as valid or invalid for swarm control via hybrid electromagnetic formation flight. In this work we aim to explore the suitability of hybrid actuation for two applications, namely satellite swarm aggregation and formation flying. Figure 11 illustrates the force experienced by a satellite in a swarm of three satellites using APF method. It is desired that the Swarm Agent 2 (SA2) move towards the final target position. Initially, SA1 exerts a repulsive force, and the target exerts an attractive force on SA 1. Then it moves to a new location in the direction of the resultant force. At this position, SA3 exerts a repulsive force and target exerts an attractive force on SA2 and it moves towards the next intermittent location. Here the target exerts the attractive force and SA2 finally moves towards its target position, thereby achieving the desired configuration. In this approach the steering direction of a particular spacecraft undergoing reconfiguration within the spacecraft swarm is determined by assuming that the other members of the constellation (obstacles) assert repulsive forces on the spacecraft and the goal (desired terminal state) asserts attractive force. Consequently, the spacecraft experiences a generalized force equal to the negative of the total potential gradient that drives the spacecraft towards the goal or the desired terminal state. In this way the APF provides a constantly active navigation, offering a

collision free trajectory for the each of the individual satellites that form part of a constellation or formation.

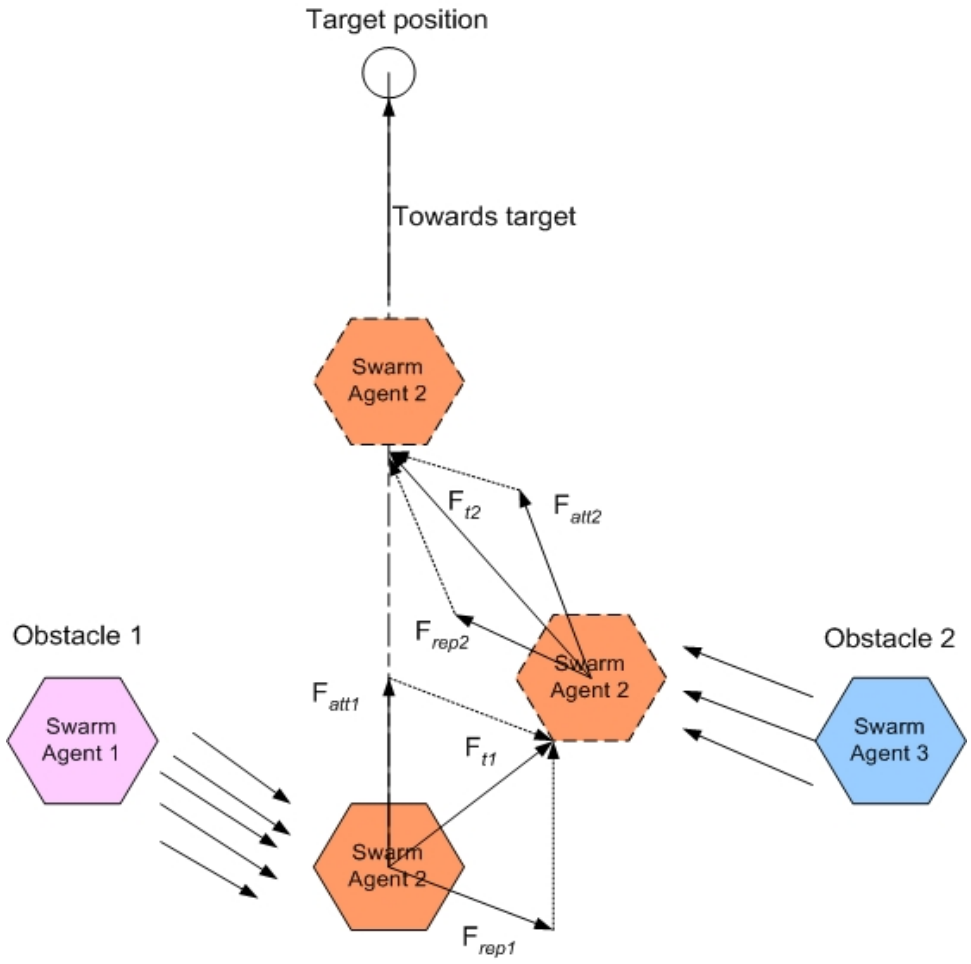

Figure 11 Schematic diagram of path planning using APF

The schematic diagram of the proposed navigation and control architecture is shown in Figure 12. It integrates various sensory signals to achieve collision-free goal oriented navigation and formation reconfiguration. The proposed sliding mode control system would integrate with hybrid actuation using electrostatic forces and electric thrusters for high Earth orbits spacecrafts. The path planning module is capable of avoiding obstacles and provides a goal-oriented navigation in an optimal time period. This approach has less computational load as compared to deliberative techniques that carry out extensive map building from raw sensory data. The proposed collision-avoidance and spacecraft-reconfiguration strategy will have all the benefits associated with the APF method along with the added advantage of utilizing Coulomb force.

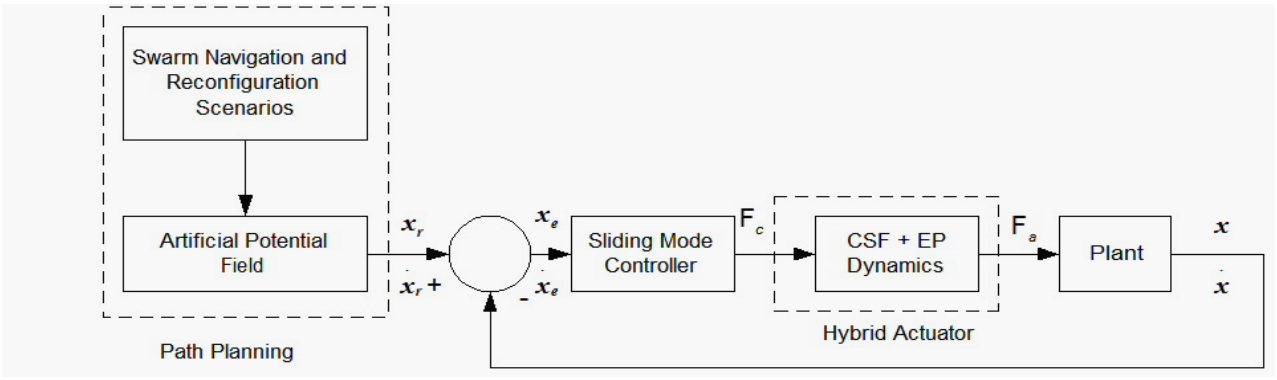

Figure 12 Schematic diagram of swarm path planning and control with hybrid actuator

4.1 COMPUTING CHARGE FROM COMMANDED FORCE (NON-LINEAR JACOBIAN)

Here we describe a method (non-linear Jacobian) to compute the charge required to achieve a desired force F_i that must act on the i^{th} spacecraft in a formation in order for its states to reach a desired target. First, we observe that F_i is the resultant of forces acting between it and each of its neighbours, according to

$$F_i = \sum_{\substack{j=1 \\ j \neq i}}^{N} k_c \frac{q_i q_j}{r_{ij}^2} e^{-\left(\frac{r_{ij}-s_i}{\lambda_i}+\frac{r_{ij}-s_j}{\lambda_j}\right)} \hat{\boldsymbol{r}}_{ij}, \tag{22}$$

which can be written as a matrix multiplication

$$\boldsymbol{F}_i = \begin{bmatrix} \hat{\boldsymbol{r}}_{i1} & \hat{\boldsymbol{r}}_{i2} & \cdots & \hat{\boldsymbol{r}}_{ij} & \cdots & \hat{\boldsymbol{r}}_{iN} \end{bmatrix} \begin{bmatrix} F_{i1} \\ F_{i2} \\ \vdots \\ F_{ij} \\ \vdots \\ F_{iN} \end{bmatrix}$$

or, for the sake of compactness,

$$\underset{3\times N}{\boldsymbol{F}_i} = \underset{3\times N}{\boldsymbol{\Gamma}_i} \underset{N\times 1}{\Phi_i}$$

Finding the resulting the scalar interbody forces $F_{ij} = \boldsymbol{F}_i \cdot \hat{\boldsymbol{r}}_{ij}$ requires merely a pseudoinverse:

$$\Phi_i = \boldsymbol{\Gamma}_i^{+} \boldsymbol{F}_i . \tag{23}$$

For N bodies, the Moore-Penrose pseudoinverse is given by

$$\begin{Bmatrix} \left(\boldsymbol{\Gamma}_i{}^T \boldsymbol{\Gamma}_i\right)^{-1} \boldsymbol{\Gamma}_i{}^T \text{ for } N \le 4 \\ \boldsymbol{\Gamma}_i{}^T \left(\boldsymbol{\Gamma}_i{}^T \boldsymbol{\Gamma}_i\right)^{-1} \text{ for } N \ge 4 \end{Bmatrix}.$$

Both solutions yield the same result for $N = 4$. This pseudoinverse is known to produce the minimum-norm solution. In the case of $N < 4$, the pseudoinverse constrains the force to lie in the range space of $\boldsymbol{\Gamma}_i$, i.e. within the plane spanned by the one or two possible force directions available from the one or two other spacecraft. With no force outside this plane (i.e. in the null space of $\boldsymbol{\Gamma}_i$), this result has the minimum norm possible. It is also a reminder that an arrangement of three CSF spacecraft cannot accelerate instantaneously outside the plane in which they lie. The three represent an underactuated system. When $N > 4$, there are more forces than strictly necessary for applying the three required force components to each body. So, the pseudoinverse minimizes the norm of the solution for the F_{ij}, with the result that it minimizes some metric involving the spacecraft power. The details of that metric are bound up in the plasma interactions described above. Given these F_{ij}, we can solve for the individual charges q_i necessary to apply them. We begin with

$$F_{ij} = k \frac{q_i q_j}{r^2} e^{-\left(\frac{r-s_i}{\lambda_i(V_i)} + \frac{r-s_j}{\lambda_j(V_j)}\right)}.$$

Let

$$\alpha_{ij} = F_{ij} \frac{r^2}{k} e^{\left(\frac{r-s_i}{\lambda_i(V_i)} + \frac{r-s_j}{\lambda_j(V_j)}\right)}.$$

Then, for three bodies, indices $i, j, \text{and } k$ we can find unsigned values

$$q_i' = \left(\frac{\alpha_{ij}\alpha_{ik}}{\alpha_{jk}}\right)^{\frac{1}{2}}. \tag{24}$$

There are two solutions for the sets of charges that impart the required force. One consists of charges opposite in polarity to the other. So, we can arbitrarily choose the polarity of one of these charges, and doing so determines the polarity of the rest. The proposed algorithm sets $q_1 = q_1'$ and then solves for $q_{i+1} = -q_{i+1}' \text{sgn}\left(q_i\right) \text{sgn}\left(\boldsymbol{F}_{i+1}^{\text{T}} \hat{\boldsymbol{r}}_{i,i+1}\right)$.

Degrees of Freedom

A CSF changes configuration thanks to internal forces only. In the absence of external forces, the angular momentum and the translational momentum of the formation are constant. Explicitly,

$$\sum_{i=1}^{N} M_i \dot{x}_i = c_1 ,$$

where M_i is the i^{th} spacecraft's mass, $\dot{x}_i$ is the i^{th} spacecraft's velocity, and c_1 is a constant. Equivalently, this result can be written as a statement that the sum of these internal forces totals zero or that the system center of mass is a constant. Angular momentum requires

$$\sum_{i=1}^{N} M_i x_i \times \dot{x}_i = c_2 ,$$

where c_2 is a constant. We take these results to describe a situation in which the spacecraft in the formation move together in such a way that the Clohessy-Wiltshire equations describe their dynamics. Then x_i and $\dot{x}_i$ represent the position and velocity, respectively, of each spacecraft relative to the formation's mass center but in an inertial frame (not the rotating CW frame). These six integrals of the motion remove six degrees of freedom from among those otherwise available among the N spacecraft. The degrees of freedom therefore number $6N - 6$.

4.2 COMPUTING CHARGE PRODUCT FROM COMMANDED FORCE (MODULATION TECHNIQUE)

For the simulation results presented in the following section we used another novel approach based on pulse modulation to derive the charge product instead of individual charges from commanded force as derived below. Consider a swarm of N spacecrafts having $p = \left(\frac{N(N-1)}{2} \right)$ charge products. For example, for $N = 4$ there are six charge products i.e.,

$$\boldsymbol{Q} = \begin{bmatrix} Q_{12} & Q_{13} & Q_{14} & Q_{23} & Q_{24} & Q_{34} \end{bmatrix}^T \tag{25}$$

For ith spacecraft, we consider all possible pairs of charge product due to the remaining $N-1$ spacecrafts as $Q_{ij} = q_i q_j$, for $j = 1, \ldots, N, i \neq j$. Then the commanded force acting on i^{th} spacecraft is

$$\boldsymbol{F}_{ci} = \sum_{j=1, i \neq j}^{N} \frac{k_c Q_{ij}}{r_{ij}^{\,2}} r_{ij} e^{-\frac{r_{ij}}{\lambda_d}} \tag{26}$$

Rewriting Equation (26) we get,

$$\boldsymbol{F}_{ci} = \left[A_i \right] \left[\tilde{\boldsymbol{Q}} \right] \tag{27}$$

where,

$$[A_i] = \left[\frac{k_c}{r_{ij}^{\,2}} \boldsymbol{r}_{i1} e^{-\frac{r_{i1}}{\lambda_d}} \quad \cdots \quad \frac{k_c}{r_{iN}^{\,2}} \boldsymbol{r}_{iN} e^{-\frac{riN}{\lambda_d}} \right],$$

$$\left[\tilde{\boldsymbol{Q}} \right] = \left[q_i q_j \quad \cdots \quad q_i q_N \right]^T.$$

Then using least-square inverse we get

$$\tilde{\boldsymbol{Q}} = \left(\boldsymbol{A}^T \boldsymbol{A} \right)^{-1} \boldsymbol{A}^T \boldsymbol{F}_{ci}. \tag{28}$$

Thus we derive the charge product $\tilde{\boldsymbol{Q}}$ for i^{th} spacecraft from its commanded force F_{ci}. The charge product thus derived is then used for computing the thrust developed by Coulomb charging of i^{th} spacecraft as

$$\boldsymbol{F}_{CSF_i} = [\boldsymbol{A}_i] \left[\tilde{\boldsymbol{Q}} \right] \tag{29}$$

and thrust required for i^{th} spacecraft from electric propulsion is

$$\boldsymbol{F}_{EP_i} = \boldsymbol{F}_{ci} - \boldsymbol{F}_{CSF\,i}. \tag{30}$$

From Equations (29) and (30) we see that the electric thrusters is used only for compensating the difference between the commanded force and that generated by electrostatic forces.

4.3 COMPUTING ACTUAL FORCE FROM CHARGE PRODUCT

The performance of Coulomb spacecraft charging is analysed using the CSF parameters like average power, peak power, specific impulse, mass flow rate, charge history and voltage on the spacecraft. Let F_{ai} denote the actual force available from the hybrid thrusters to $i\text{th}$ spacecraft for changing its manoeuvre. Due to the actuator dynamics, F_{ai} will differ in magnitude from the commanded thrust F_{ci}. For simulation purpose, we first determine the charge product from the commanded force F_{ci} using Equation (28) and then determine $F_{CSF\,i}$ and $F_{EP\,i}$ according to Equations (29) and (30) respectively. We adopt a kind of pulse modulation in which we assume that over a time step t (i.e. over the period control is applied), the total charge product $\boldsymbol{Q}$ for the entire swarm is computed based on the following representation. For example, consider again the case of $N = 4$ with four individual charges $q_i, i = 1, \ldots, N,$ and p charge products as in Equation (26). Then we have the charge distribution over time t as shown in Table 2. The time period $t = \Delta t_1 + \Delta t_2 + \Delta t_3 + \Delta t_4 + \Delta t_5 + \Delta t_6$ and at every fast sampling instant (bang-bang) $\Delta t_k, k = 1, \ldots, p$, we assume that a pair of spacecrafts in the swarm are charging and we compute their respective charge product using Equation (28). Note that we do not compute the individual charges. For example, say at Δt_1, spacecrafts 1 and 2 are has a charge product

Q_{12} while it is assumed that the rest of the spacecrafts has zero charge. Note that this assumption is justified, as the sampling period Δt_k is much smaller than a fraction of a second. Over time t the actual force/thrust F_{ai} acting on ith spacecraft is derived back from the cumulative effect of all these charge products.

t	Δt_1	Δt_2	Δt_3	Δt_4	Δt_5	Δt_6
p	Q_{12}	Q_{13}	Q_{14}	Q_{23}	Q_{24}	Q_{34}
S/c1	q_1	q_1	q_1	×	×	×
S/c2	q_2	×	×	q_2	q_2	×
S/c3	×	q_3	×	q_3	×	q_3
S/c4	×	×	q_4	×	q_4	q_4

Table 1 CSF Charge distribution

4.4 CSF PERFORMANCE EVALUATION

Next we list a set of formulae derived based on the above concept for evaluating the various CSF parameters.

1. Charge history $q_{hist} = \dfrac{\sum_i^N \left| \tilde{q}_i \right|}{N-1}$, where $\tilde{q}_i = \sqrt{\tilde{\boldsymbol{Q}}}$

Note that in order to compute the individual charges $\tilde{q}_i$ from the charge products, there $N-1$ possible solutions for each of the N charges based on possible p charge products.

2. Using Gauss's law and assuming that the spacecraft is spherical with radius ρ, the surface potential is

$$V_{sc_i} = \frac{\tilde{q}_i}{4\pi\varepsilon_0 r_i}$$

and average spacecraft voltage is

$$V_{sc} = \frac{\sum_{i=1}^{N} \left(\dfrac{\sum_{i=1}^{N} \left| V_{sc_i} \right|}{N-1} \right)}{N}.$$

3. CSF mass flow rate is

$$\dot{m} = \frac{I_e m_{ion}}{q_{ion}}$$

where I_e is the emission current, m_{ion} is the mass of ions and q_{ion} is charge of the ion. Then the average average mass flow is

$$\dot{m}_{avg} = \frac{\sum\left(\sum \dot{m}\right)}{p}$$

Note that here we sum all the mass flow rate of individual spacecrafts for each pulse time Δt_k and then average over t for p charge products.

4. The specific impulse

$$I_{sp} = \frac{F_{CSF}}{\dot{m}_{avg}\, g_0}$$

where $g_0 = 9.81\,\mathrm{m/s^2}$ is the gravitational constant.

5. Power generated due to Coulomb charging is $P_i = \left|V_{sc} I_e\right|$, where $\left|I_e\right| = 4\pi\varepsilon_0 \rho^2 \left|J_p\right|$ is the emission current and J_p is the current density to the spacecraft from the plasma. The peak power is

$$P_{peak} = \max \frac{\left(\sum P_i\right)}{N-1}$$

and the average power is

$$P_{avg} = \frac{\sum\left(\frac{\sum P_i}{N}\right)}{N-1}.$$

4.5 SNECMA PPS 1350 EP THRUSTER

EP Thruster Features	**Value/Units**
Power (nominal)	1500W
Thrust	88 mN
Specific Impulse	1650 sec
Mass (including 2 Xe flow control systems)	5.3 kg
Supply voltage	350 V
Efficiency	55 %

Table 2 Snecma PPS 1350 thruster specifications

The Snecma PPS 1350 EP thrusters was successfully flown on-board the European Space Agency's Smart-1 lunar probe. This electric thruster is suitable for operating over 5000 hours and has stable operation over a power range of 1200W to 1600W. Moreover, the starting power requirement is also low and it suits for the applications considered in this work. The Table 2

describes its salient features. We chose the Snecma PPS 1350 EP thruster for our simulation study.

4.6 SIMULATION STUDY

Simulation parameter	**Value/Units**
Spacecraft individual mass M	150 kg
Lower bound on mass $\underline{M}$	0.5 M
Upper bound on mass $\overline{M}$	1.5 M
Spacecraft radius η (assumed spherical)	0.5 m
Debye length (GEO)	200 m
Charge saturation limit	2 μC
Number of spacecrafts N	4 and 30
Initial separation	5 km and 10 km
Final inter spacecraft formation separation d	50m
Manoeuvre time	24 hrs
Peak magnitude of differential disturbance in GEO	2 μN

Table 3 CSF simulation parameters

This section illustrates the results of the simulation studies performed for the various scenarios considered in this study using hybrid thrusters in conjunction with PD control, sliding mode control and artificial potentials discussed in the preceding sections. The main scenarios considered in this study under various operating conditions are as follows:

1. Four spacecraft forming a tetrahedron formation in R^3
    (a) Initial spacecraft separation of ~ 5 km using simple PD control
    (b) Initial spacecraft separation of ~ 5 km using SM control
2. Thirty spacecraft swarm aggregation problem in R^3
    (a) Initial spacecraft separation of ~ 10 km using simple PD control
    (b) Initial spacecraft separation of ~ 10 km using SM control

The specifications common to all the four simulations presented here are listed in Table 3.

4.6.1. FOUR SPACECRAFT FORMING A TETRAHEDRON FORMATION IN R^3

In this section we present the simulation results for tetrahedron formation using simple PD control and SMC assuming the initial position is randomly chosen with a maximum inter agent separation around 5 km. Refer the Appendix for more details. For simulation purpose using PD control, the settling time is chosen as 70 sec and the damping ratio is chosen as 1. We used $N = 4$, $n = 3$, $\varepsilon_i = 1$, $\overline{J} = 0.01N$ and $\overline{f_i} = 2\mu N$. The uncertainty acting in the system is $f_i(x^i, \dot{x}^i) = 2\times10^{-6}\sin(2*(2*\pi/t))$ where $t = 24*3600$ sec is the manoeuvre time and it satisfies the assumption on the bound i.e., $\left\| f_i(x^i, \dot{x}^i) \right\| = \left\| 2\times10^{-6}\sin(0.2t) \right\| \le 2\times10^{-6} \stackrel{\Delta}{=} \bar{f}_i$. Note that individuals with point mass dynamics with uncertainties are considered for sliding mode controller design in (Gazi 2005). For formation control each agent in the swarm is pre-assigned a desired position in the final formation. The potential function considered for formation control problem has linear attraction and exponential repulsion terms given by

$$g(y) = -y\left(a - b\exp\left(-\frac{\|y\|^2}{c}\right)\right)$$

where, $a = b\exp\left(-d^2/c\right)$, $b = 0.5\times10^{-4}$, $c = 2500$ and $d = 50$. For formation control each agent in the swarm is pre-assigned a desired position in the final formation. The parameter a is computed in order to achieve the balance of attraction and repulsion between any two agents at the desired distance d in the final tetrahedron formation. By increasing the repulsive force (i.e. by increasing b) we could guarantee collision avoidance. From the plot of this potential function in Figure 13a, we see that the attraction range the repulsion range and the point it crosses the horizontal axis is the desired formation separation $(d = 50\,\text{m})$. The distance at which attraction balance the repulsion is at a unique distance $\delta = \sqrt{\dfrac{c}{\ln\left(\dfrac{b}{a}\right)}} = 50$. Figure 13-18 shows the results with PD control and Figure 19-24 shows the results with SMC respectively. Figure 13b shows the trajectories of the spacecrafts initialised at rest with random initial positions. The maximum initial separation between spacecrafts is approximately 5km. With time the four spacecrafts move to their required inter spacecraft separation of 50m and form the required tetrahedron formation while avoiding collisions. Figure 13c shows the final formation positions and the center of the formation $\bar{x}$ is represented by '*'. With PD control there is much drift of formation centre. Figure 13d shows the minimum, average and maximum of the distances of the individual spacecraft positions to the formation center. The average distance to the center $\bar{x}$ is greater

than the expected value of $50\sqrt{\frac{3}{8}}$ due to centre drift. Figure 15f shows the plot of formation center movement. Figure 14a shows the minimum, average and the maximum distances between the individuals in the formation. It is seen that the average distance between spacecrafts in the tetrahedron formation is equal to the side length of the tetrahedron or the final inter- spacecraft separation of 50m. The plot of center movement is shown in Figure 14b. The plots of hybrid actuator parameters are shown in Figure 14c to Figure 18. The charge history is shown in Figure 14c. The charge saturation limit is 2μC. The average potential of the Coulomb formation is shown in Figure 14d. The average power is shown in Figure 15a. The peak power (worst case) is roughly $P_{peak} = 10\text{W}$ and is shown in Figure 15b. The commanded force F_{ci} from the sliding mode controller for the four spacecrafts in the formation is shown in Figure 15c. The actual force F_{ai} available to individual spacecraft is contributed by F_{CSF_i} and F_{EP} and these are shown in Figure 15d and Figure 16a respectively. As expected (refer King et al. 2003), we observe that for Coulomb formation of 50m separation, C is of the order of tens of micro-Newtons. The tracking error or the formation error settles to very close zero and hence the desired formation is achieved. In ideal case with zero disturbance and no charge saturation, F_{CSF_i} would contribute a major proportion of F_{ci} with minimum effort from the electric propulsion. The mass flow rate of the electric thrusters is shown in Figure 16b. The specific impulse history and mass flow rate are shown in Figure 16c and 16d respectively. Figure 17 and 18 shows the comparison of the vector components (x, y, z components) of the commanded force F_{ci}, the generated Coulomb force F_{CSF_i} and the EP force F_{EP} for each of the four spacecrafts. The commanded force F_{ci} is of the order of 10^6 μN, the EP force F_{EP} is of the order of 10^3 μN and the generated Coulomb force F_{CSF_i} is of the order < 10^2 μN. From these plots we see the vector sum of F_{CSF_i} and F_{EP} does not exactly match F_{ci} due to the saturation imposed on F_{EP} (88 mN or 8.8×10^4 μN) and CSF charge saturation limit of 2μC. It is observed that by tuning the PD gains Coulomb forces of 500 μN can be generated. However, the formation center movement is tremendous and is not appropriate. This shows that there is a huge trade-off between CSF and path planning behaviour with respect to formation geometry when we use simple PD control. Nevertheless, better performance is expected if PID control is used instead of PD control as the incorporation of the integral term will improve the steady state response of the over all formation. However, this is not addressed in this report. In this study, we have used a more advanced robust control technique using SMC originally designed for addressing swarm aggregation and formation control problems (refer Gazi and Passino, 2005). The simulation plots using SMC are shown in Figure 19 - Figure 24 and it is observed that the

SM controller gives better performance compared to the PD control considered in this study. The trade-off between CSF and path planning or formation behaviour is only minimal. As expected, the average distance to the center $\bar{x}$ is equal to $50\sqrt{\frac{3}{8}}$. It is observed that during transient before the occurrence of sliding mode it is possible for the center $\bar{x}$ to move. However, once the sliding mode occurs the center is expected to be almost stationary. For practical implementations, there might be small deviations even after transient, which are due to chattering effects. Comparing Figure 13c with Figure 19c and Figure 14b with Figure 20b, it is observed that the formation centre is almost stationary with SMC than with PD control. In Figure 23 and 24, we observe that the vector sum of F_{CSF_i} and F_{EP} nearly match F_{ci} as F_{ci} is of the order of 10^4 μN and is close to the saturation limit of F_{EP}. The Table 3 lists a basic comparison between the two types of control schemes used in this work.

Performance/parameter	**SMC**	**PD**
Speed of convergence	Fast	Fast
Transient response	Good and is governed by the reaching phase	Good, Tailorable
Steady state response	Very good and governed by sliding surface	Good
Complexity of tuning controller	Slightly more complex as there are more design parameters	Simple
Robustness	Highly insensitive to the class of ext. disturbance considered here. The more number of design parameters makes the controller robust.	Poor
Formation center movement	Stationary after SM begins	More prominent
Final inter agent separation	50m±001%	50m±002%

Table 3. Comparison between SMC and PD Control

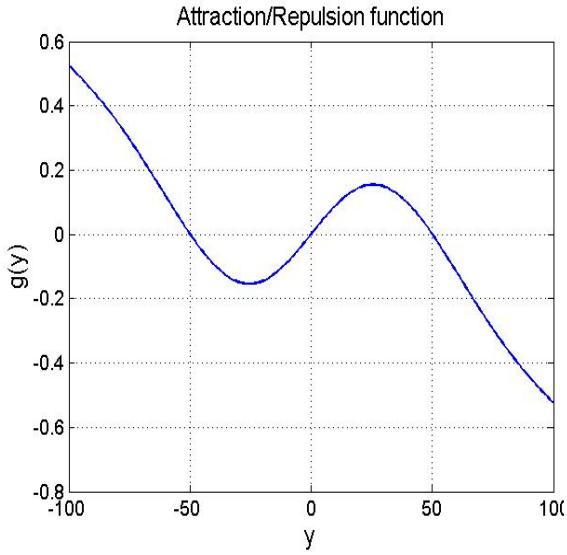

(a)

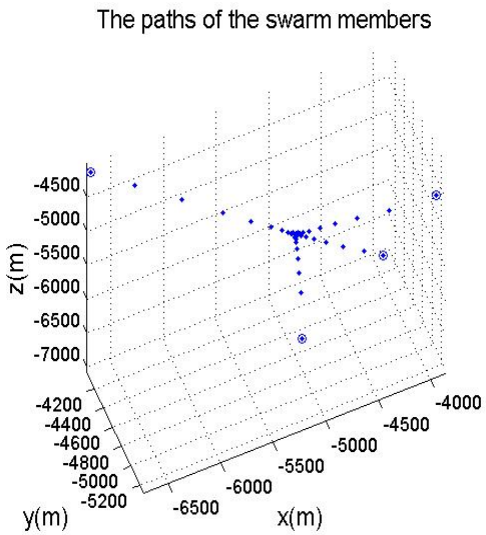

(b)

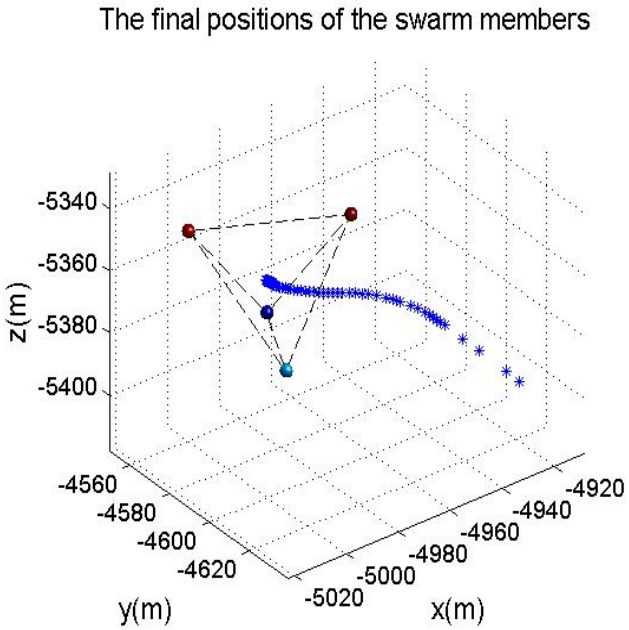

(c)

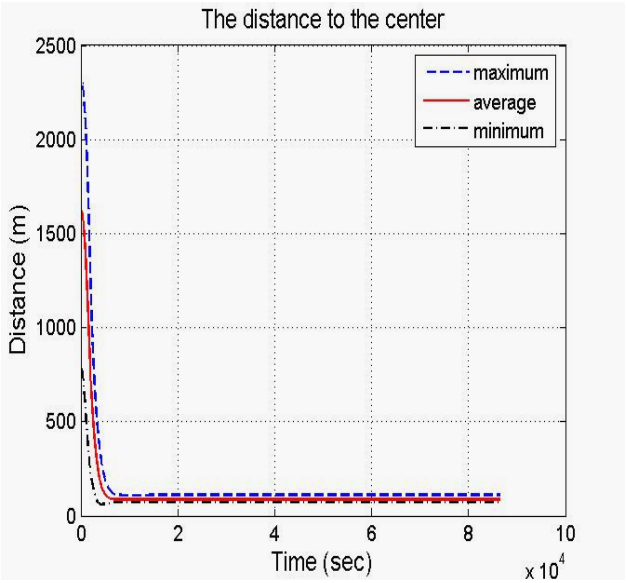

(d)

Figure 13 Simulation plots for tetrahedron formation using PD and maximum initial separation of 5km: Path planning (a)-(d).

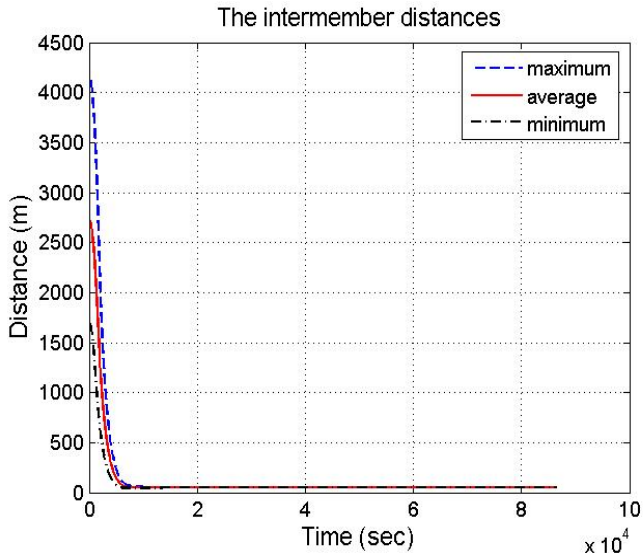

(a)

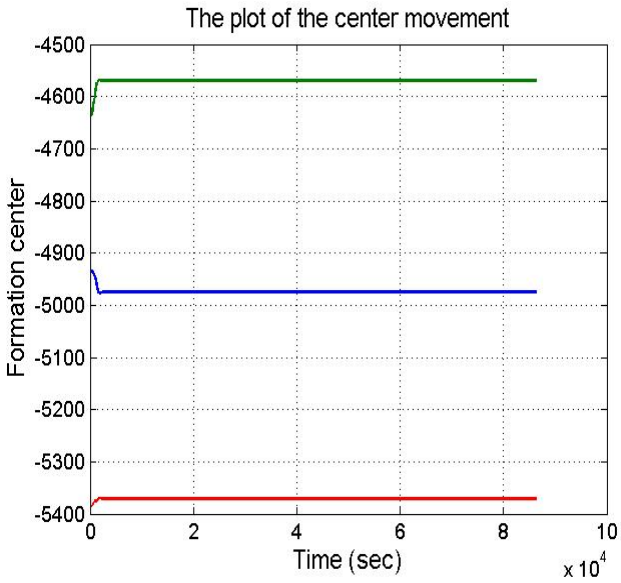

(b)

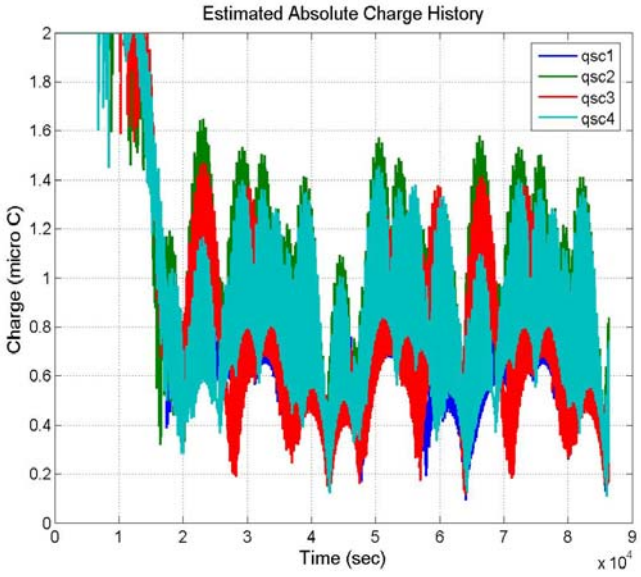

(c)

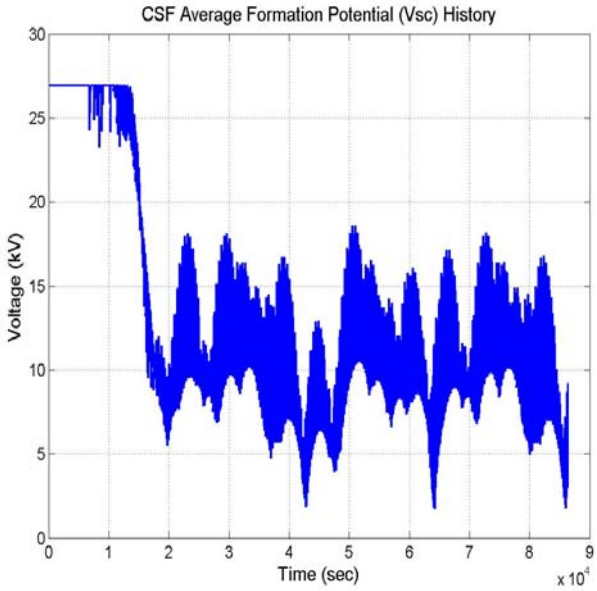

(d)

Figure 14 Simulation plots for tetrahedron formation using PD and maximum initial separation of 5km: Path planning (a)-(b) and hybrid actuator parameters (c)-(d).

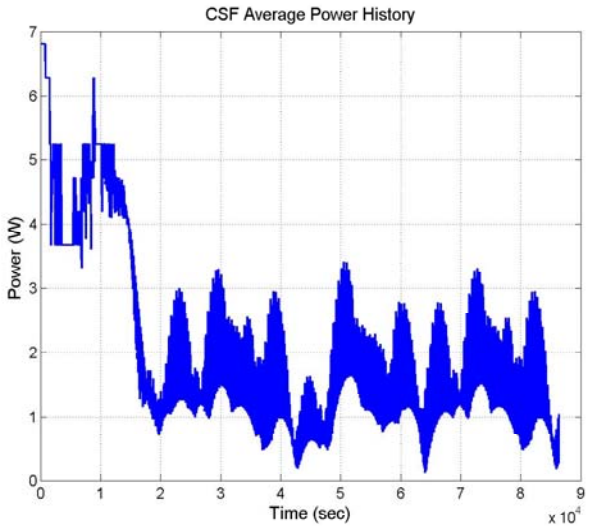

(a)

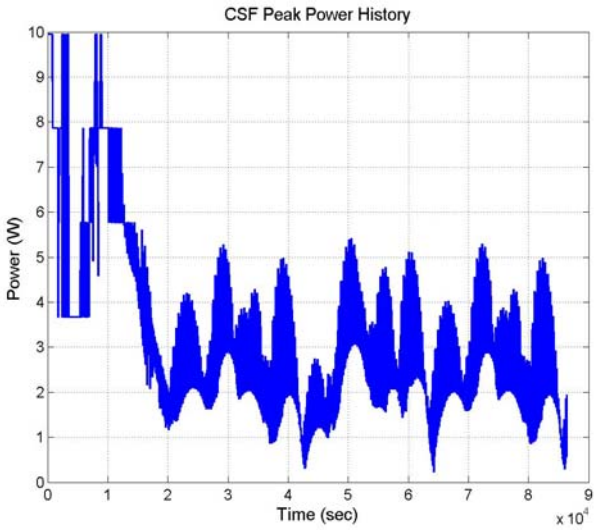

(b)

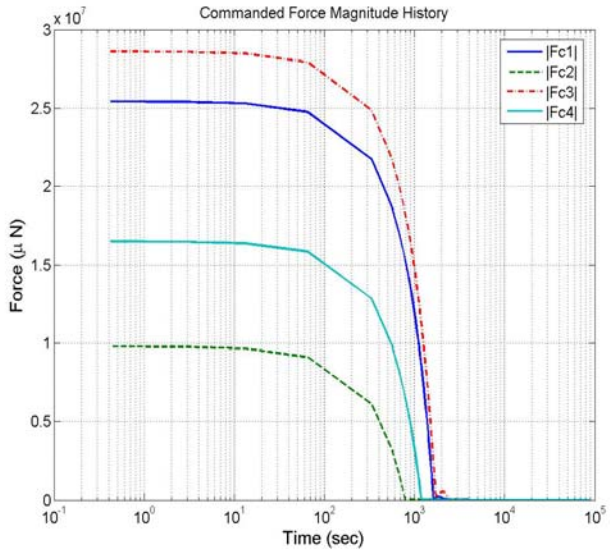

(c)

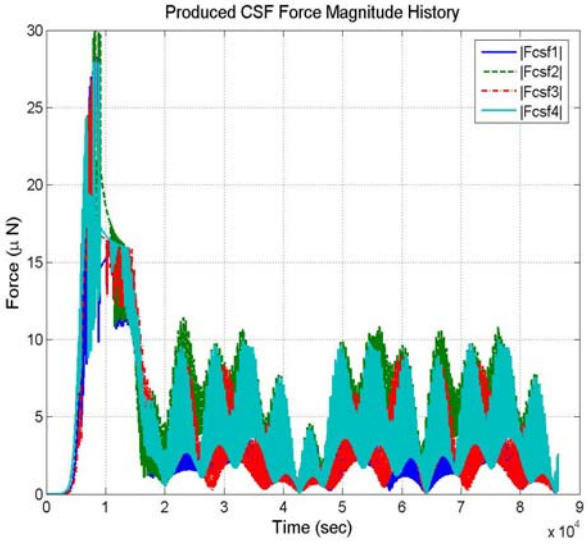

(d)

Figure 15 Simulation plots for tetrahedron formation using PD and maximum initial separation of 5km: Hybrid actuator parameters (a)-(d).

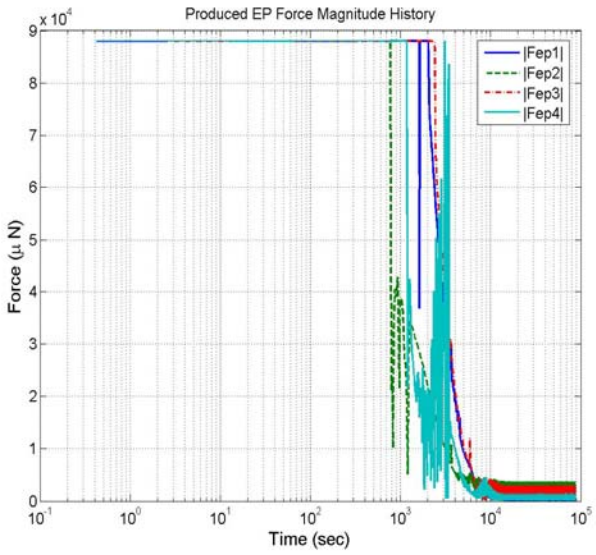

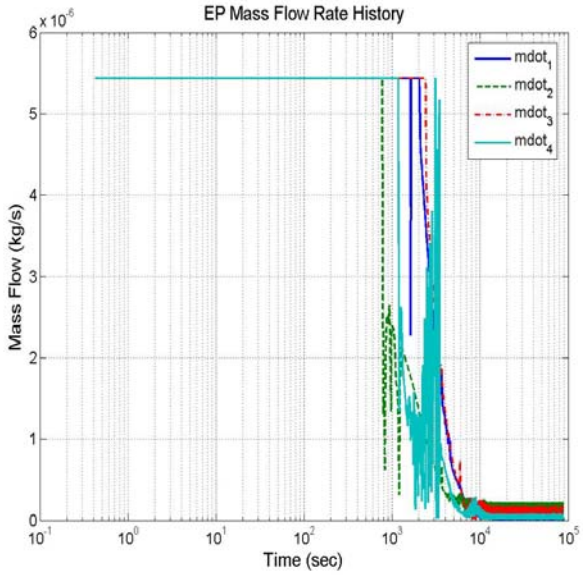

(a) **(b)**

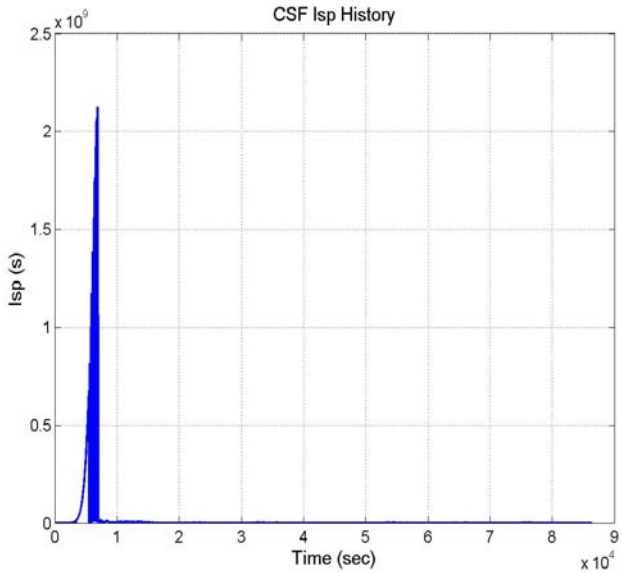

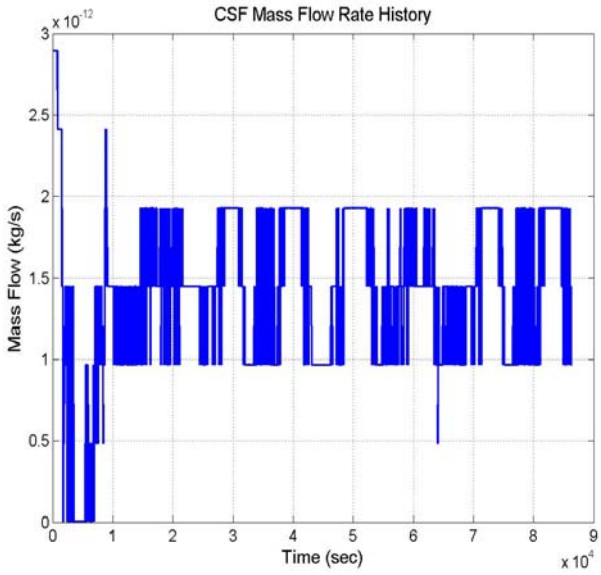

(c) **(d)**

Figure 16 Simulation plots for tetrahedron formation using PD and maximum initial separation of 5km: Hybrid actuator parameters (a)-(d).

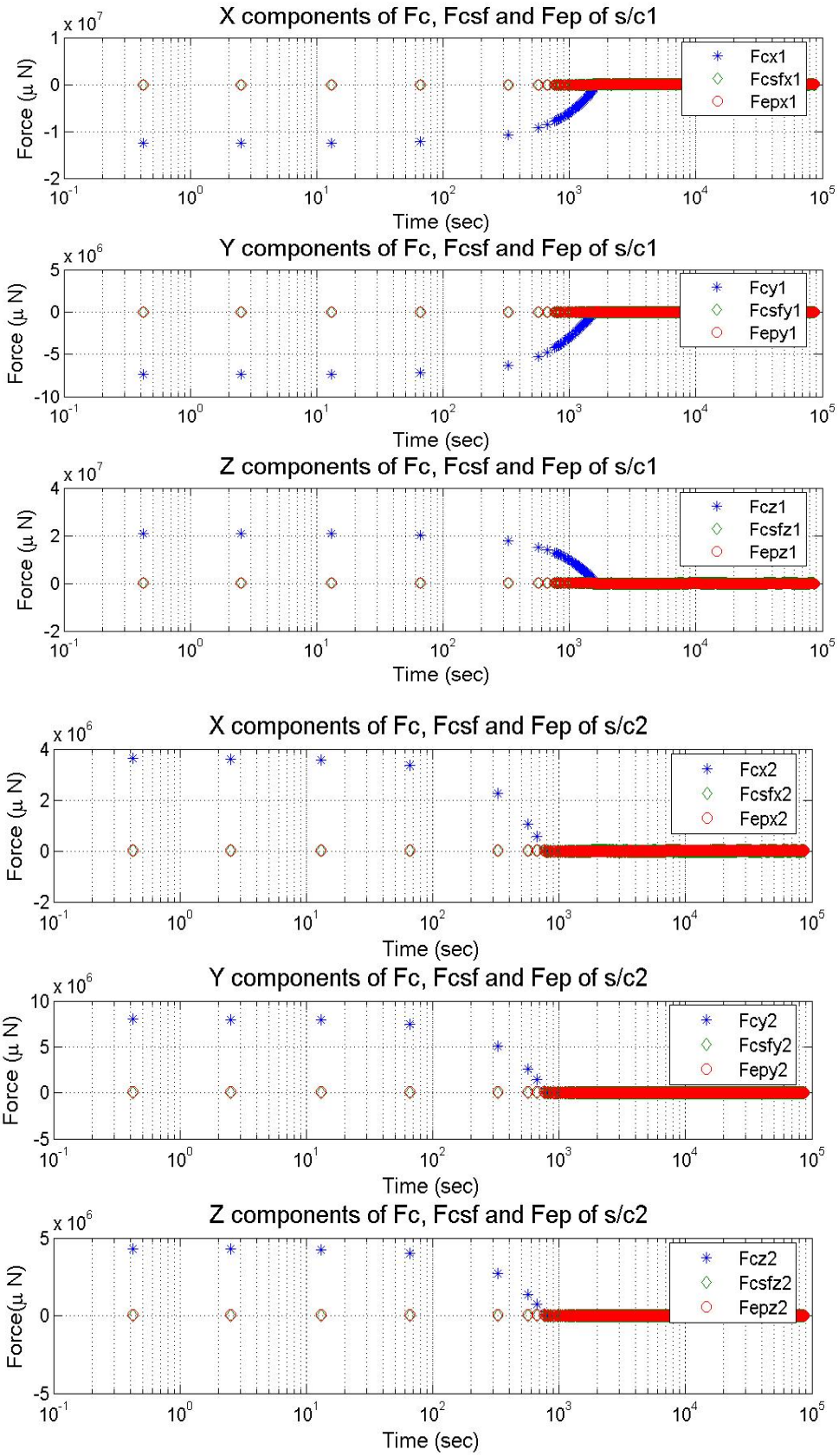

Figure 17 Simulation plots for tetrahedron formation using PD and maximum initial separation of 5km: X, Y and Z componets of commanded, CSF and EP force vectors for spacecraft 1 and 2

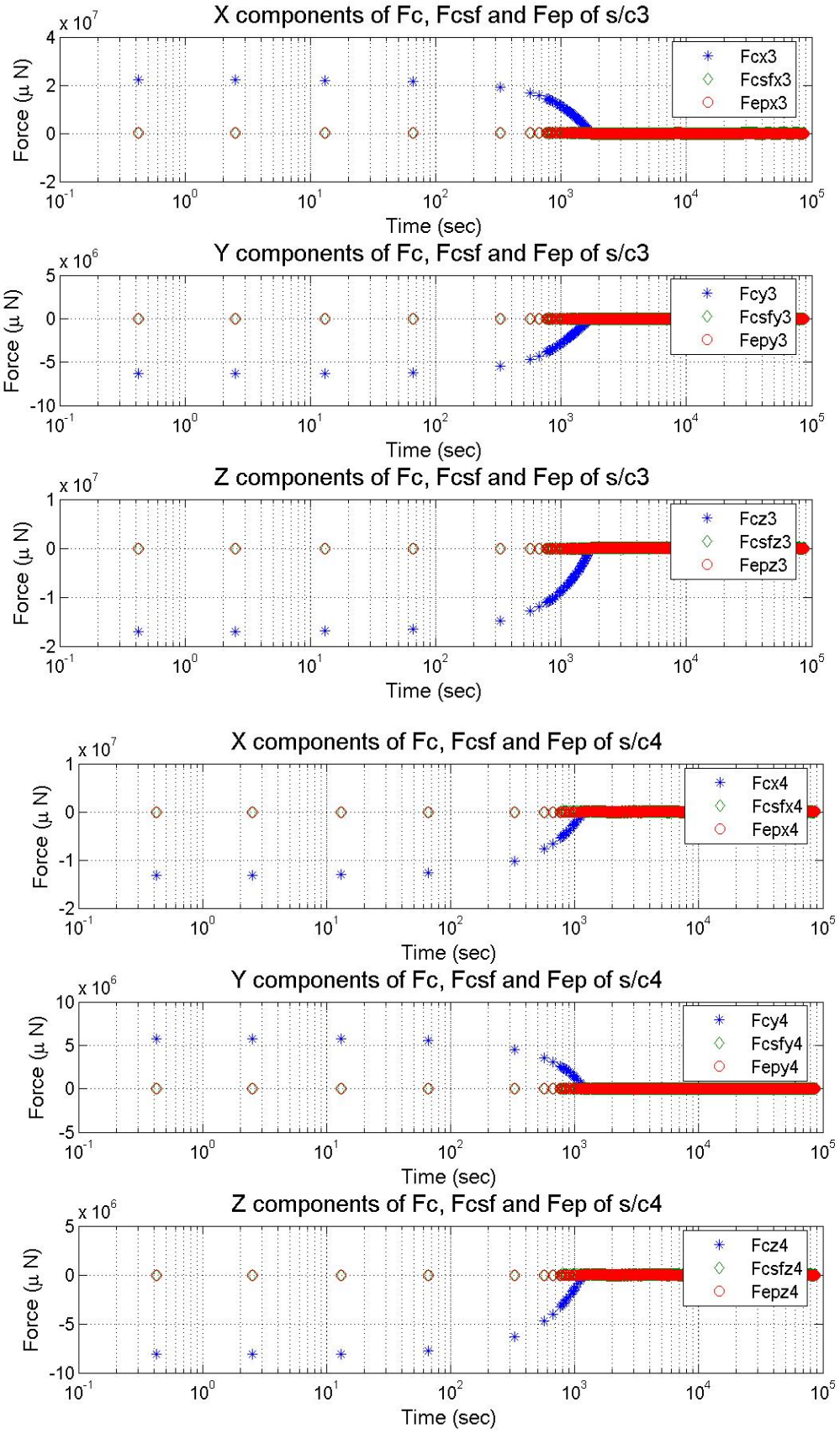

Figure 18 Simulation plots for tetrahedron formation using PD and maximum initial separation of 5km: X, Y and Z componets of commanded, CSF and EP force vectors for spacecraft 3 and 4

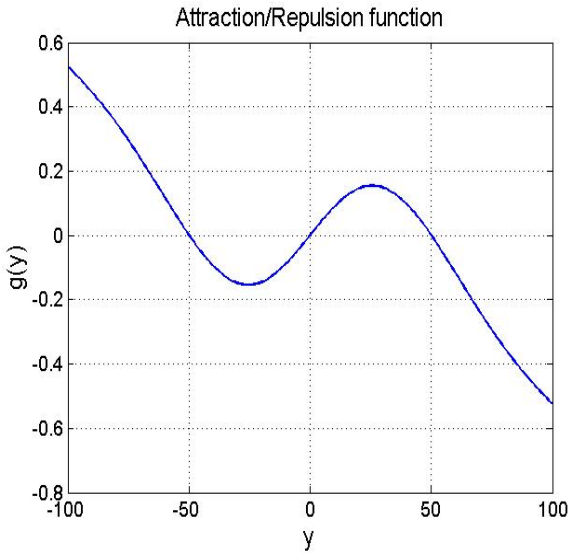

(a)

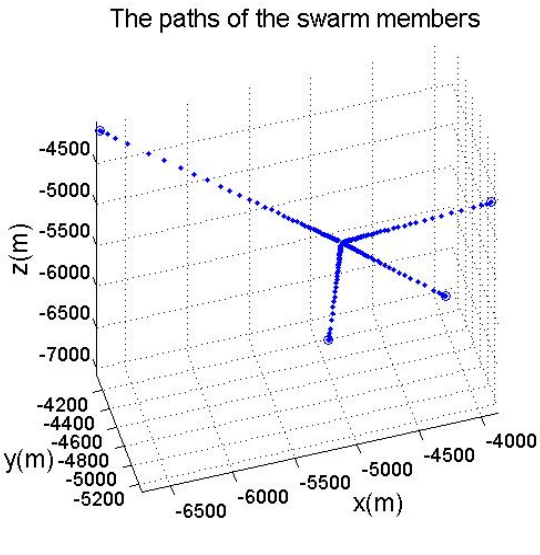

(b)

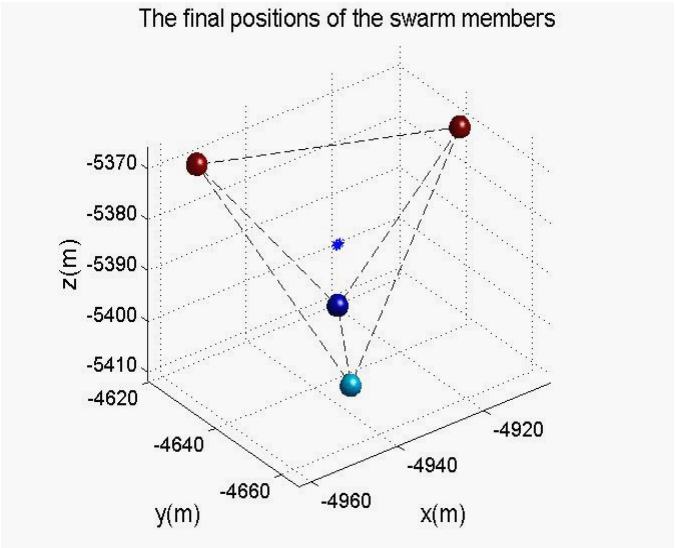

(c)

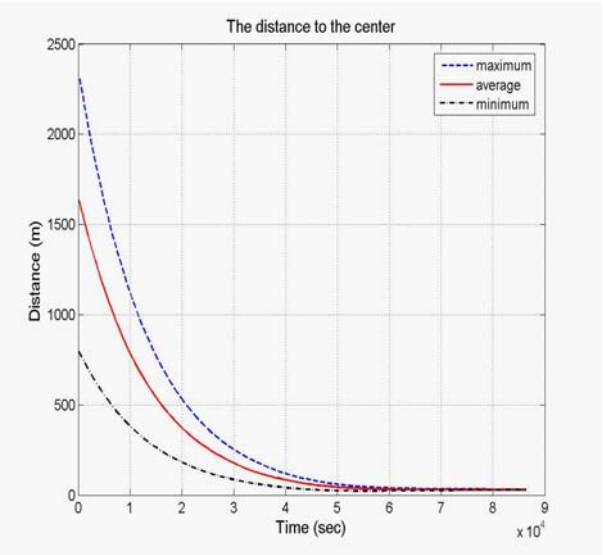

(d)

Figure 19 Simulation plots for tetrahedron formation using SMC and maximum initial separation of 5 km: Path planning (a)-(d).

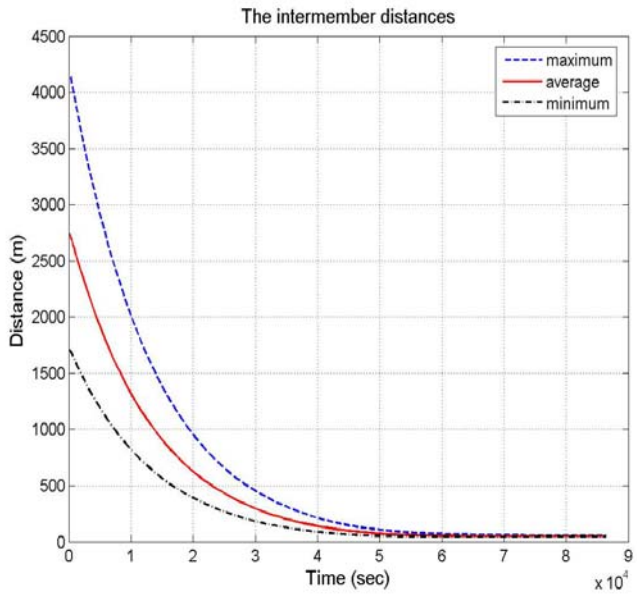

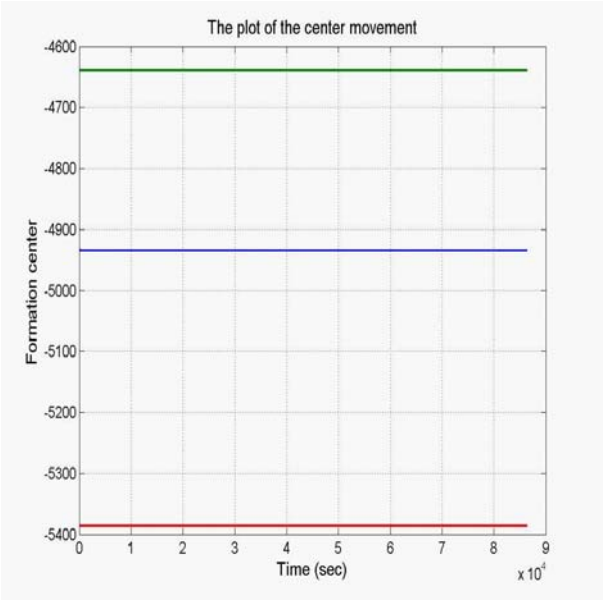

(a) **(b)**

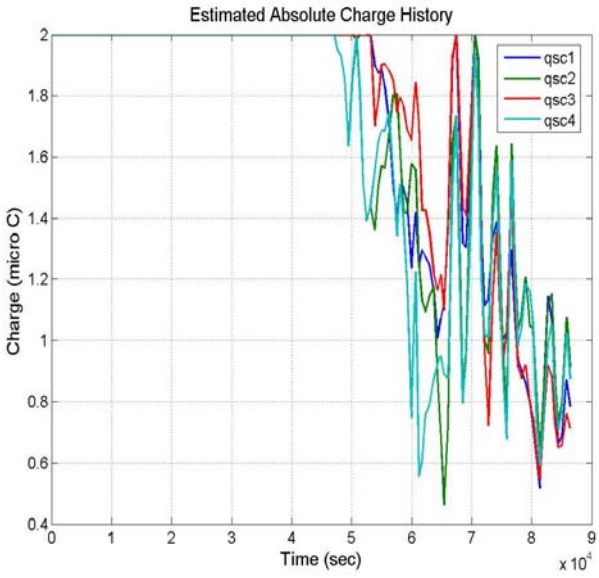

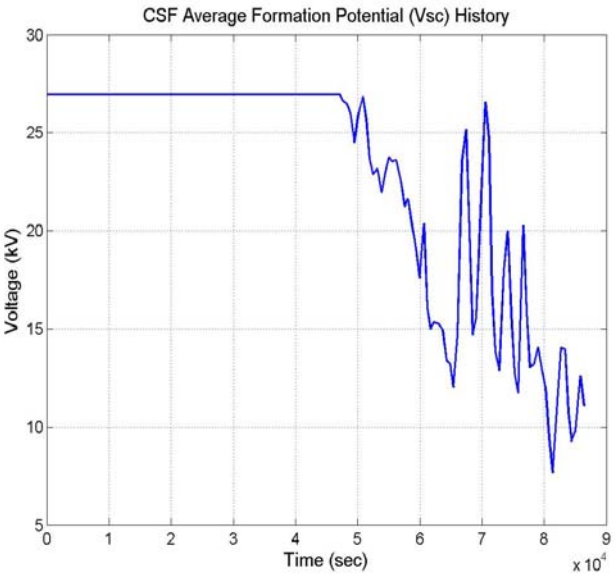

(c) **(d)**

Figure 20 Simulation plots for tetrahedron formation using SMC and maximum initial separation of 5 km: Path planning (a)-(b) and hybrid actuator parameters (c)-(d).

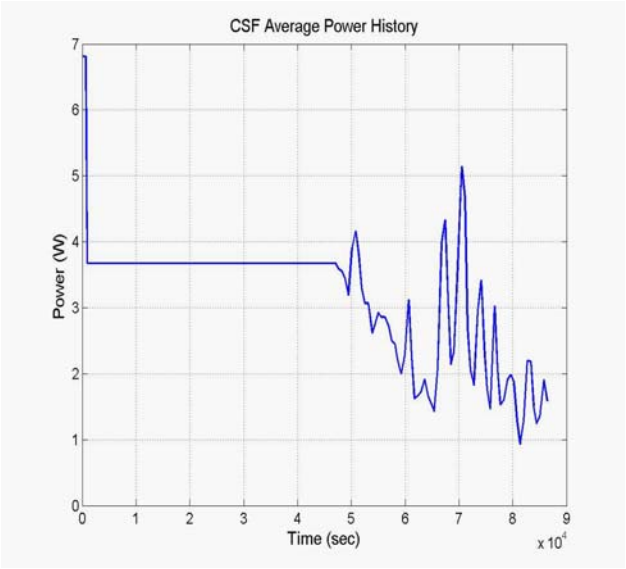

(a)

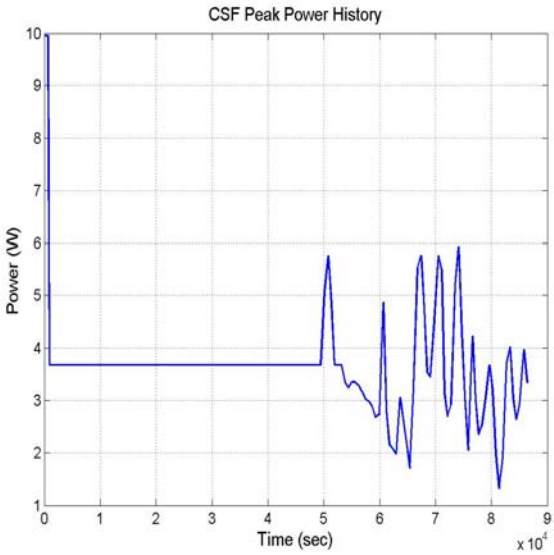

(b)

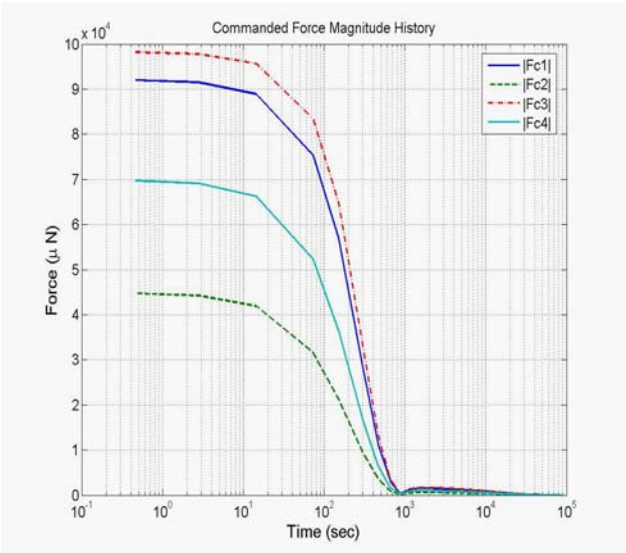

(c)

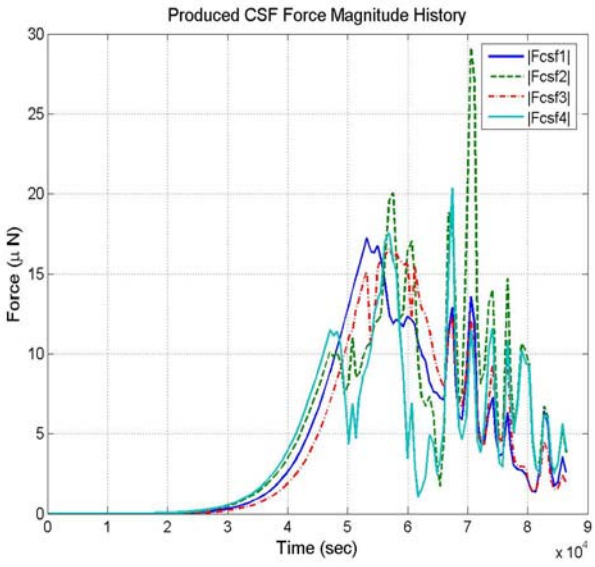

(d)

Figure 21 Simulation plots for tetrahedron formation using SMC and maximum initial separation of 5 km: Hybrid actuator parameters (a)-(d).

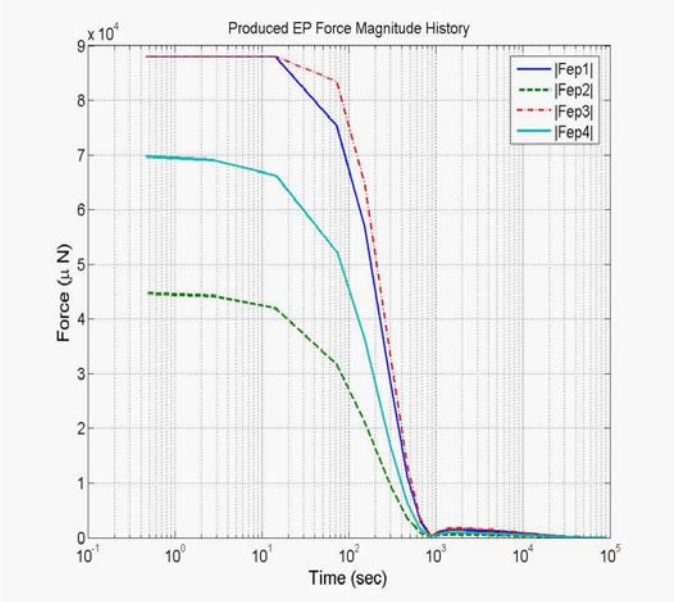

(a)

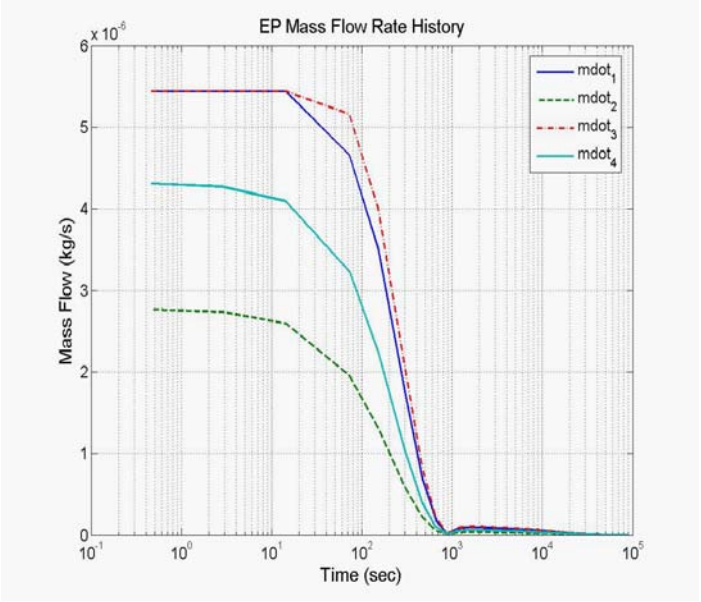

(b)

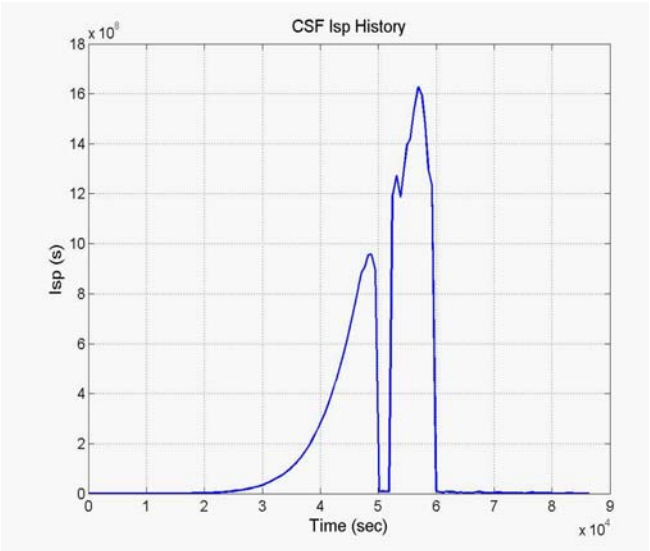

(c)

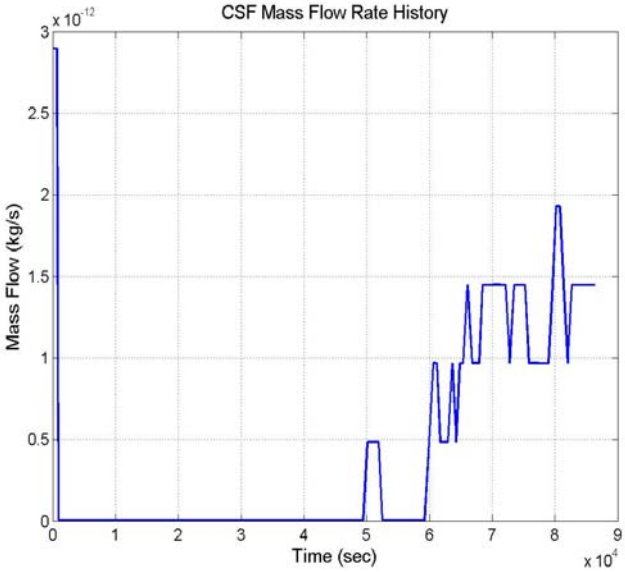

(d)

Figure 22 Simulation plots for tetrahedron formation using SMC and maximum initial separation of 5 km: Hybrid actuator parameters (a)-(d).

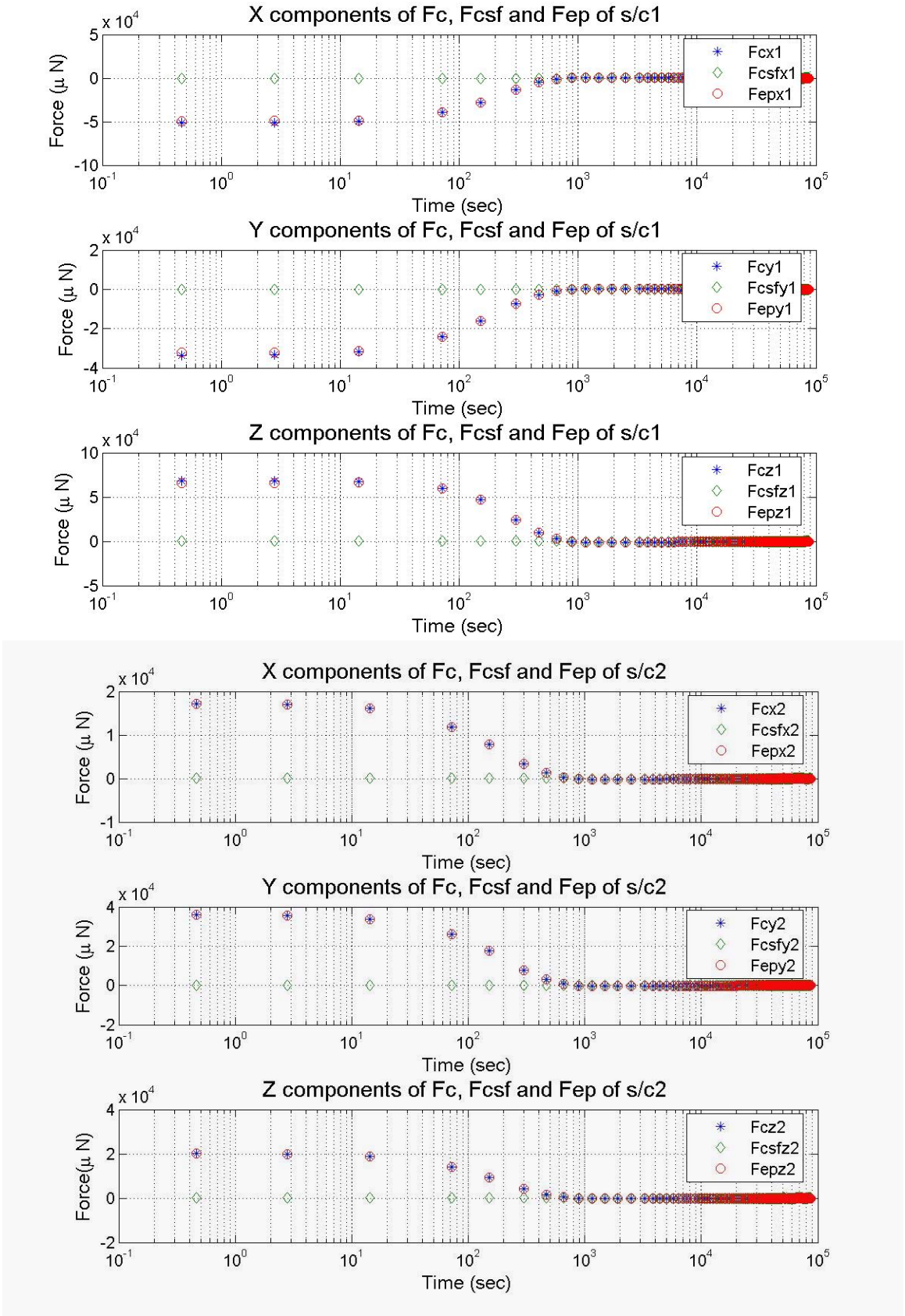

Figure 23 Simulation plots for tetrahedron formation using SMC and maximum initial separation of 5 km: X, Y and Z components of commanded, CSF and EP force vectors for spacecraft 1 and 2

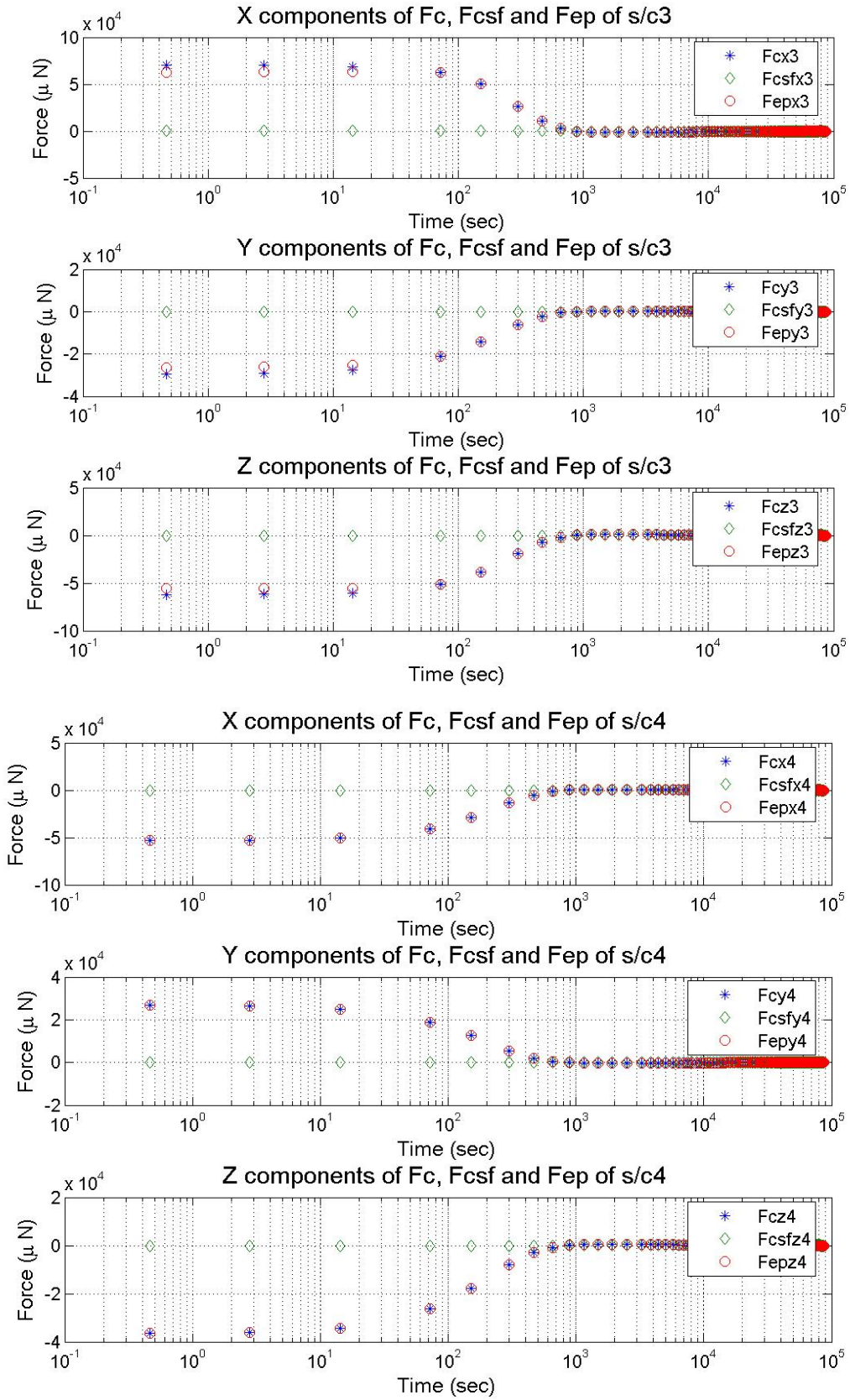

Figure 24 Simulation plots for tetrahedron formation using SMC and maximum initial separation of 5 km: X, Y and Z components of commanded, CSF and EP force vectors for spacecraft 3 and 4

4.6.2. N - SPACECRAFT SWARM AGGREGATION PROBLEM IN R^3

The algorithm developed for spacecraft swarm aggregation works for any number of spacecrafts. For simulation purpose using PD control, the settling time is chosen as 50 sec and the damping ratio is chosen as 1. For simulation purpose we used $N = 30$, $n = 3$, $\varepsilon_i = 1$, and $\bar{J} = 0.01N$. The uncertainty acting in the system is $f_i(x^i, \dot{x}^i) = 2 \times 10^{-6} \sin(2(2\pi/t))$. The potential function considered is the linear attraction and hard-limiting type repulsion discussed in Section 3 given by $g(y) = -y\left(a - \frac{b}{\left(\left\|x^i - x^j\right\| - 2\eta\right)^2}\right)$, where we select $a = 0.2 \times 10^{-6}$ and $b = 0.01$ for $\eta = 0.5$. There would be a safety area of radius $\eta = 0.5$ for all the spacecrafts in the swarm Figure 25-28 shows the results using PD control and Figure 29-32 shows the plots using SMC respectively. Figure 25a shows in R^3 the paths of the spacecrafts in the swarm. We chose the initial positions of the spacecrafts randomly and their initial velocities as zero (as is needed by condition **R2**). The initial positions of the spacecrafts are represented by circles and their paths with dots. Their positions after 24 hrs are represented by spheres. We observe that all the members of the swarm move towards each other and form a swarm cluster. Figure 25b shows in R^3 the positions of the individual spacecrafts represented by spheres after the swarm has been formed and the individuals have almost stopped. As can be seen from the figure the spacecrafts keep a distance $\left\|x^i(t) - x^j(t)\right\| > 2\eta$ for all pairs (i, j) as desired. In R^3, the lower bound on the radius of the smallest sphere, which can enclose all the N spacecrafts, is $r_{\min} = \eta\sqrt[n]{N}$. Also it is possible to avoid collision by setting the magnitude of repulsion high at the expense of getting a larger swarm size, which is feasible for spacecraft swarm applications. Figure 25c shows the minimum, average and maximum of the distances of the individual spacecraft positions to the swarm center and Figure 25d shows the minimum, average and the maximum distances between the individuals in the swarm. Figure 26a shows the plot of the center movement. The centre movement is prominent using simple PD control. Figure 26b to Figure 28 shows the plots of hybrid propulsion parameters. Figure 26b shows the charge history. The charge saturation limit is 2μC. The average Coulomb formation potential is shown in Figure 14c. The peak power (worst case) is roughly is shown in Figure 26d. The average power is shown in Figure 27a. The commanded force F_{ci} from the sliding mode controller for all the 30 spacecrafts in the swarm is shown in Figure 27b (Note that x-axis in log scale). The actual force F_{ai} available to individual spacecraft is contributed by F_{CSF_i} and F_{EP} and these are shown in Figure 27c and Figure 27d respectively. The CSF mass flow rate and specific impulse

history are shown in Figure 28a and 28b respectively. The mass flow rate of the EP thrusters is shown in Figure 28c. The plots using SMC are shown in Figure 29-32. From the x, y, z co-ordinates of the formation centre (see Figure 29b and Figure 30a) it is noted that the center is almost stationary when compared to the corresponding plots (Figure 24b and Figure 26a) using PD control. Nevertheless, we would like to emphasis two issues here. First issue is related to the assumption that the initial velocities of the spacecrafts are zero. If the initial velocities are non-zero then condition **R2** is violated and hence the bound on the derivative of the potential function $J(x)$ would no longer hold (Equation (7) in (Gazi 2005)). It might be possible to derive such a bound with the assumption that initial velocities are bounded. In any case for the bound in Equation (7) in reference (Gazi 2005) we will have more complicated expression. This issue needs to be further investigated and is outside the scope of this study. The second issue is with the sliding mode control and the hard-limiting potential. The gradient ($\nabla_y \boldsymbol{J}_r(\|\boldsymbol{y}\|) = \boldsymbol{y}\boldsymbol{g}_r(\|\boldsymbol{y}\|)$) of the hard-limiting potential can become infinite if the inter-spacecraft distance becomes close to the critical distance. Therefore, the gain of the sliding mode control (due to infinite $\bar{J}$) has to become also infinite and hence cannot be implemented. Nevertheless, we conjecture that this issue is less likely to happen in the case of spacecraft swarming because we do not need tight swarming as is the case with biological swarms.

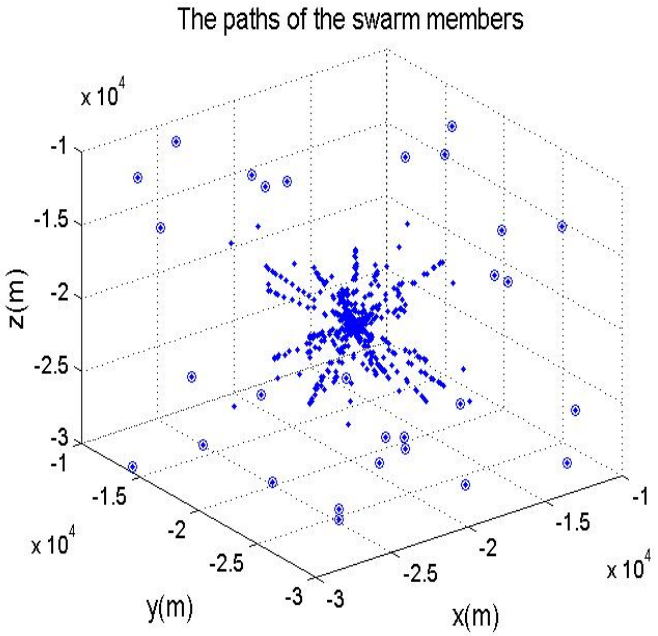

(a)

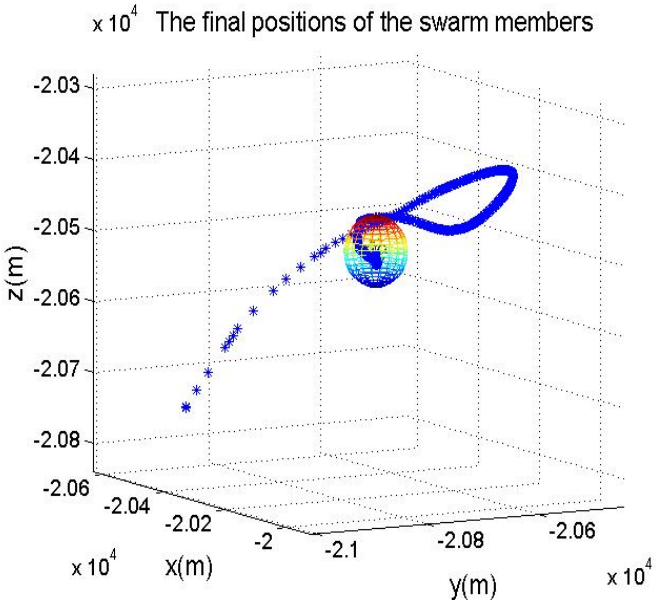

(b)

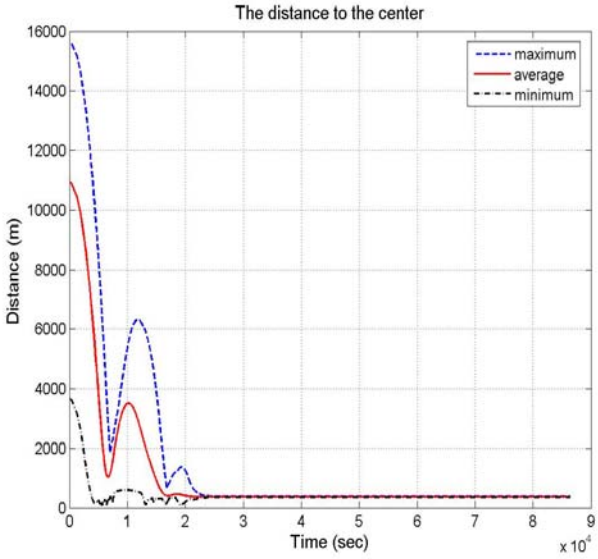

(c)

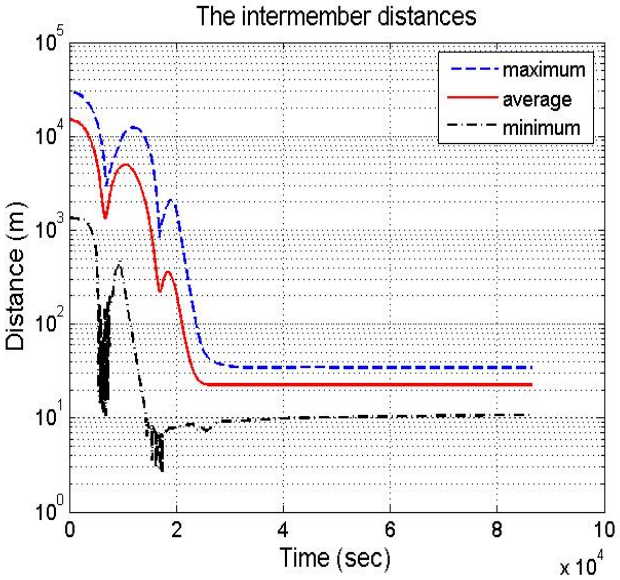

(d)

Figure 25 Simulation plots for 30 spacecraft swarm aggregation using PD and maximum initial separation of 10 km: Path planning (a)-(d)

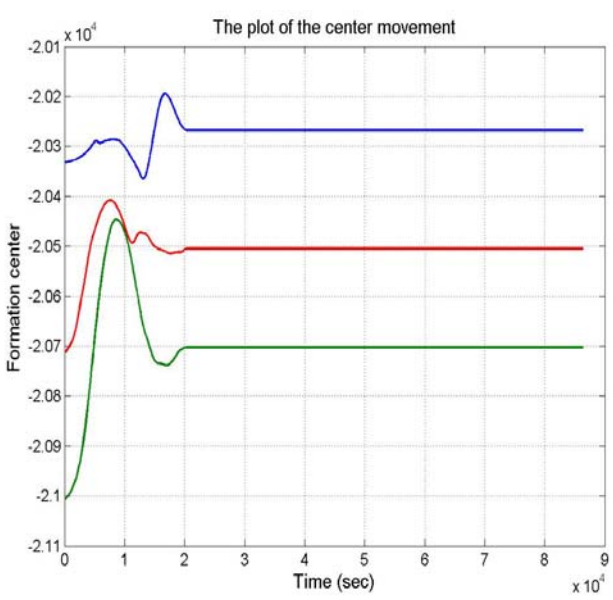

(a)

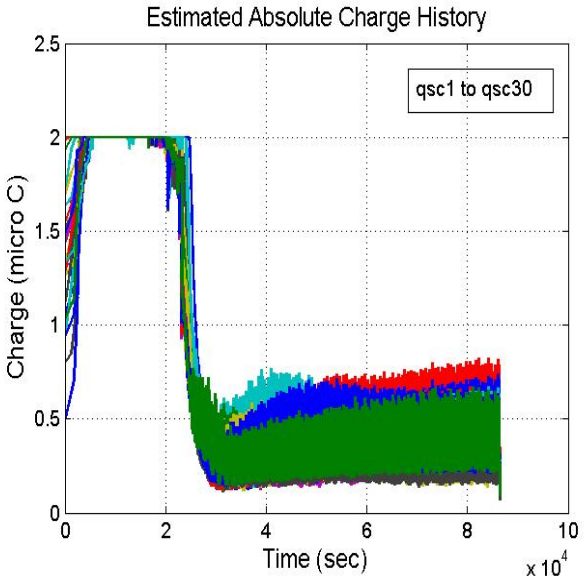

(b)

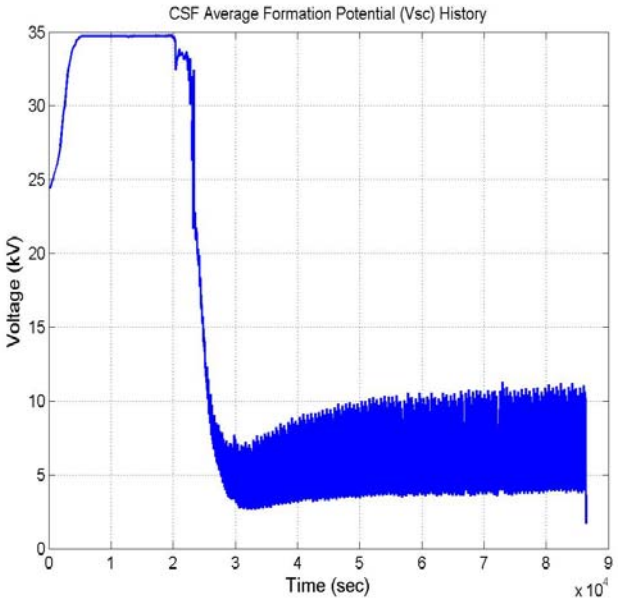

(c)

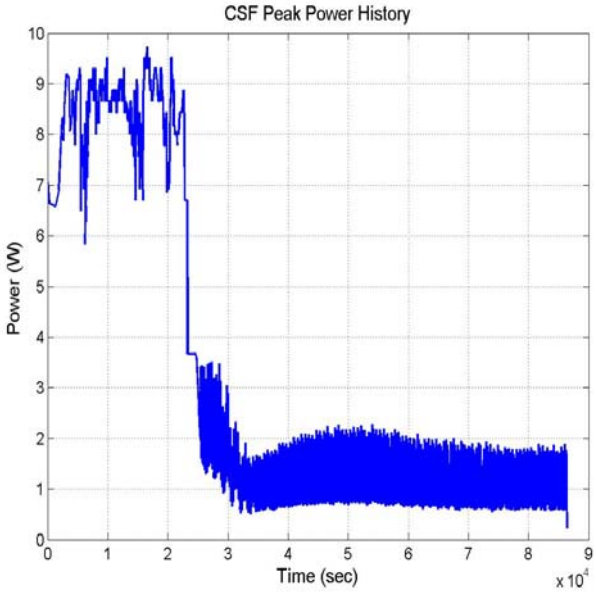

(d)

Figure 26 Simulation plots for 30 spacecraft swarm aggregation using PD and maximum initial separation of 10 km: Path planning (a) and hybrid actuator parameters (b)-(d).

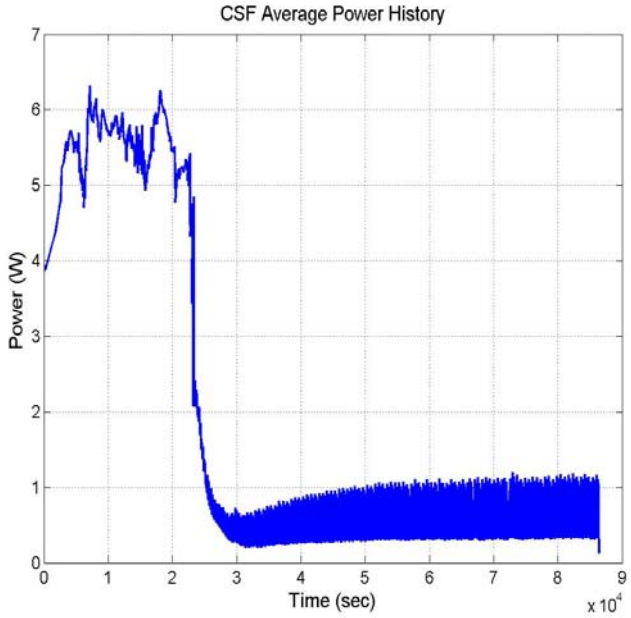

(a)

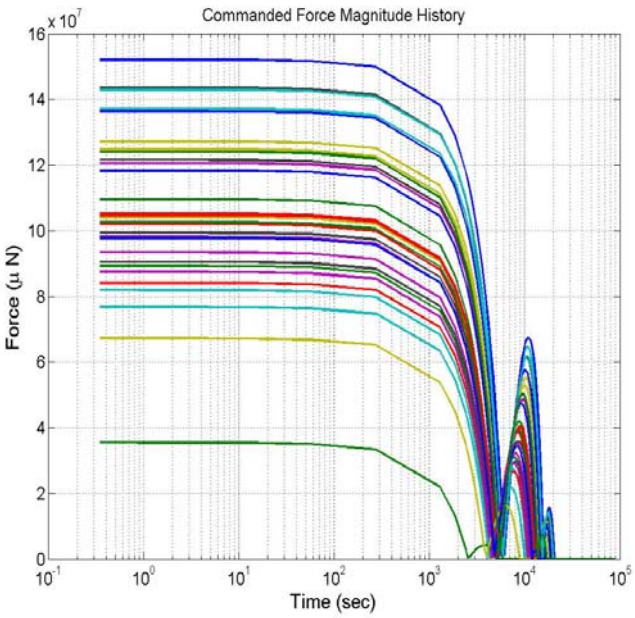

(b)

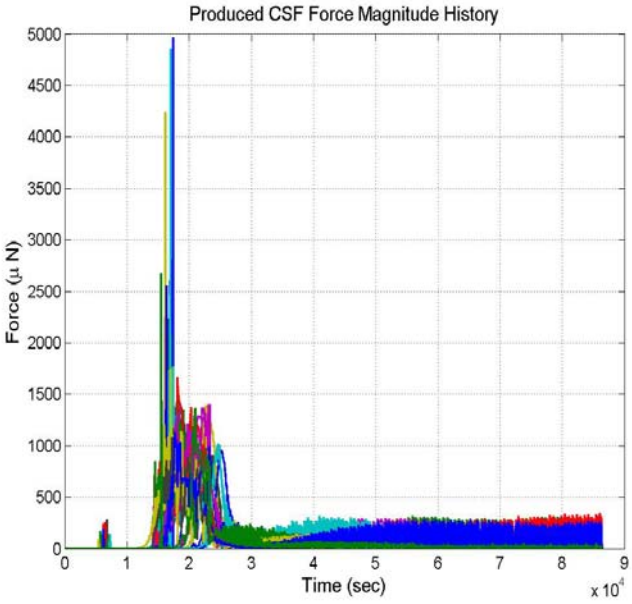

(c)

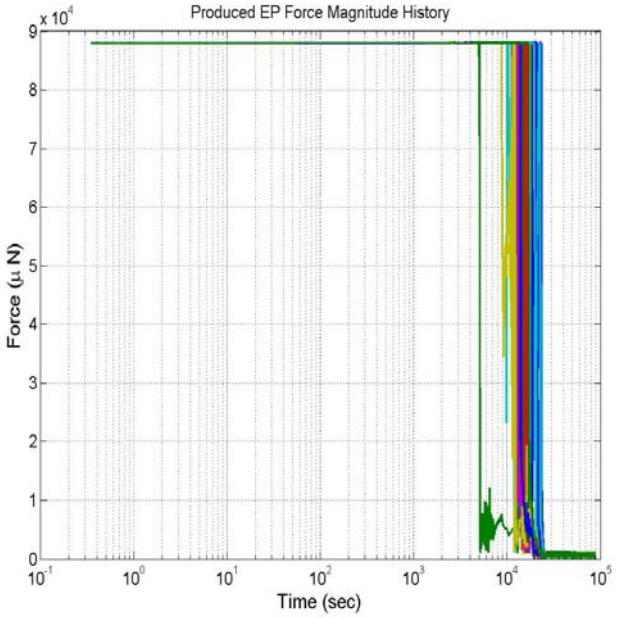

(d)

Figure 27 Simulation plots for 30 spacecraft swarm aggregation using PD and maximum initial separation of 10 km: Hybrid actuator parameters (a)-(d).

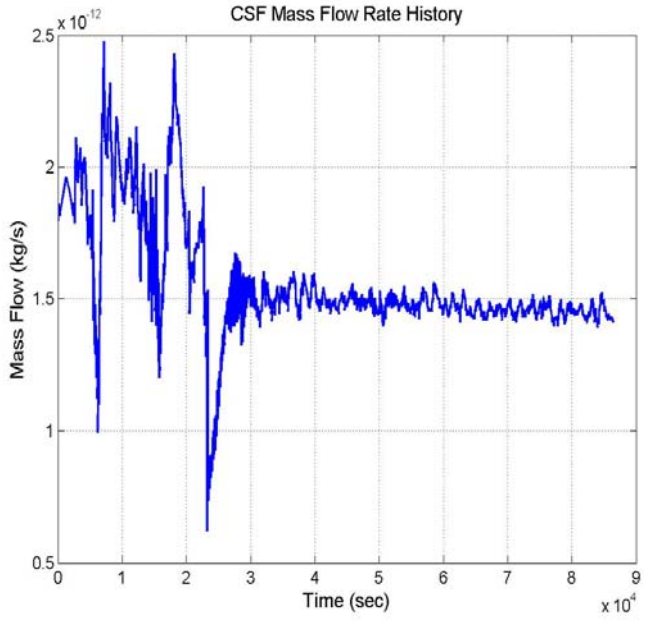

(a)

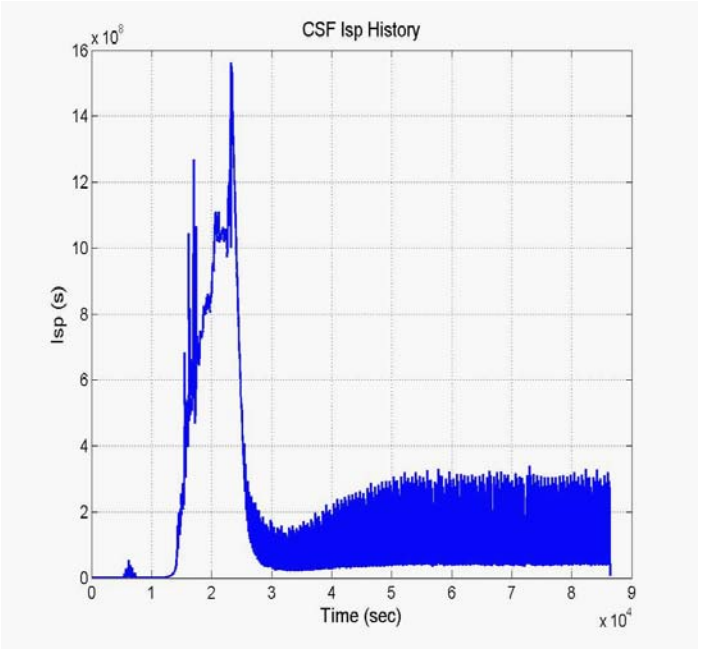

(b)

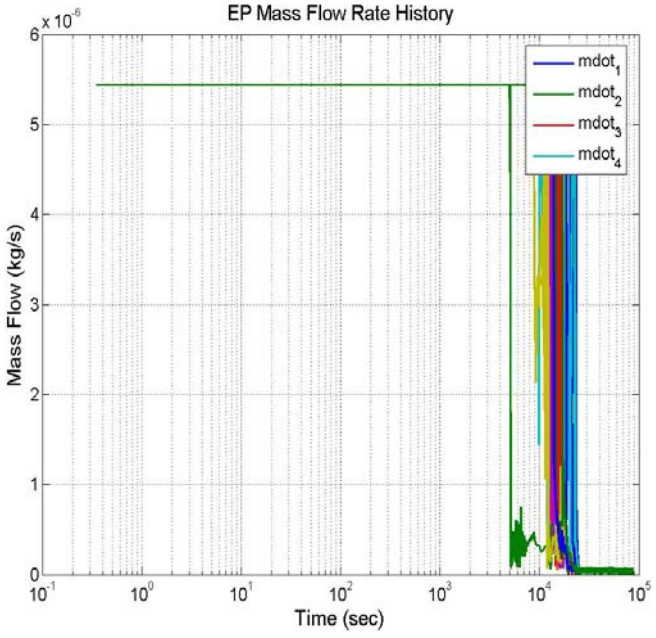

(c)

Figure 28 Simulation plots for 30 spacecraft swarm aggregation using PD and maximum initial separation of 10 km: Hybrid actuator parameters (a)-(c).

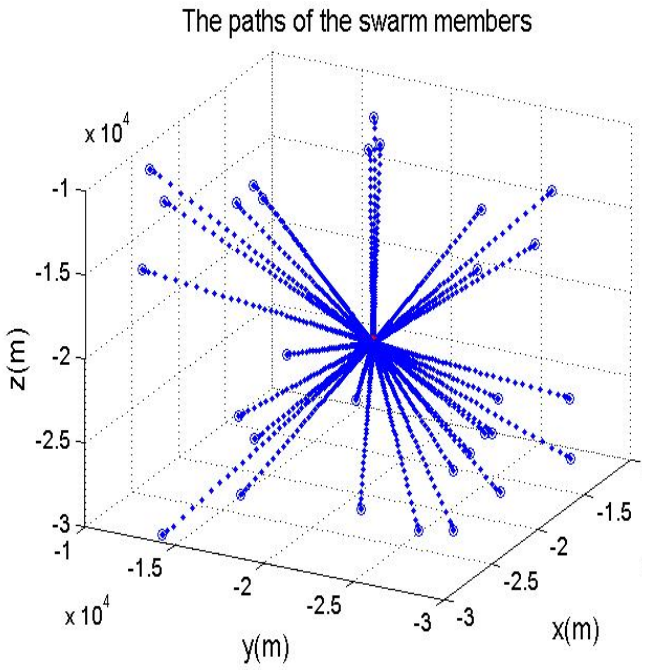

(a)

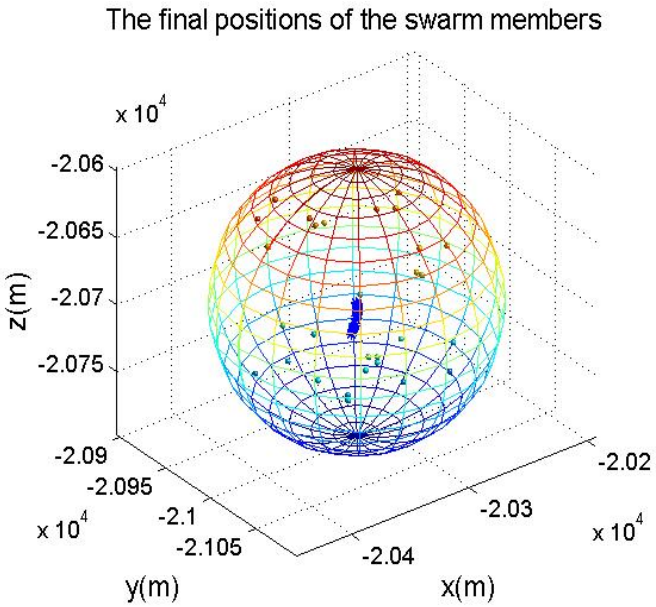

(b)

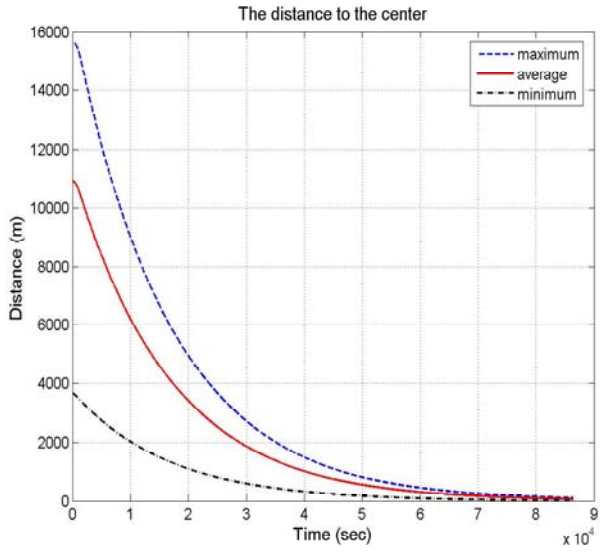

(c)

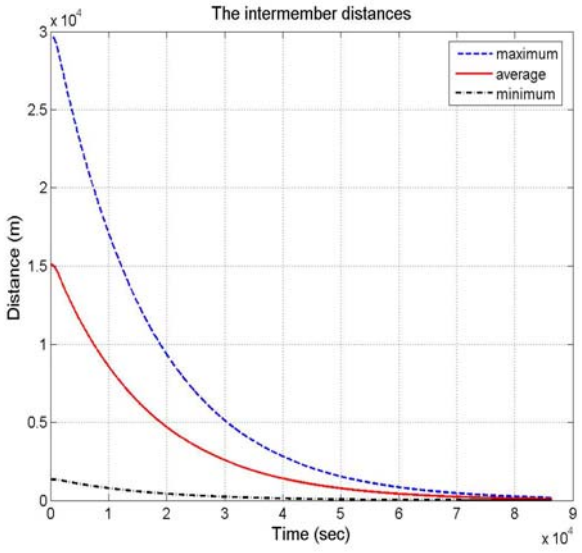

(d)

Figure 29 Simulation plots for 30 spacecraft swarm aggregation using SMC and maximum initial separation of 10 km: Path planning (a)-(d)

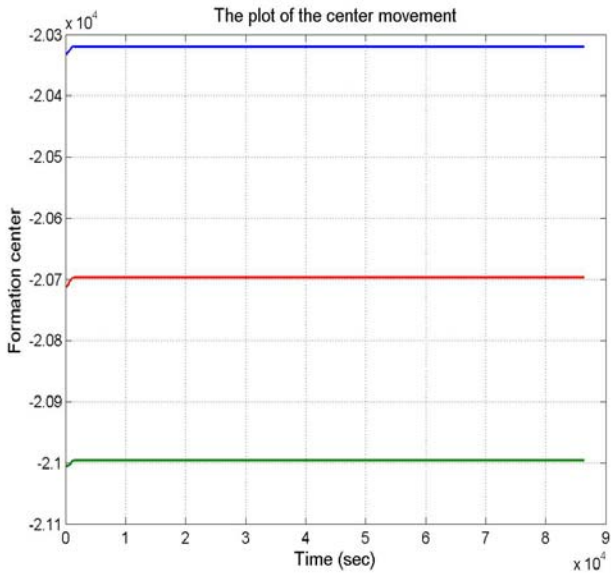

(a)

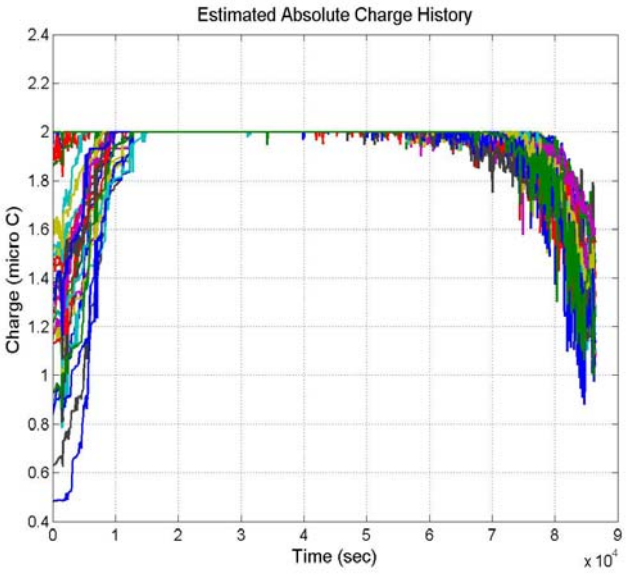

(b)

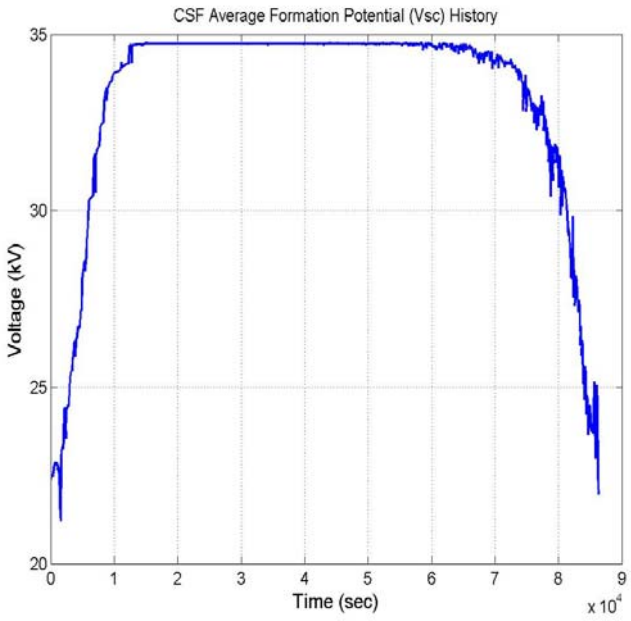

(c)

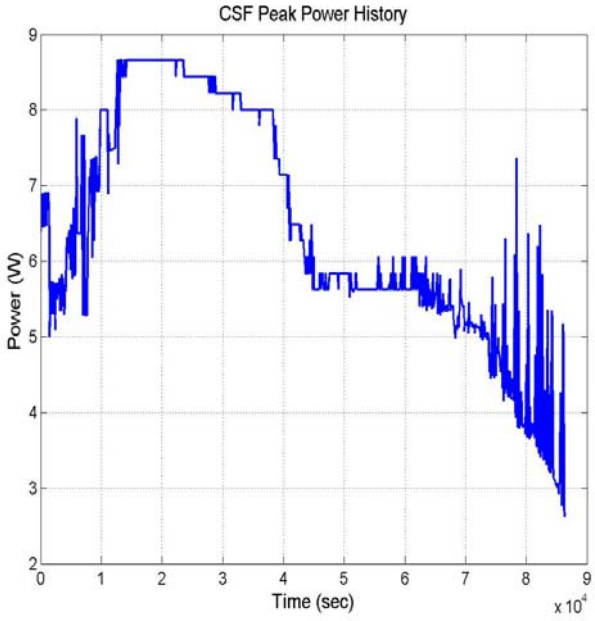

(d)

Figure 30 Simulation plots for 30 spacecraft swarm aggregation using SMC and maximum initial separation of 10 km: Path planning (a) and hybrid actuator parameters (b)-(d).

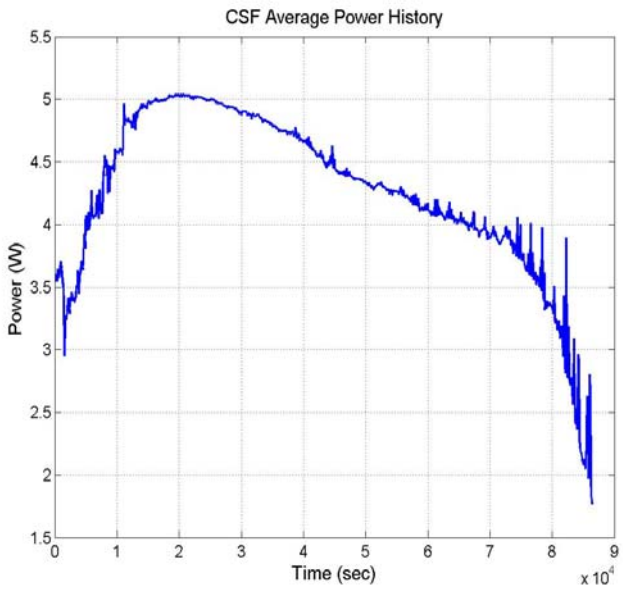

(a)

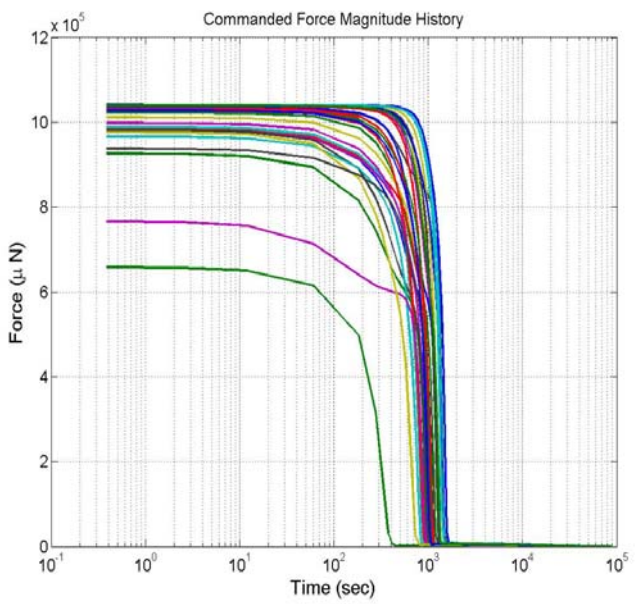

(b)

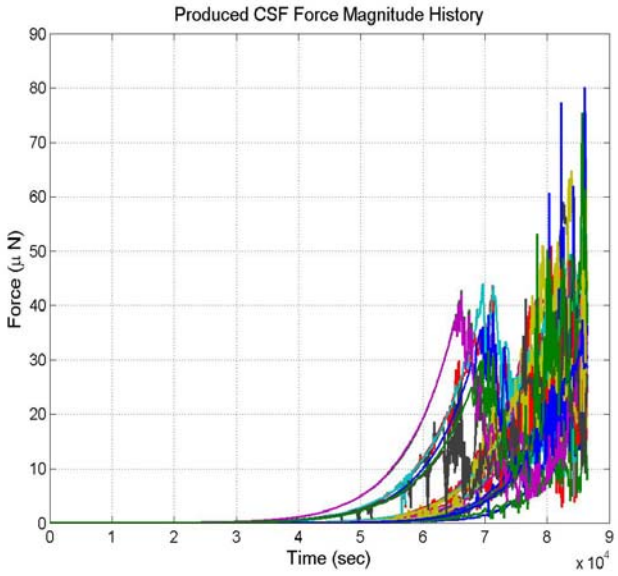

(b)

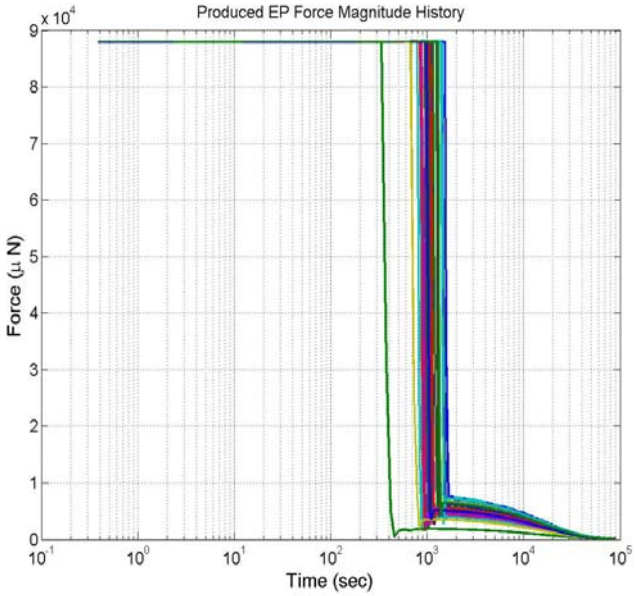

(d)

Figure 31 Simulation plots for 30 spacecraft swarm aggregation using SMC and maximum initial separation of 10 km: Hybrid actuator parameters (a)-(d).

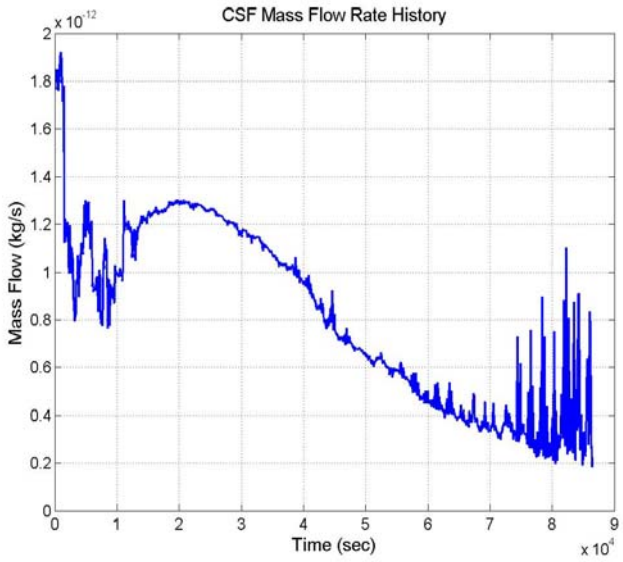

(a)

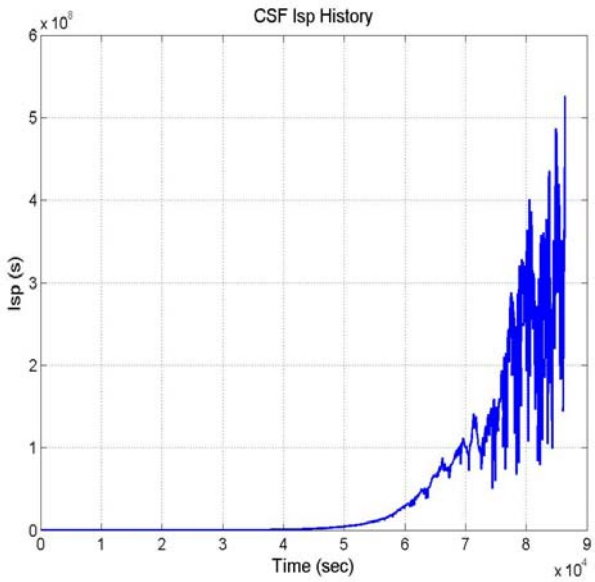

(b)

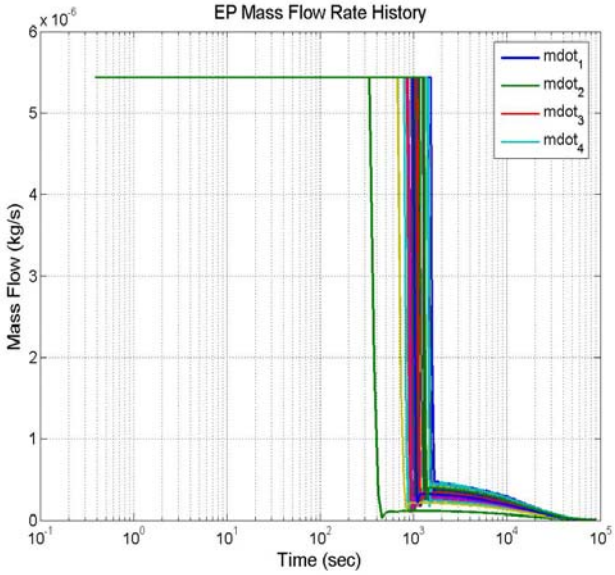

(c)

Figure 32 Simulation plots for 30 spacecraft swarm aggregation using SMC and maximum initial separation of 10 km: Hybrid actuator parameters (a)-(c).

5. SIMPLE LAO FORMATION MANEUVER

A simple formation maneuver is performed entirely using the Lorentz force. The formation is a three-satellite, planar triangle. This triangle is in the Earth's equatorial plane. One spacecraft, Satellite A, in the formation is used as a reference satellite. This satellite is in a Keplerian circular, equatorial, orbit. The two remaining spacecraft begin the maneuver in 'levitating' LAO-type orbits. The 'levitating' orbit entails having a small nominal charge on a satellite. The Lorentz force experience by this will be generally in the radial direction, in essence, augmenting or decrementing the influence of gravity. This radial force allows the satellite to have a stable circular orbit with an angular velocity different from that of a Keplerian orbit. Thus, the two LAO satellites orbit with the same angular speed as the reference satellite but slightly further from Earth. One LAO satellite, Satellite B, is leading the reference and one, Satellite C, is trailing, forming a triangular formation. The goal of the maneuver is to have the leading and trailing LAO satellites switch roles. They must exit their LAO hovering and perform a phasing correction, using only the Lorentz force. The reconfiguration is accomplished by calculating an open loop trajectory that achieves this goal, and using a closed loop PD controller to follow this trajectory. The trajectory is formed by inputting the size of the desired phasing action, dr , and calculating the time, t_{man}, to perform such a maneuver with respect to a known reference maneuver. These quantities are related by the simple linear expression

$$t_{man} = \frac{dr}{dr_{ref}} t_{ref}$$

where dr_{ref} and t_{ref} are the reference manoeuvre size and duration, respectively. The inputs to the controller are the satellite's desired angular velocity, radial position, and radial velocity. These inputs come from the previously calculated trajectory. The controller outputs a charge to mass ratio commanded to the spacecraft. Thus, the controller is of the form

$$\frac{q}{m} = K \begin{bmatrix} \omega_{des} - \omega \\ r_{des} - r \\ \dot{r}_{des} - \dot{r} \end{bmatrix}$$

where K is a 1x3 hand-tuned gain matrix. The PD controller is also used to maintain the hovering state of the satellite when desired.

5.1 LAO MODELLING

The Lorentz Augmented Orbit scenario is modelled using the 2-body Newtonian gravity assumption. The spacecraft is assumed to be a point mass orbiting a spherically-symmetric Earth. The simulation considers no charging dynamics. A commanded charge-to-mass ration is assumed to be instantly and perfectly actuated. Schaub et al, has shown that charging

occurs on small timescales (under one second), thus charging dynamics are ignored (Schaub et al. 2003). The LAO dynamics are modelled in an inertial, Earth-centered reference frame using spherical coordinates. This coordinate system is shown in Figure 25. Expressing the equations of motion of the spacecraft in these coordinates yields

$$\ddot{r} = r\dot{\theta}^2 \sin^2\phi + r\dot{\phi}^2 - \frac{\mu}{r^2} - \vec{F}_L \cdot \hat{r}$$

$$r\ddot{\phi} = -2\dot{r}\dot{\phi} + r\dot{\theta}^2 \sin\phi\cos\phi + \vec{F}_L \cdot \hat{\phi}$$

$$r\ddot{\theta}\sin\phi = -2\dot{r}\dot{\theta}\sin\phi - 2r\dot{\phi}\dot{\theta}\cos\phi + \vec{F}_L \cdot \hat{\theta}$$

where, μ is the Earth's gravitational parameter, and $\vec{F}_L$ is the Lorentz force (per unit mass) experienced by the satellite. The Lorentz force is calculated based on the charge-to-mass ratio of the satellite and its position and velocity, as in

$$\vec{F}_L = \frac{q}{m}(\vec{v} - \vec{\omega}_E \times \vec{r}) \times \vec{B}$$

where *q*/m is the charge-to-mass ratio of the satellite, $\vec{v}$ is the spacecraft velocity, $\vec{\omega}_E$ is the Earth's angular velocity, and $\vec{B}$ is the vector geomagnetic field. The magnetic field is modeled as a dipole field with arbitrary orientation. The position of the magnetic north pole is given by two parameters: α, the angle between magnetic north and true north, and $\Omega_m(0)$, the initial longitude of the magnetic pole. The vector magnetic field is the calculated using the standard dipole field equation:

$$\vec{B} = \frac{B_0}{r^3}\left[3(\hat{N}\cdot\hat{r})\hat{r} - \hat{N}\right]$$

where $\hat{N}$ is the unit vector on the magnetic north pole direction.

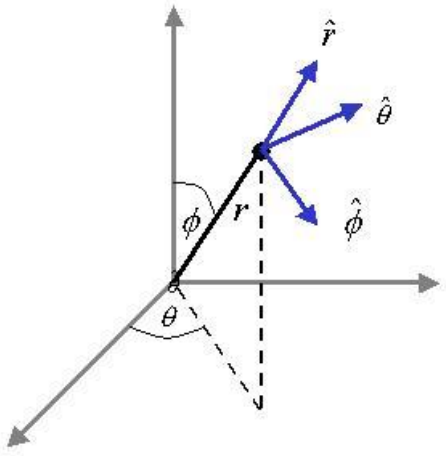

Figure 33 Coordinates used in LAO modelling

5.2 SIMULATION STUDY

The results of spacecraft formation flying in low Earth orbits using Lorentz force is discussed here. The simulation is valid for any initial orbit and magnetic field. Table 4 shows the parameters common to all simulations. The above equations are numerically integrated using a Runge-Kutta 4-5 algorithm in Matlab. The charge-to-mass value for each simulation is either constant or can be set at each time step with an integrated controller. When working with a formation of satellites, the simulation treats each satellite as a separate entity. The motion of each member is integrated independently of all others. This strategy assumes no Coulomb interactions between the individual spacecraft. This assumption nearly always remains valid in LEO as the Debye length is on the order of cm. However, in GEO the satellites must remain several Debye lengths away from each other in order to keep the simulation valid.

Simulation parameters	Value
ω_E	7.272e-5 rad/s
μ	3.986e14 m^3/s^2
B_0	-8.000e15 Wb-m

Table 4 LAO Simulation parameters

The simulation used to demonstrate this manoeuvre is a full three-dimensional system, integrating full dynamics for all three satellites. The orbit of the reference satellite is a 400 km altitude, circular, equatorial orbit. In this simulation the value of *K* is given by [-14e4, 0.3, -5]. The reference maneuver is a manually tuned 50 m phasing maneuver that takes one orbit to complete. The desired maneuver is 25 m phasing change that allows the two moving satellites to switch positions in the triangular formation. The maneuver lasts for 2.5 orbits of the reference satellite. During the first orbit the triangle formation is maintained by the controller in order to show that it is stable throughout an orbit. During the following half-orbit of Satellite A, the maneuver is performed by Satellites B and C. The final full orbit shows that the new configuration is stable as well, again with the controller active. The magnetic field model used is a dipole field tilted 10^o with respect to Earth's true north pole. The resulting path of the satellites is shown in Figure 1. This figure shows the track of each spacecraft relative to Satellite A. Circular points represent initial positions, with triangular points denoting final positions. Figure 1 shows that the maneuver is a success. Figure 2 shows the charge to mass ratio, *q/m*, commanded by the controller to each LAO satellite. The charge to mass ratio was capped at 0.005 C/kg to provide a more realistic current-technology actuator maximum. This saturation

limit shows no decrease in the effectiveness of the maneuver, and could be removed is the gains were tuned to prevent actuator saturation.

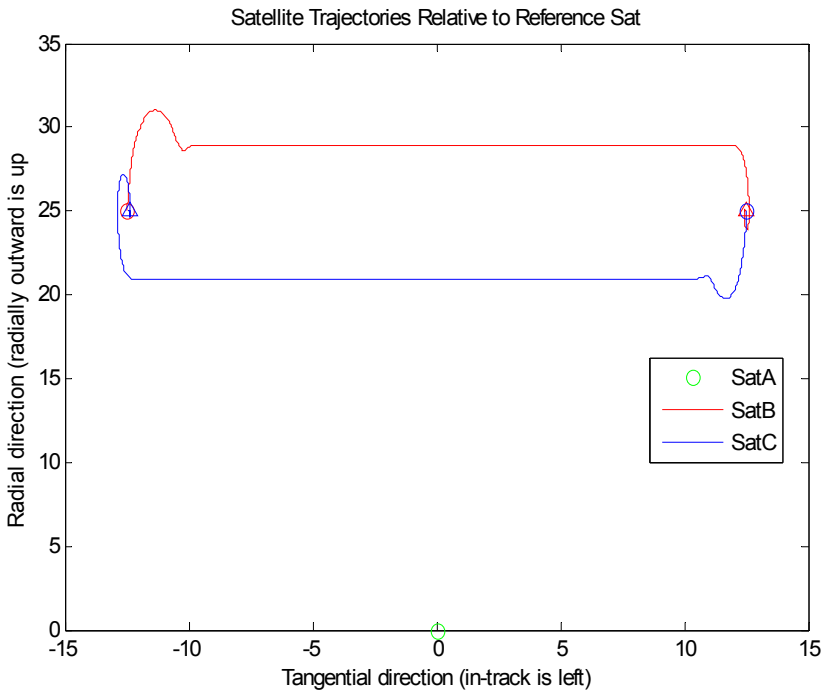

Figure 34 Track of the formation satellites with reference frame centered on Satellite A

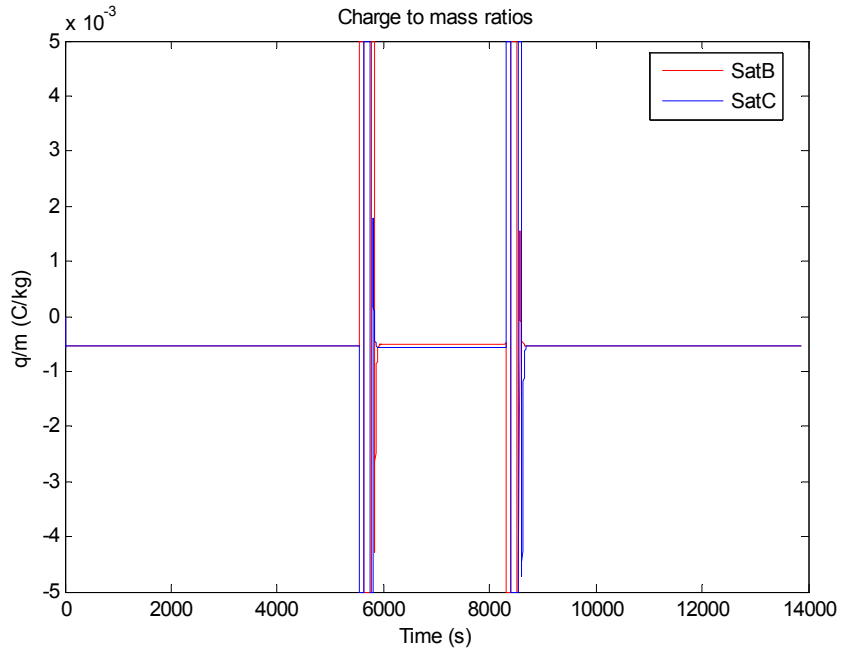

Figure 35 Charge to mass ration in C/kg for each LAO satellite in the formation.

6. CONCLUSIONS

The philosophy of hybrid propulsion using electrostatic forces oriented to satellite swarm navigation and reconfiguration is introduced. This report presents Coulomb force and Lorentz force and studied how these two natural forces interact with conventional electric propulsion system. With respect to the spacecraft swarming and formation flying, electrostatic forces have been extensively studied over the years. However, there still exists the opportunity for more novel techniques and methods – in particular, we investigated how these Coulomb forces will interact with the standard electric thrusters and how the Lorentz force can be used so that the system optimally takes advantage of the physics. We developed a novel hybrid propulsion system for Satellitrons, which optimally limits the required fuel based on leveraging these effects. Furthermore, we developed an algorithm for autonomous path planning and navigation of swarm of satellites. Artificial potential field method combined with classical PD control and modern robust control method using sliding mode control form the basis for these approaches. It is expected that this method will ensure safe and autonomous navigation and reconfiguration of the satellites in the formation. We examined various candidate architectures in sufficient technical detail to evaluate the merits and demerits associated with their eventual implementation. The major conclusions drawn from this study are the following:

- The concept of propellant-less propulsion using electrostatic forces could be successfully used for spacecraft swarms and formation flying applications and is capable of generating 10-1000 micro Newton thrust. This helps to reduce the thrust required from the electric or ion thrusters on-board the spacecraft.
- If the influence of external disturbance due to interaction with plasma environment can be neglected, then the hybrid actuation system developed for satellitron formation flying missions could prove to be more fuel-efficient as it can take full advantage of Coulomb forces in high Earth orbits.
- This method could help though not fully to reduce the weight and contamination issues that are associated with conventional ion thrusters.
- Further investigations are required to fully validate if Coulomb forces can truly replace electric propulsion for future missions.
- Our expectation is that the revolutionary concept of propellant-less spacecraft propulsion using the Lorentz force will offer significant potential for stable LEO spacecraft formations.
- The autonomous navigation and reconfiguration using artificial potential field is suitable for both spacecraft swarm aggregation as well as formation flying.
- The major advantage of using sliding mode controller compared to classical control is the inherent insentivity to parameter variations and disturbances once in the sliding mode, thereby

eliminating the necessity of exact modeling. Proper chatter elimination technique should be used to make this suitable for practical missions. The results presented in this report shows that the algorithm using artificial potential field and sliding mode control is very efficient for autonomous path planning and navigation of spacecrafts.

The results in this report help to understand the whole motion process of electrostatic forces and Lorentz force and design of hybrid propulsion system with good performance for satellite swarm aggregation and formation flying using minimum power from electric propulsion.
The use of Coulomb and Lorentz force as opposed to conventional electric/ion thrusters reduces the risk of contamination and reduces the cost as only minimum power is utilized from electric thrusters. This can make the novel hybrid propulsion system a viable alternative to conventional thrusters in near future. It is important to highlight that the results presented in this report are novel and will definitely throw light in the area of hybrid propulsion for spacecraft path planning and navigation. We hope that this study will prove valuable for ESA's future efforts and will advance the state of the art in this area.

7. FUTURE WORK

There are many exciting open problems that could be addressed in future studies. This includes the following:

- To implement the hybrid propulsion system developed in this study for a real mission in order to validate this feasibility study.
- To investigate the use of hybrid propulsion using Coulomb and Lorentz forces for precise attitude control of spacecrafts flying in formation or for station keeping applications.
- To further explore the field of artificial potential field for path planning. In this study we addressed local minima problem by redefining or changing the philosophy in defining the potential function with minimum local minima. Instead one could use simulated annealing to address the local minima problem.
- Continuous-time sliding mode control using state feedback has practical limitations. A feasible solution would be to extend these results using discrete-time output feedback sliding mode control.

ACKNOWLEDGEMENTS

The European Space Agency Advanced Concepts Team under the Ariadna programme supported this research work. This support is gratefully acknowledged. We are grateful to Dr. Dario Izzo who served as the project manager and contract monitor for his guidance. We would

also like to express our sincere thanks and gratitude to Dr. Veysel Gazi (Department of Electrical and Electronics Engineering, TOBB University of Economics and Technology, Turkey) for the fruitful discussions that led to successful completion of this project.

REFERENCES

Akishita S., Kawamura S. and Hisanobu T. (1993), "Velocity potential approach to path planning for avoiding moving obstacles", *Advanced Robotics*, vol. 7, no. 5, pp. 463-478.

Alfven H. (1954), "*On the Origin of the Solar System*", Newyork, NY.

Aoki M. and Li M. T. (1973), "Partial Reconstruction of State Vector in Decentralized Dynamic Systems," *IEEE Transactions on Automatic Control*, pp. 289–292.

Ayre M., Izzo D. and Pettazzi L. (2005), "Self Assembly in Space Using Behaviour Based Intelligent Components" *TAROS 2005, Towards Autonomous Robotic Systems,* Imperial College, London, UK.

Berryman J. and Schaub H. (2005), "Static Equilibrium Configurations in GEO Coulomb Spacecraft Formations," *AAS Spaceflight Mechanics Meeting*, Copper Mountain, CO, Paper No. 05-104.

Burns J. A. and Schaffer L. (1989), "Orbital Evolution of Circumplanetary Dust by Resonant Charge Variations," *Nature*, vol. 337, no. 6205, pp. 340-343.

Bilen S. G., Gilchrist B. E., Bonifazi C. and Melchioni E. (1995), "Transient Response of an Electropdynamic Tether System in the Ionosphere: TSS-1 First Results," *Radio Science*, vol. 30, no. 5, pp. 1519-1535.

Balch T. and Arkin R. C. (1998), "Behavior-Based Formation Control for Multirobot Teams," *IEEE Transactions on Robotics and Automation*, vol. 14, pp. 926–939.

Beard R., Lawton J. and Hadaegh F. (2001), "A feedback architecture for formation control," *IEEE Transactions on Control Systems Technology*, vol. 9, no. 6, pp. 777–790.

Beard R. (1998), "Architecture and algorithms for constellation control", *Technical report*, Jet Propulsion Laboratory, California Institude of Technology, 4800 Oak Grove Dr., Pasadena, CA 91109, Available online http://www.ee.byu.edu/grad1/users/beard/www docs/research formation.html

Beard R. and Hadaegh F. Y. (1998), "Constellation templates: An approach to autonomous formation flight", *World Automation Congress*, ISIAC, Anchorage, Alaska, pp. 177.1 – 177.6.

Balch T. and Arkin R. C. (1998), "Behavior-based formation control for multi-robot teams," *IEEE Transactions on Robotics and Automation*, vol. 14, no. 6, pp. 926–939.

Choi S. B., Cheong C. C. and Park D. W. (1993), "Moving switching surfaces for robust control of a second order variable structure systems," *Int. J. Control.*, vol. 58, no. 1, pp. 229–245.

L Chengqing et al. (2000) Proc. IEEE Int. Conference on Robotics & Automation, San Francisco, pp. 983-988.

Chutijian A. (2000), “Recent applications of gaseous discharges: Dusty plasmas and upward-directed lightning”, *Advances in Atomic, Molecular and Optical Physics*, New York, NY: Academic, vol. 2000, pp. 373-398.

Cui, Chunshi, and Goree J. (1994), “Fluctuations of the Charge on a Dust Grain in a Plasma,” *IEEE Transactions on Plasma Science*, vol. 22, no. 2.

Cort´es J. and Bullo F. (2004), “Coordination and geometric optimization via distributed dynamical systems,” *SIAM Journal of Control and Optimization*.

Campbell M. (2003), “Planning Algorithm for Multiple Satellite Clusters”, *J. Guidance Control and Dynamics*, vol. 26, no. 5, pp. 770-780.

Das A., Cobb R. and Stallard M. (1998), “TechSat 21 - A Revolutionary Concept in Distributed Space Based Sensing,” *Proc. of the Guidance, Navigation and Control Conference*, vol. AIAA-98-5255, Boston, MA, pp. 1–6.

Davison E. (1974), “The Decentralized Stabilization and Control of a Class of Unknown Non-Linear Time-Varying Systems,” *Automatica*, vol. 10, pp. 309–316.

DeCou A. (1991), “Orbital station-keeping for multiple spacecraft interferometry,” *J. Astronautical Sciences*, vol. 39, no. 3, pp. 283–297.

Dimarogonas D. V., Zavlanos M. M., Loizou S. G., and Kyriakopoulos K. (2003), “Decentralized motion control of multiple holonomic agents under input constraints,” *Proc.* 42nd *IEEE Conf. on Decision and Control*, Hawaii, pp. 3390–3395.

Drazenovic B. (1969), “The invariance conditions in variable structure systems,” *Automatica*, vol. 6, pp. 287–295.

Emel’yanov S. V. (1964), “Design of variable structure control systems with discontinuous switching functions,” *Eng. Cybern.*, vol. 1, pp. 156–160.

Egerstedt M. and Hu X. (2001), “Formation constrained multi-agent control,” *IEEE Trans. on Robotics and Automation*, vol. 17, no. 6, pp. 947–951.

Friedrich M. and Torkar K. M. (1991), “Plasma Observations of the Active Mother-Daughter Payload MAIMIK in the Lower Thermosphere,” *Planetary and Space Sciences,* vol. 39, no. 3, pp. 453-467.

Fredslund J. and Matari´c M. J. (2002), “A general algorithm for robot formations using local sensing and minimal communications,” *IEEE Transactions on Robotics and Automation*, vol. 18, no. 5, pp. 837–846.

Friedman and Kennedy, “*Plasma Physics and Engineering*”, London: Taylor & Francis Publishing, 2004.

Garett H. B. (1981), “The Charging of Spacecraft Surfaces”, *Rev. Geophy*., vol. 19, pp. 577-616.

Garrett H. B. and Whittlesey A. C. (2000), “Spacecraft Charging, An Update,” *IEEE Transactions on Plasma Science*, vol. 28, no. 6, pp. 2017-2028.

Gazi V. (2005), “Swarm aggregations using artificial potentials and sliding mode control”, IEEE Transactions on Robotics, Vol. 21, No. 6, pp. 1208-1214.

Gazi V. and Passino K. M. (2004), “A class of attraction/repulsion functions for stable swarm aggregations”, *International Journal of Control*, Vol. 77, No. 18/15, pp. 1567-1579.

Gazi V. and Passino K. M. (2003), “Stability analysis of swarms”, *IEEE Transactions on Automatic Control*, Vol. 48, No. 4, pp. 692-696.

Guldner J. and Utkin V. I. (1995), “Sliding mode control for gradient tracking and robot navigation using artificial potential fields,” *IEEE Trans. On Robotics and Automation*, vol. 11, no. 2, pp. 247–254.

Hasting D. and Garret H. (1996), “*Spacecraft-Environment Interactions*”, Cambridge University Press, Cambridge, UK, pp. 44-71.

Heck B. S. and Ferri A. A. (1989), “Application of output feedback to variable structure systems,” *Journal of Guidance*, vol. 12, pp. 932–935.

Hoskins W. A., Wilson M. J., Willey M. J., Meckel N. J., Campell M. and Chung S. (1999), AIAA Meeting Papers on Disk vol. 4, No. 3, *Proc. 35th AIAA/ASME/SAE/ASEE Joint Propulsion Conference*, Los Angeles, CA.

Hough M. E. (1982), “Lorentz Force Perturbations of a Charged Ballistic Missile”, *Proc. AIAA Guidance and Control Conference*, San Diego, pp. 277-287.

Hung J. Y., Gao W. and Hung J. C. (1993), “Variable structure control: A survey”, *IEEE Trans. Industrial Electronics*, vol. 40, no. 1, pp. 2-22.

Izzo D. (2002), “Formation Flying Linear Modelling”, *Proc. 5th Int. Conference in Space, Cambridge*, UK, pp. 283-289.

Izzo. D., Sabatini M. and Valente C. (2003), “A new Linear Model Describing Formation Flying Dynamics Under J_2 Effect”, *Proc. XVII AIDAA Congress*, pp. 493-500.

Izzo D. and Pettazzi L. (2005), “Autonomous and Distributed motion planning for satellite swarm”, accepted for publication in *Journal of Guidance Control and Dynamics*, also *8th International Symposium on Artificial Intelligence*, Robotics and Automation in Space, 5-9 Sept., Munich, Germany, 2005. (available at www.esa.int/act)

Inalhan G., Busse J. and How J. (2000), “Precise Formation Flying Control of Multiple Spacecraft using Carrier-Phase Differential GPS”, *Proc. Guidance, Control and Navigation Conference*, AAS 00-109.

Itkis U. (1976) , *Control Systems of Variable Structure*. New York: Wiley.

Janson S. W., Helvajian, H., Hansen, W. W., and Lodmell, J. (1999), “Microthrusters for nanosatellites”, *2nd Int. Conf. on Integrated Micro Nanotechnology for Space Applications*, Pasadena, CA.

Janardhanan S. and Bandyopadhyay B. (2006), "Discrete Sliding Mode Control of Systems with Unmatched Uncertainty using Multirate Output Feedback", *IEEE Transactions on Automatic Control*, vol. 51, no. 6, pp. 1030-1035.

Joe H., Schaub H. and Parker G. G. (2004), “Formation Dynamics of Coulomb Satellites,” *6th Int. Conf. on Dynamics and Control of Systems and Structures in Space*, Cinque Terre, Liguria, Italy.

James B. F., Norton O. W. and Alexander M. B. (1994), “The Natural Space Environment: Effects on Spacecraft,” *NASA Reference Publication* 1350.

Kang W. and Yeh H. (2002), “Co-ordinated attitude control of multi-satellite systems”, *Int. J. Robust and Nonlinear Control*, vol.12, pp. 185–205.

Khatib O. (1986), “Real-Time Obstacle Avoidance for Manipulator and Mobile Robots”, *The Int. J Robotics Research*, vol. 5, no. 1, pp. 90-98.

Khatib O . and Chatila R. (1995), “ ”, *Intelligent Autonomous Systems (IAS’4)*, Karlsruhe, Germany, pp. 490-496.

Khosla and Volpe R. (1988), “ Superquadratic artificial potentials for obstacle avoidance and approach“, *IEEE Conf Robotics Automat*, pp.1778-1784.

Kim J. O. and Khosla P. (1992), “Real time obstacle using harmonic potentials”, *IEEE Trans Robotics and Automation*, vol. 8, no. 3, pp. 338-349.

King L. B., Parker G. G., Deshmukh S. and Chong J. H. (2002a), “Propellantless Control of Spacecraft Swarms using Coulomb Forces” *NIAC Final Report*.

King L. B., Parker G. G., Deshmukh S. and Chong J. H. (2002b), “Spacecraft Formation-Flying using Inter-Vehicle Coulomb Forces” *Tech. Report, NASA/NIAC,* http://www.niac.usra.edu/

King L. B., Parker G. G., Deshmukh S. and Chong J. H. (2003), “Study of Inter-spacecraft Coulomb Forces and Implications for Formation Flying”, *AIAA Journal of Propulsion and Power*, vol. 19, no. 3, pp. 497-505.

Kirkpatrick S., Gelatt C. D. and Vecchi M. P. (1983), “Optimization by simulated annealing”, *Science*, vol. 220, no. 4598, pp. 671-680.

Klavins E. (2003), “Toward the control of self-assembling systems,” in *Control Problems in Robotics*, ser. Springer Transactions in Advanced Robotics, A. Bicchi, H. Christensen, and D. Prattichizzo, Eds. Springer,, vol. 4, pp. 153–168.

Kong, E.M.C., Kwon, D.W., Schweighart, S.A., Elias, L.M., Sedwick, R.J., Miller, D.W. (2004), “Electromagnetic Formation Flight for Multi-Satellite Arrays,” J. Spacecraft and Rockets, vol. 41, no. 4, pp. 659-666.

Kong E. M. (2002), “Spacecraft Formation Flights Exploiting Potential Fields”, *PhD Thesis*, Department of Aeronautics and Astronautics, Massachusetts Institute of Technology.

Krogstad T. R. (2005), “Attitude Control of Satellites in Clusters”, Master’s Thesis, Norwegian University of Science and Technology.

Kumar R. and Seywald H. (1995), “Fuel-optimal station keeping via differential inclusions”, *J. Guidance, Control and Dynamics*, vol. 18, no. 5, pp. 1156-1162.

Lai S.T. and Murad E. (1989), “Critical ionization velocity experiments in space”, *Planet Space Sci*., vol. 37, no. 7, pp. 865-872.

Lai S. T. (1989), “An Overview of Electron and Ion Beam Effects in Charging and Discharging of Spacecraft,” *IEEE Transactions on Nuclear Science*, vol. 36, no. 6.

Lai S. T. (2002), “On Supercharging; Electrostatic Aspects,” *J. Geophysical Research*, vol. 107, No. A4.

Lawton J., Young B. and Beard R. (2000), “A decentralized approach to elementary formation maneuvers,” *Proc. of the IEEE International Conference on Robotics and Automation*, San Francisco, CA, pp. 2728–2733.

Lewis M. and Tan K. (1997), “High precision formation control of mobile robots using virtual structures”, *Autonomous Robots*, vol. 4, pp. 387–403.

Leonard N. E. and Fiorelli E. (2001), “Virtual leaders, artificial potentials and coordinated control of groups,” *Proc. of Conf. Decision Contr.*, Orlando, FL, pp. 2968–2973.

Leitner J., Bauer F., Folta D., Moreau M., Carpenter R. and How J. (2002), “Formation Flight in Space,” *GPS World*.

Lin Z., Broucke M. and Francis B. (2004), “Local control strategies for groups of mobile autonomous agents,” *IEEE Transactions on Automatic Control*, vol. 49, no. 4, pp. 622–629.

Lin J., Morse A. and Anderson B. (2003), “The multi-agent rendezvous problem,” *Proc. 42th IEEE Conference on Decision and Control*, Maui HI, pp. 1508–1513.

Littlejohn, R. G. (1982), “Hamiltonian Perturbation Theory in Non-Canonical Coordinates,” *Journal of Mathematical Physics*, Vol. 23 pp. 742-747.

Littlejohn, R. G. (1979), “A Guiding Center Hamiltonian: A New Approach,” *Journal of Mathematical Physics*, Vol. 20, pp. 2445-2458.

Martinez-Sanchez M. and Pollard J. E. (1998), “Spacecraft Electric Propulsion-An Overview”, *J. Propulsion and Power*, vol. 14, no. 5, pp. 688-699.

Mullen E. G., Gussenhoven M. S. and Hardy D. A. (1986), “SCATHA Survey of High-Voltage Spacecraft Charging in Sunlight”, *Journal of the Geophysical Sciences*, vol. 91, pp.1074–1090.

Mandell M. J., Jongeward G. A., Cooke D. L. and Raitt W. J. (1998), “SPEAR 3 Flight Analysis: Grounding by Neutral Gas Release, and Magnetic Field Effects on Current Distribution,” *J. Geophysical Research,* vol. 103, no. A1, pp 439-445.

Milam M. B., Petit N. and Murray R. M. (2001), “Constrained Trajectory Generation of Micro-Satellite Formation Flying”, *AIAA Guidance Navigation and Control Conference,* 4030*.*

McInnes C. R. (1995), “Potential Function Methods For Autonomous Spacecraft and Control”, *Paper AAS 95-447*.

McQuade F. (1997), “Autonomous Control for On-Orbit Assembly Using Artificial Potential Functions”, *Ph.D. thesis*, Faculty of Engineering University of Glasgow.

Mesbahi M. and Hadaegh F. (2001), “Formation Flying Control of Multiple Spacecraft via Graphs, Matrix Inequalities, and Switching*”, J. Guidance Control, and Dynamics*, vol. 24, no. 2, p. 369-377.

Natarajan A. and Schaub H. (2005), “Linear Dynamics and Stability Analysis of a Coulomb Tether Formation,” *AAS Spaceflight Mechanics Meeting*, Copper Mountain, CO, Paper No. 05-204.

Olfati-Saber R. and Murray R. M. (2004), “Consensus problems in networks of agents with switching topology and time-delays,” *IEEE Transactions on Automatic Control*, vol. 49, no. 9, pp. 1520–1533.

Olfati-Saber R. and Murray R. M. (2002), “Distributed cooperative control of multiple vehicle formations using structural potential functions,” *Proc. IFAC World Congress*, Barcelona, Spain, [CD ROM].

Ogren P., Egerstedt M., and Hu X. (2002), “A control Lyapunov function approach to multiagent coordination”, *IEEE Trans. Robot. Autom*., vol.18, pp. 847–851.

Parker G. G., Passerello C. and Schaub H. (2004), “Static Formation Control Using Inter-spacecraft Coulomb Forces,” *2nd International Symposium on Formation Flying*, Washington, D.C.

Peck M. A. (2005), “Prospects and Challenges for Lorentz-Augmented orbits” *AIAA Guidance, Navigation, and Control Conference*, Paper no. 2005-5995.

Peck M. A. and Morgowicz B. (2006), “LEOSynch: A Low-Earth Orbiting, Geosynchronous Spacecraft”, *Summary Concept White Paper*, Northrop Grumman Space Technologies, Technology Development.

Personal Communications (2006) with L. King, M. Peck, H. Schaub on ‘Plasma-Spacecraft Iteraction Modelling’, June 16 and September 6.

Pan H. and Kapila V. (2000), “Adaptive nonlinear control for spacecraft formation flying with coupled translational and attitude dynamics”, *Proc. 40th IEEE Conference on Decision and Control.*

Park M. G., Jeon J. H. and Lee M. C. (2001), “Obstacle Avoidance for Mobile Robots using Artificial Potential Field Approach with Simulated Annealing”, *IEEE Int. Symposium on Industrial Electronics*, Pusan, Korea, pp. 1530-1535.

Rustan P., Garrett H., and Schor M. J. (1993), “High Voltages in Space: Innovation in Space Insulation,” *IEEE Transactions on Electrical Insulation*, vol. 28, no. 5.

Ren W. and Beard R. (2004), “A Decentralized Scheme for Spacecraft Formation Flying via the Virtual Structure Approach”, *AIAA Journal of Guidance, Control and Dynamics*, vol. 27, no. 1, pp.73-82.

Ren W., and Beard, R.W. (2002), “Virtual structure based spacecraft formation control with formation feedback”, *Proc. AIAA Guidance, Navigation, and Control Conf*., Monterey, CA.

Rimon E. and Koditschek D. E. (1992), “ Exact robot navigation using artificial potential functions”, *IEEE Trans. Robotics & Automation*, vol. 8, no. 5, pp. 501-518.

Saaj C. M., Bandyopadhyay B. and Unbehauen H. (2002), “A new algorithm for discrete-time sliding mode control using fast output sampling feedback”, *IEEE Transaction on Industrial Electronics*, vol. 49, pp. 518-523.

Schaub H., Parker G. G. and King L. B. (2003), “Challenges and Prospects of Coulomb Spacecraft Formations,” *AAS John L. Junkins Astrodynamics Symposium*, College Station, TX, Paper No. AAS-03-278.

Schaub H. (2004), “Stabilization of Satellite Motion Relative to a Coulomb Spacecraft Formation,” *AAS Spaceflight Mechanics Meeting*, Maui, Hawaii, Paper No. AAS 04-259.

Schaub H. and Kim M. (2004), “Orbit Element Difference Constraints for Coulomb Satellite Formation,” *AAS Astrodynamics Specialist Conference*, Providence, Rhode Island, Paper No. 04-5213.

Schaffer L. and Burns J. A. (1987), “The Dynamics of Weakly Charged Dust: Motion Through Jupiter’s Gravitational and Magnetic Fields”, *J. Geophysical Research*, vol. 92, pp. 2264-2280.

Schaffer L. and Burns J. A. (1994), “Charged Dust in Planetary Magnetospheres: Hamiltonian Dynamics and Numerical Simulations for Highly Charged Grains,” *J. Geophysical Research*, vol. 99, no. A9, pp. 17,211-223.

Streetman B. and Peck M.A. (2006), “Synchronous Orbits and Disturbance Rejection Using the Geomagnetic Lorentz Force” *Proceedings of the AIAA Guidance, Navigation, and Control Conference* (Accepted).

Schaffer L. and Burns J. A. (1987), “The Dynamics of Weakly Charged Dust: Motion through Jupiter’s Gravitational and Magnetic Fields,” *J. Geophysical Research*, vol. 92, no. A3, pp. 2264-2280.

Sandoval-Rodriguez R. and Abdallah C. T. (2003), “Internet-like protocols for the control and coordination of multiple agents with time delay,” *Proc. IEEE International Symposium on Intelligent Control*, Houston, TX.

Scharf D. P., Hadaegh F. Y. and Polen S. R. (2003), “A Survey of Spacecraft Formation Flying Guidance and Control (Part I:) Guidance”, *Proc. American Control Conference*, Denver, Colorado, pp. 1733-1736.

Smith R. S. and Hadaegh F.Y. (2002), “Control Topologies for Deep Space Formation Flying Spacecraft”, American Control Conference, Anchorage, AK.

Tajmar M., Mitterauer J. and Wang J. (1999), “Field-Emission-Electric-Propulsion (FEEP) Plasma Modeling: 3D Full Particle Simulations”, *AIAA/ASME/SAE/ASEE Joint Propulsion Conference*, June 20-24, Los Angeles, CA.

Tribble A.C. (2003), *The Space Environment: Implications for Spacecraft Design*, Princeton University Press.

Torkar K., Riedler W., Escoubet C. P. and Fehringer R., Schmidt R., Grard R. J. L., Arends H., Rudenauer F., Steiger W., Narheim B. T., Svenes K., Torbert R., Andre M., Fazakerley A., Goldstein R., Olsen R. C., Pedersen A., Whipple E. and Zhao H. (2001), “Active Spacecraft Potential Control for Cluster-Implementation and First Results”, *Annales Geophysicae*, vol. 19, pp. 1289-1302.

Tanner H. G., Jadbabaie A. and Pappas G. J. (2003), “Stable flocking of mobile agents, Part I: Fixed topology,” in *Proc. IEEE Conference on Decision and Control*, Maui, Hawaii, December 9-12, pp. 2010–2015.

Tanner H. G. and Kumar A. (2005a), “Towards decentralization of multi-robot navigation functions,” *Proc. IEEE Conference on Robotics and Automation*.

Utkin V. I. (1977), “Variable structure systems with sliding modes”, *IEEE Trans. Automatic Control,* vol. 22, no. 2, pp. 212-222.

Utkin V. I. (1971), “Equations of the slipping regime in discontinuous systems: I,” *Autom. Remote Control*, vol. 32, pp. 1897–1907.

Utkin V. I., Drakunov S. V., Hashimoto H., and Harashima F. (1991), “Robot path obstacle avoidance control via sliding mode approach,” *IEEE/RSJ International Workshop on Intelligent Robots and Systems*, Osaka, Japan, pp. 1287–1290.

Vitale S., Bender P., Brillet A., Buchman S., Cavalleri A., Cerdonio M., Cruise M., Cutler C., Danzmann K., Dolesi R., Folkner W., Gianolio A., Jafry Y., Hasinger G., Heinzel G., Hogan C., Hueller M., Hough J., Phinney S., Prince T., Reinhard R., Richstone D., Robertson D., Rodrigues M., Ruediger A., Sandford M., Schilling R., Shoemaker D., Schutz B., Stebbins R., Stubbs C., Sumner T., Thorne K., Touboul P., Ward H., Weber W. and Winkler W. (2002), "LISA and its In-Flight Test Precursor SMART-2", in Proceedings of the Astroparticle Conference TAUP2001, *Nuclear Physics B, Proc.* Suppl., 10, pp. 209-216.

Walker J. G. (1982), “The Geometry of Cluster Orbits”, *J. Brit. Interplan. Soc*., vol. 35, pp. 345.

Wang P., Hadaegh F. and Mokuno M. (2003), “Formation flying of multiple spacecraft with automatic rendezvous and docking capability”, *AIAA Guidance, Navigation and Control Conference and Exhibit Proceedings*.

Wang P., Hadaegh F. and Lau K. (1999), “Synchronized formation rotation and attitude control of multiple free-flying spacecraft”, *J. Guidance, Control and Dynamics* pp. 28–35.

Young B., Beard R., and Kelsey J. (2001), “A control scheme for improving multi-vehicle formation manoeuvres”, *Proc. American Control Conf*., Arlington, VA, pp. 704–709

Young K. D., Utkin V. I. and Ozguner U. (1999), “A control engineer’s guide to sliding mode control”, *IEEE Trans. Control System*, vol. 7, no. 3, pp. 328-342.

APPENDIX

1. $N = 4$ ***Spacecraft forming a tetrahedron formation in*** R^3

The initial conditions of the spacecrafts are randomly chosen as x0=[5000*(rand(3, 4)-1.5]. Both PD control and SMC use the same initial conditions. The co-ordinates of the initial positions of each of the four spacecrafts along X, Y and Z-axis are listed below.

Initial Position co-ordinates	x0: X-axis	x0: Y-axis	x0: Z-axis
s/c1	-7823.65578534303	-8073.30605282212	-14159.2093924956
s/c2	-10456.4485024445	-10581.7170309366	-11467.4954499931
s/c3	-13463.9363747651	-8243.55350366588	-8007.86672258738
s/c4	-7724.90870782069	-10216.1561904334	-9451.58013658323

The final position co-ordinates after t=86400 sec are as follows:

1. Using PD Control

Final position co-ordinates	xf: X-aixs	xf: Y-axis	xf: Z-axis
s/c1	-4963.2	-4551.7	-5393.2
s/c2	-4988.3	-4594	-5383.8
s/c3	-4995.1	-4553.9	-5354.7
s/c4	-4952	-4579.1	-5352.9

Maximum distance to center of formation after 86400 sec =109.76 m

Average distance to center of formation after 86400 sec = 86.17 m

Minimum distance to center of formation after 86400 sec = 71.065 m

Maximum inter-member distance after 86400 sec = 50.00 m

Average inter-member distance after 86400 sec = 50.00 m

Minimum inter-member distance after 86400 sec = 50.00 m

2. Using Sliding Mode Control

Final position co-ordinates	xf: X-aixs	xf: Y-axis	xf: Z-axis
s/c1	-4921.7	-4623.3	-5409.7
s/c2	-4948.1	-4661.6	-5398.6
s/c3	-4956.5	-4626	-5368.4
s/c4	-4911.1	-4646.4	-5367.6

Maximum distance to center of formation after 86400 sec = 31.72 m

Average distance to center of formation after 86400 sec = 30.545 m

Minimum distance to center of formation after 86400 sec = 29.516 m

Maximum inter-member distance after 86400 sec = 54.083m

Average inter-member distance after 86400 sec = 49.838 m

Minimum inter-member distance after 86400 sec = 47.482 m

2. $N = 30$ **- *Spacecraft swarm aggregation problem in*** R^3

The initial conditions of the spacecrafts are randomly chosen as x0=[10000*(rand(3, 30)-1.5]. Both PD control and SMC use the same initial conditions. The co-ordinates of the initial positions of each of the four spacecrafts along X, Y and Z-axis are listed below.

Initial Position co-ordinates	x0: X-axis	x0: Y-axis	x0: Z-axis
s/c1	-1.5742×10^4	-1.9020×10^4	-1.1173×10^4
s/c2	-2.3403×10^4	-1.5910×10^4	-1.1131×10^4
s/c3	-1.8368×10^4	-1.2397×10^4	-1.5008×10^4
s/c4	-2.2408×10^4	-1.5489×10^4	-2.6744×10^4
s/c5	-1.0876×10^4	-2.6075×10^4	-1.4476×10^4
s/c6	-1.7734×10^4	-2.6754×10^4	-2.9379×10^4
s/c7	-2.4227×10^4	-1.0579×10^4	-1.0990×10^4
s/c8	-2.5439×10^4	-1.0829×10^4	-1.6403×10^4
s/c9	-2.8901×10^4	-1.8003×10^4	-2.2137×10^4
s/c10	-2.5693×10^4	-2.6352×10^4	-2.8465×10^4
s/c11	-2.9852×10^4	-1.4224×10^4	2.9644×10^4
s/c12	-1.2441×10^4	-2.2949×10^4	-1.5557×10^4
s/c13	-1.0631×10^4	-2.6887×10^4	-2.6741×10^4
s/c14	-2.3732×10^4	-2.9412×10^4	-2.2847×10^4
s/c15	-2.9456×10^4	-1.4127×10^4	-1.0015×10^4
s/c16	-2.7795×10^4	-1.7548×10^4	-2.7349×10^4
s/c17	-2.3799×10^4	-2.7304×10^4	-2.5533×10^4
s/c18	-2.2069×10^4	-2.7297×10^4	-2.5179×10^4
s/c19	-1.1450×10^4	-2.2178×10^4	-1.9775×10^4
s/c20	-2.8142×10^4	-2.9566×10^4	-2.6809×10^4
s/c21	-1.3110×10^4	-1.2417×10^4	-2.6260×10^4
s/c22	-1.0174×10^4	-1.5759×10^4	-1.2573×10^4
s/c23	-2.0407×10^4	-2.0080×10^4	-2.4249×10^4
s/c24	-2.8781×10^4	-2.4751×10^4	-2.6275×10^4
s/c25	-1.1658×10^4	-2.7534×10^4	-2.9731×10^4
s/c26	-2.2606×10^4	-1.6027×10^4	-1.2213×10^4
s/c27	-1.8125×10^4	-2.6866×10^4	-2.3666×10^4
s/c28	-2.5332×10^4	-2.9832×10^4	-2.2062×10^4
s/c29	-1.7003×10^4	-2.8300×10^4	-1.4624×10^4
s/c30	-1.0606×10^4	-1.5704×10^4	-1.4361×10^4

The final position co-ordinates after t=86400 sec are as follows:

1. Using PD Control

Maximum distance to center of swarm after 86400 sec = 389.3 m
Average distance to center of swarm after 86400 sec = 373.25 m
Minimum distance to center of swarm after 86400 sec = 356.92 m
Maximum inter-member distance after 86400 sec = 34.44 m
Average inter-member distance after 86400 sec = 22.469 m
Minimum inter-member distance after 86400 sec = 10.769 m

2. Using SMC

Maximum distance to center of swarm after 86400 sec = 193.59 m
Average distance to center of swarm after 86400 sec = 177.69 m
Minimum distance to center of swarm after 86400 sec = 161.09 m
Maximum inter-member distance after 86400 sec = 33.979 m
Average inter-member distance after 86400 sec = 22.481 m
Minimum inter-member distance after 86400 sec = 10.137 m